The Mediterranean Journal of Measurement and Control

Volume 2 / Number 1 / 2006

ISSN: 1743-9310

Published by SoftMotor Ltd.

The Mediterranean Journal of Measurement and Control

Aims and Scope

The journal publishes papers from worldwide in the field of instrumentation, measurement, and control. Its scope encompasses cutting-edge research and development, education and industrial applications. The journal publishes peer-reviewed papers designed to appeal to both researchers and practitioners. It presents up-to-date coverage of the latest developments, offering a unique interdisciplinary perspective. It also includes invited papers, book reviews, conference notices, calls for papers, and announcements of new publications and special issues. The journal covers - but not limited to: All Aspects of Control Theory and its Applications (Linear, Nonlinear, Robust, State Space and Multivariable, Self-Tuning, Adaptive, Optimal, and others), System Identification and Parameter Estimation, and Mathematical Modeling and Simulation, Intelligent Systems and Applications (fuzzy logic, neural networks, genetic algorithms, and others), Machine Vision and Pattern Recognition, Mechatronics and Robotics, and Advanced Manufacturing Systems, Sensors, Measuring Instruments, and Signal Processing, Computing for Measurement, Control and Automation, and Industrial Networks and Communication protocols (FieldBuses, OPC, and others). Papers may be from the following categories: Design: Present a complete “how-to” guide. Connect design procedures to first principles. Explicitly state necessary heuristics and limits of applicability. Provide evidence that the procedures are practicable. Analysis: Clearly develop a fundamental, theoretical analysis of a practice-relevant issue. Explicitly state implications and recommendations for its application. Provide credible examples. Application: Present the results of new (or under-utilized) techniques or novel applications. Provide a complete description of results, including pilot- or plant-scale experimental data, and a revelation of heuristics and shortcomings.

 ISSN: 1743-9310

WELCOME TO THE MEDITERRANEAN JOURNAL OF MEASUREMENT AND CONTROL

We would like to welcome you all to the second volume - first issue - of The Mediterranean Journal of Measurement and Control. This issue of the journal, comprising of five papers, is dedicated to the latest research work being done in the analyses of modeling and control of dynamic systems.

The first paper by Dotoli deals with the issues of modeling and managing the Supply Chain (SC) at the operational level. The system is modeled as a timed discrete event dynamical system, whose evolution depends on the interaction of discrete events such as the arrival of components at the facilities, the departure of the transporters from the suppliers or the manufacturers, the start of assembly operations at the manufacturers. More precisely, generalized stochastic Petri nets model the system in a modular way and describe its behavior.

The second paper by Rimlinger deals with the control of solution copolymerization reactors**.** This paper proposes a new observer-based control structure in order to control the composition and the molecular weight of the polymer. A high gain observer that allows estimating the concentration of radicals and the residual number of moles of monomers is developed.

The third paper by Chin deals with the control of an underactuated remotely operated vehicle**.** This paper, proposes a new pipeline tracking control of an underactuated remotely operated vehicle (ROV) based on a thruster allocation and a nonlinear PD heading control for inner and outer loops respectively. Generalized ROV models for decoupled horizontal and vertical plane motions are derived based on small roll and pitch angles that are self-stabilizing during operations.

The fourth paper by Röbenack deals with the problem of observer design for nonlinear differential-algebraic equations. This approach is based on an approximate observer error linearization technique. The design method is applicable to a class of semi-explicit differential-algebraic equations. The observer design is illustrated on an example system.

Finally, the fifth paper by AbdulRahman deals with nonlinear predictive control based on radial basis function (RBF) networks for nonlinear dynamical systems. The RBF model of the nonlinear process is developed using the orthogonal least squares (OLS) training algorithm. The nonlinear sequential quadratic programming (SQP) optimisation technique is employed to calculate the optimal actuation sequence for the nonlinear predictive control based on the RBF model of the system.

January 2006

Dr. Mohamed H. Mahmoud
Editor-in-Chief

A GENERALIZED STOCHASTIC PETRI NET MODEL FOR SUPPLY CHAIN MANAGEMENT

M. Dotoli *, M. P. Fanti
Dipartimento di Elettrotecnica ed Elettronica, Politecnico di Bari, Italy

ABSTRACT

A Supply Chain (SC) is a collection of independent companies possessing complementary skills and integrated with transportation and storage systems. This paper deals with the issues of modeling and managing the SC at the operational level, in order to study the performance measures of the systems controlled by different management strategies. The system is modeled as a timed discrete event dynamical system, whose evolution depends on the interaction of discrete events such as the arrival of components at the facilities, the departure of the transporters from the suppliers or the manufacturers, the start of assembly operations at the manufacturers. More precisely, generalized stochastic Petri nets model the system in a modular way and describe its behavior. Moreover, two well known broad policies are considered to manage the SC: make-to-stock and make-to-order. In order to compare the two management strategies and to show the effectiveness of the modeling technique, a case study is presented.

Keywords

Supply Chains, Management, Modeling, Discrete Event Systems, Petri Nets, Performance Evaluation.

1. INTRODUCTION

The global market economy is constantly forcing companies to focus on the production of high-value-adding core components. Companies respond to this pressure by reengineering their processes, integrating geographically distributed facilities with international logistics. This process has given rise to the formation of the Supply Chain (SC), that may be defined as a collection of independent companies possessing complementary skills and integrated with transportation and storage systems, information and financial flows, with all entities collaborating to meet the market demand. The analysis, design and management of SC is currently an active area of research [1, 10, 15, 18-20, 22]. In particular, SC management deals with the planning and execution issues involved in the entire SC network in order to enhance the system operation. Following a firm and systematic way to organize decisions in automated manufacturing systems, an analogous guideline has been proposed to manage SC and classify the related decision problems [3]. This guideline is based on the three levels of a decision hierarchy: strategic, tactical and operational decision levels. The classes of SC problems encountered in the strategic level planning involve location-allocation decisions, demand planning, strategic alliances, new product development, supplier selection and pricing. This level of the hierarchy considers time horizons of a few years and requires approximate and aggregate data models. Moreover, tactical level planning basically refers to layout and network design, production/distribution coordination, equipment and material handling selection. Finally, operational level planning is short-range planning, which involves coordination across the stages and optimization of operational policies to reduce costs while improving services to customers. Moreover, important aspects at the SC operational decision level are the specification of the control strategy managing customer orders to trigger the production and determining the synchronization of paths, information and material flows.

Obviously, different models have to be defined at each level of the decision hierarchy to describe the multiple aspects of the SC, with respect to different time horizons. In particular, numerous models, that are basically optimization models, have been formulated for the strategic and tactical design of SC [5, 8, 12, 17, 18]. On the other hand, few contributions focus on modeling the SC at the operational level to determine the performances, taking into account transportation operations, capacity constraints and different management strategies. At the time horizon of the operational level, SC can be viewed as Discrete Event Dynamical Systems (DEDS), in which the evolution depends on the interaction of discrete events such as customer demands, departure of parts or products from the entities, arrival of the transporters at the facilities, start of assembly operations at the manufacturers, arrivals of finished goods at the customers etc. [20]. Thanks to the well known ability of Petri Nets (PN) to model concurrency and asynchrony, while capturing precedence relations and structural interactions, PN based models may be suitably derived for SC. In [7] a two product SC is modeled by complex-valued token PN and the performance measures are determined by simulation. Moreover, in [9] timed event graphs, that are a subclass of PN, are employed to model, analyze and control a supply link. In addition, in [21] the authors propose an extension of PN based on the XML standard for inter-organizational data exchange to model and manage supply chains, while colored PN are employed in [16] to model each SC entity. Furthermore, a network-based technique extending PN and proposing the so-called formalism Trans-Net, is presented in [23] for supply chain network

*Corresponding author: *E-mail:* dotoli@deemail.poliba.it

 ISSN: 1743-9310

modeling. However, to take into account the stochastic values of process and transportation times, Generalized Stochastic Petri Nets (GSPN) may be successfully applied for SC modeling. In this direction, in [20] GSPN are employed to describe a particular example of SC and determine the decoupling point location, i.e., the facility from which all finished goods are assembled after customer order confirmation. More recently, in [2] an extension of GSPN named batch deterministic and stochastic PN is proposed for describing and testing inventory policies. Even if such a paper applies the effective model to an inventory system with independent demand, it does not face a basic aspect of the supply chain operations: the SC management problem [11].

The aim of this paper is twofold: i) presenting a GSPN model in order to describe in a modular and simple way a generic SC at an operational level, ii) applying and testing two management strategies. The aim of SC control methodologies is triggering a series of activities, to synchronize the production and transport facilities so that the end customer order is satisfied. There are three SC managing policies followed in practice [14, 20]: *Make-To-Stock* (MTS), *Make-To-Order* (MTO) and *Assemble-To-Order* (ATO). In particular, the MTS strategy manages the system by a push strategy, so that end customers are satisfied from stocks of inventory of finished goods. On the other hand, in the MTO technique customer orders trigger the flow of materials and the requirements at the different stages of the SC. In addition, the ATO policy is a hybrid of the former two strategies, basically applying MTS in the first stages of the SC, up to the so-called customer order decoupling point, and MTO in the last stages. In this paper, we apply the MTO and the MTS strategies to an example case study modeled by GSPN. However, we remark that the proposed approach may straightforwardly be employed while other management strategies are applied, e.g. ATO. In particular, in the paper we realize the MTO control policy by using the just in time philosophy employing Kanbans. Moreover, the MTS strategy is performed by introducing appropriate finite inventory capacities of each product and material. In order to compare the two management techniques, we evaluate the steady state probabilities of the Markov chain embedded in the corresponding GSPN modeling the SC.

This paper is organized as follows. Section 2 describes the structure and the model of a generic SC and Section 3 defines the performance measures obtained by the analysis of the associated GSPN. Moreover, Section 4 introduces the case study and its performance measures are analyzed in Section 5. Finally, Section 6 summarizes the conclusions.

2. THE SYSTEM MODEL

2.1 The System Description

A SC may be described as a set of facilities with materials that flow from the sources of raw materials to subassembly producers and onwards to manufacturers and consumers of finished products. The SC facilities are connected by transporters of materials, semi-finished goods and finished products. More precisely, the entities of an SC may be summarized as follows:

1) *Suppliers:* a supplier is a facility that provides raw materials, components, semi-finished products to manufacturers that make use of them.

2) *Manufacturers:* a manufacturer is a facility that transforms input raw materials/components into desired output products. It is the place where transformation processes occur. Important attributes of such an entity are lead-time, production costs, minimum production lot size and bill-of-material.

3) *Retailers:* retailers or (groups of) customers are sink nodes of material flows. Demands of different types of products are generated from customers and fulfilled by periodic delivers. Important attributes related to these components are demand quantity, demand frequency and expected delivery date.

4) *Logistics:* distributors and transporters play a crucial role in SC. The handling capacity of a distributor usually depends on the size of the delivery fleet and the delivery frequency. Moreover, the attributes of logistics facilities are storage capacities, handling capacities, transportation times, operation and inventory costs.

We assume that the considered SC performs a set of activities such as transportation, manufacturing operations, assembling operations and distribution to retailers. In the following we use the term *resources* only to refer to logistics entities such as transporters, buffers and warehouses. In some cases, the resources may exhibit finite capacity. Let J be the set of final products that the SC has to produce. Moreover, if the SC is managed by a MTO technique, customer orders trigger the flow of material. In particular, Kanbans [19] are used to order the delivery of final products and to trigger the assembly and procurement of intermediate products. More precisely, available Kanbans enable the lot of products that are produced by each stage of the SC.

The dynamics of the production system is traced by the flow of products among resources. However, from a general point of view, we can model a SC as a timed DEDS. As time lapses, the state of the DEDS changes at each event occurrence. In particular, we assume that an event of the DEDS occurs whenever a product acquires and/or releases a resource, starts or finishes an operation. Therefore, we consider the following events:

a)arrival of components at a supplier, a manufacturer or a customer;

b) departure of a truck from a supplier or a manufacturer;

c) start of assembling or transport operation;

d) start of a request.

Example 1: We consider a system where the product set $J = \{E,F\}$ is produced by the four stages depicted in Figure 1 (dashed lines). The first stage includes a number of component suppliers, the second stage is composed by subassembly manufacturers, the third stage is composed by brand manufacturers and the last stage is constituted by a set of retailers. Note that a stage is a collection of SC entities, which are schematically represented by solid boxes and are not connected by any logistics link (see Figure 1): indeed, in the considered model material flows though different stages. On the contrary, facilities belonging to different stages, that are located in different geographical sites, may be connected by logistics service providers, represented by arrows (see Figure 1). Here, we consider an example where two buyers order two brand of products (E and F). Such products are obtained by two manufacturers (M_3 and M_4) that are located at different sites. The two manufacturers assemble two types of products (C and D) obtained from two subassembly suppliers. The subassemblies C and D are in turn produced by the manufacturers of the second stage (M_1 and M_2), which receives the components of type A and B by the first supplier stage. Transporters connect the different stages and transfer material or product lots from a stage to another.

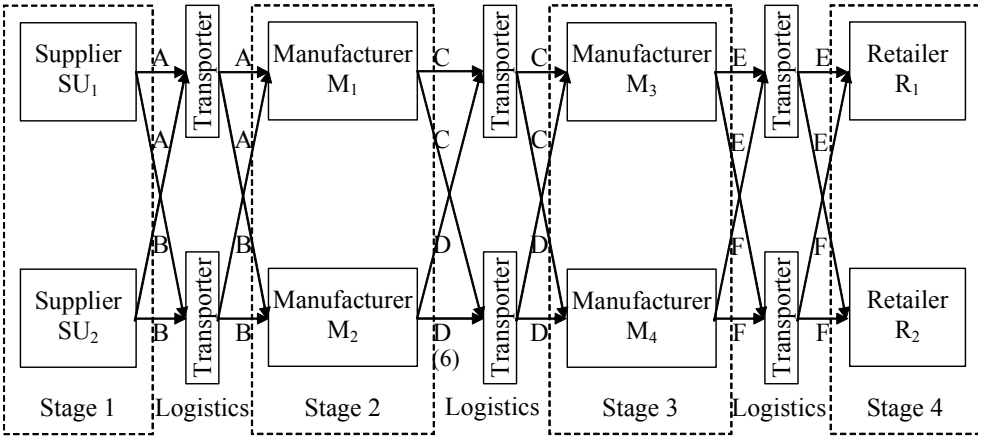

Figure 1. The supply chain configuration

2.2 Introduction to Generalized Stochastic Petri Nets

A Generalized Stochastic (marked) Petri Net (GSPN) [1] is a bipartite digraph described by the seven-tuple *GSPN*=(P, T, ***Pre***, ***Post***, ***F***, S, ***M***), where P is a set of places, T is a set of transitions partitioned in the set T_I of immediate transitions and the set T_E of exponential transitions, ***Pre*** and ***Post*** are the pre-incidence and the post-incidence matrices, respectively, of dimension $|P|$x$|T|$. Note that we use symbol $|A|$ to denote the cardinality of the generic set A. More precisely, the element $Pre(p_i,t_j)$ is equal to 1 if an arc joining p_i and t_j exists and 0 otherwise; the element $Post(p_i,t_j)$ is equal to 1 if an arc joining t_j and p_i exists and 0 otherwise. Moreover, ***F*** is a firing time vector. The firing time of transition $t_j \in T_E$ is an exponentially distributed random variable with mean F_j (i.e., the j-th element of vector **F**). Each $t_j \in T_I$ has zero firing time, i.e., F_j=0. In addition, S is a set of elements called random switches, which associate probability distributions to subsets of conflicting immediate transitions.

The state of a GSPN is given by its current marking, that is a mapping $\boldsymbol{M}: P \to N$, where N is the set of non-negative integers. ***M*** is described by a $|P|$-vector and the i-th component of ***M***, indicated with $M(p_i)$, represents the number of tokens in the i-th place $p_i \in P$.

Given a GSPN and a transition $t \in T$, the following sets of places may be defined: $\bullet t = \{p \in P: Pre(p,t) > 0\}$, named pre-set of t; $t \bullet = \{p \in P: Post(p,t) > 0\}$, named post-set of t. Analogously, for each place $p \in P$, the following sets of transitions may be defined: $\bullet p = \{t \in T: Post(p,t) > 0\}$, named pre-set of p; $p \bullet = \{t \in T: Pre(p,t) > 0\}$, named post-set of p.

A transition $t_j \in T$ is enabled at a marking ***M***, i.e., ***M***[t_j>, if and only if for each $p_i \in \bullet t_j$, $M(p_i)>0$. When fired, t_j produces a new marking ***M'***, denoted as ***M***[t_j>***M'***, where for each $p_i \in P$ it holds $M'(p_i)=M(p_i)+Post(p_i,t_j)-Pre(p_i,t_j)$. A marking ***M'*** is said reachable from ***M*** if and only if there exists a sequence of transitions $t_1 t_2 \ldots t_n$ such that $\boldsymbol{M}[t_1>\boldsymbol{M_1}[t_2>\boldsymbol{M_2}\ldots\boldsymbol{M_{n-1}}[t_n>\boldsymbol{M'}$. The set of markings reachable from ***M*** in the GSPN is denoted by $R(\boldsymbol{M})$.

2.3 The SC Model

We introduce the *GSPN*=(P, T, ***Pre***, ***Post***, ***F***, S, $\boldsymbol{M_0}$) modeling the SC as a GSPN, whose elements are defined as follows.

1) P is the set of places, partitioned into three subsets: P_A (modeling activities such as transportation, storage in manufacturers or in warehouses), P_C (modeling the resource capacities) and P_K (modeling orders).

2) T is the set of transitions, partitioned into two subsets: stochastic transitions T_E (modeling the activity durations, i.e., transportation and manufacturer operations) and immediate transitions T_I (modeling a resource acquisition or the start of an order).

In particular, each logistics provider is modeled by the subnet shown in Figure 2 (solid lines): the immediate transition t models the transport beginning, the stochastic transition t' models the transport of the product, a token in $p \in P_A$ means that a lot is under transport.

Moreover, Figure 3 (solid lines) shows the subnet modeling a manufacturer, that is described by a stochastic transition (t), modeling the production of a lot of products, and two places ($p \in P_A$ and $p' \in P_A$): a token in p or in p' represents a lot of material under operation or ready to be transported, respectively.

In addition, a customer is modeled by a place $p \in P_A$, where ready lots of products are stored, and an immediate or a stochastic transition t (see Figure 4), modeling the start of a lot request. If the transition is considered stochastic, a stochastic interval time is expected between orders.

Note that a supplier can be simply modeled by the starting transition t of a transporter (see Figure 2).

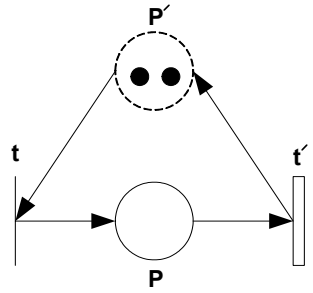

Figure 2. The logistics provider model

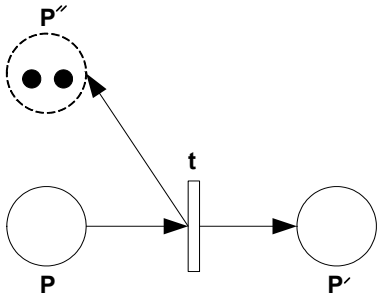

Figure 3. The manufacturer model

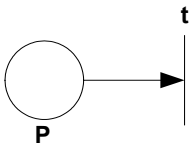

Figure 4. The customer model

After the identification of activity places and transitions, the net can be completed by adding capacity and order places, respectively belonging to sets P_C and P_K, and properly connecting them to the transitions. For example, when a transport is completed or a lot leaves a buffer, the corresponding resource is released and a token appears in the related transporters place. Figure 2 shows the transport subnet with two available transporters completed by the capacity place $p' \in P_C$ and two tokens (see dashed lines). Analogously, dashed lines in Figure 3 show the capacity assigned to a manufacturer, i.e., an available inventory of two lots, modeled by place $p'' \in P_C$.

Obviously, the net structure determines the ***Pre*** and ***Post*** matrices. Moreover, elements of ***F***, *S* and the initial marking $\mathbf{M_0}$ are properly defined in each model.

3. ANALYSIS OF THE GSPN

The marking process of a *GSPN*=(*P*, *T*, ***Pre***, ***Post***, ***F***, S, $\boldsymbol{M_0}$) can be shown to be a semi-Markov process with discrete state space, given by the reachability set $R(\boldsymbol{M_0})$ [19]. The embedded Markov Chain (MC) of this marking process comprises tangible markings as well as vanishing markings. More precisely, markings in which at least one immediate transition is enabled are vanishing markings. On the other hand, markings in which only exponential transitions are enabled are called tangible markings. The transition probability matrix of this MC can be computed using the firing rates of each transition $t_j \in T$ and the random switches [19]. The marking process of a GSPN leaves each vanishing marking as soon as it enters the marking, because an immediate transition fires. Thus the sojourn time in each vanishing marking is zero and consequently, from the performance evaluation point of view, it suffices to study the evolution of tangible markings alone. In order to remove vanishing markings from the MC, a reduced embedded MC is defined, including only tangible markings and the transition probabilities in the reduced MC are deduced from those in the MC.

3.1 Computation of Performance Measures

To study the MC embedded in the GSPN, we can examine the GSPN properties that are closely related to the existence of the steady-state probability distribution of the equivalent MC. This distribution exists if the following conditions are simultaneously verified [6]:

i) the GSPN is bounded (i.e., the reachability set is finite);

ii) the initial marking is reachable from all the reachable markings;

iii) the firing times are exponentially distributed random variables.

For a MC with *K* tangible states, the limiting or steady-state probabilities of the MC are given by π_k with $k = 1 \ldots K$, which are independent of the initial state. They are combined into the steady-state probability vector, $\boldsymbol{\pi}$, which is calculated from the matrix of the *infinitesimal generator* $\boldsymbol{Q}$, which is a Kx K matrix. The off-diagonal elements of $\boldsymbol{Q}$ q_{ij} with $i \neq j$ are the rates at which the process transfers from state i to state j. The diagonal terms q_{ij} are chosen in such a way that each row of $\boldsymbol{Q}$ sums to zero. The steady-state probabilities satisfy the following equations:

$$\boldsymbol{\pi Q} = 0 \tag{1}$$

subject to

$$\boldsymbol{\pi e} = 1 \tag{2}$$

where $\boldsymbol{e}$ is a column vector of ones.

The steady-state probabilities can be used to determine the performance measures of the GSPN, such as throughput and mean waiting time as follows:

- the probability that a place p_i has exactly *h* tokens:

$$\mathrm{Prob}(p_i, h) = \sum_{k \in U_1} \pi_k \tag{3}$$

where $U_1 = \{k : k \in \{1, 2 \ldots K\}, \mathrm{M}_k(p_i) = h\}$;

- the expected number of tokens in a place p_i:

$$ET(p_i) = \sum_{h=1}^{H} h \,\mathrm{Prob}(p_i, h) \tag{4}$$

where *H* is the maximum number of tokens that p_i may contain in any reachable marking;

- the throughput rate of an exponential transition t_j

$$TR(t_j) = \sum_{k \in U_2} \pi_k F_j \tag{5}$$

where $U_2 = \{k : k \in \{1, 2 \ldots K\}, \boldsymbol{M}[t_j>\}$;

- the mean waiting time in a place p_i:

$$WAIT(p_i) = \frac{ET(p_i)}{\sum_{t_j \in p_i^\bullet} TR(t_j)} \quad (6)$$

4. THE CASE STUDY

In this section, we consider the SC described in Example 1 and Figure 1 and we manage the system using two broad strategies: MTO and MTS. More precisely, in the MTO technique the customer orders trigger the flow of materials and the requirements at the different stages of the SC. On the other hand, the MTS strategy manages the system by a push strategy, so that the end customers are satisfied from stocks of inventory of finished goods.

4.1 The System Under the MTO Strategy

The MTO technique can be considered as a pull strategy that is here realized by Kanbans in a just in time philosophy. In the SC behavior, we suppose that Kanbans represent message orders that in short time trigger the transport of product and material lots. Since in this context the transportation resources are very important and can significantly influence the system performance, we consider two different transport facilities: system S_1 exhibits only one logistics to manage transportation between each couple of connected entities, while system S_2 considers different transportation pools, each devoted to transport a particular type of parts/products. Figure 5 shows the GSPN modeling system S_1 and Figure 6 shows the GSPN describing system S_2. Note that places p_3, p_4, p_{19}, p_{20}, p_{35} and p_{36} in Figure 5, representing available transporters for the first, second and third stage respectively, are doubled by adding places p'_3, p'_4, p'_{19}, p'_{20}, p'_{35} and p'_{36} in Figure 6, to model the available transporters for each type of products. The interpretations of places and of transitions are reported in Tables 1 and 2 respectively. In addition, Table 2 shows the mean firing times of the stochastic transitions (a zero firing time indicates that the transition is immediate). Both in Figure 5 and 6 places p_{13}, p_{14}, p_{15} and p_{16}, p_{29}, p_{30}, p_{31} and p_{32}, p_{41}, p_{42}, p_{45} and p_{46} represent available Kanbans for the goods produced by the first, second and third stage of Figure 1, respectively. Furthermore, in this example transitions t_{29}, t_{30}, t_{31} and t_{32} modeling order arrivals are chosen stochastic (see Table 2). As soon as a lot of type E or F is delivered to the retailer, a new order starts the transport of the corresponding good (E or F, respectively) from the preceding stage of the SC. This order message triggers in turn the transport of products C and D, necessary to assemble the E and F products. Analogously, a message arrives to the first stage so that available material of type A and B is transported to the manufacturers of the subsequent stage.

4.2 The system Under the MTS Strategy

The MTS strategy manages the system in a push perspective. In order to limit the input of raw materials, the inventory capacities are introduced in each facility. Figure 7 shows the GSPN describing Example 1 under the MTS strategy (i.e., system S_3) and the relative place and transition interpretations are respectively listed in Tables 3 and 2. It is evident that the system under the MTS strategy exhibits limited buffer capacities for all the products in order to bound the production in each manufacturer. Moreover, the elements of S for all systems S_1, S_2 and S_3 associate a uniform probability distribution to the subsets of conflicting immediate transitions. Finally, the initial marking $\boldsymbol{M_0}$ of each system is defined as follows: $M_0(p_i)=0$ if $p_i \in P_A$, $M_0(p_i)=C_i$ if $p_i \in P_C$ and $M_0(p_i)=K_i$ if $p_i \in P_K$, where C_i and K_i denote the capacities and the number of available Kanbans, respectively. For the sake of simplicity, the initial marking of systems S_1, S_2 and S_3 is omitted in the corresponding Figures 5, 6 and 7.

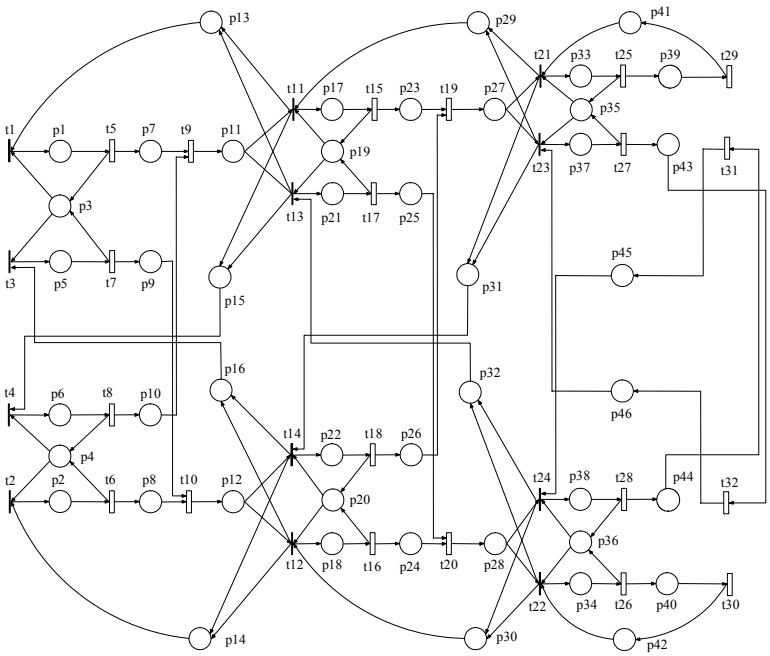

Figure 5. GSPN model of system S_1

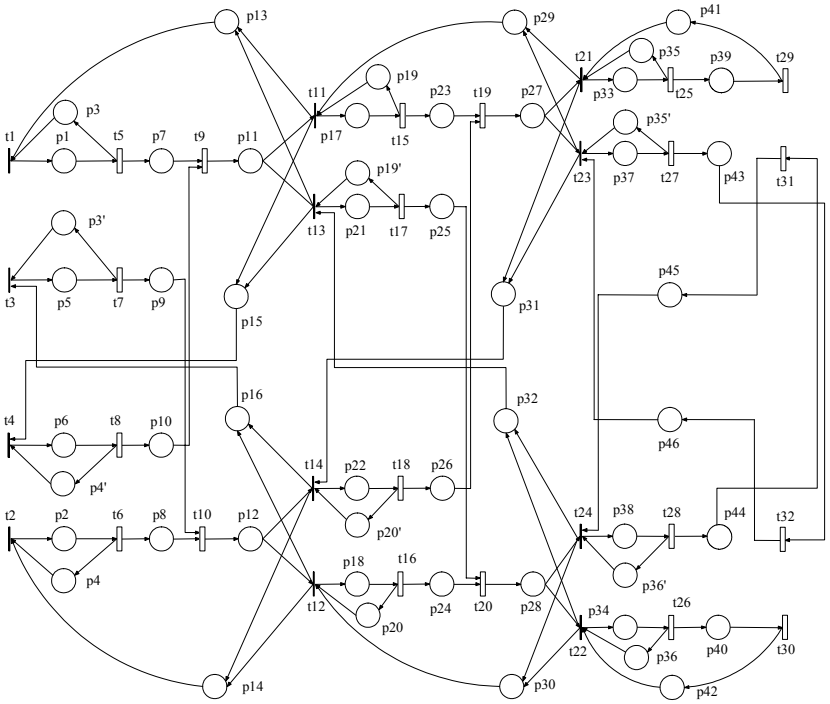

Figure 6. GSPN model of system S_2

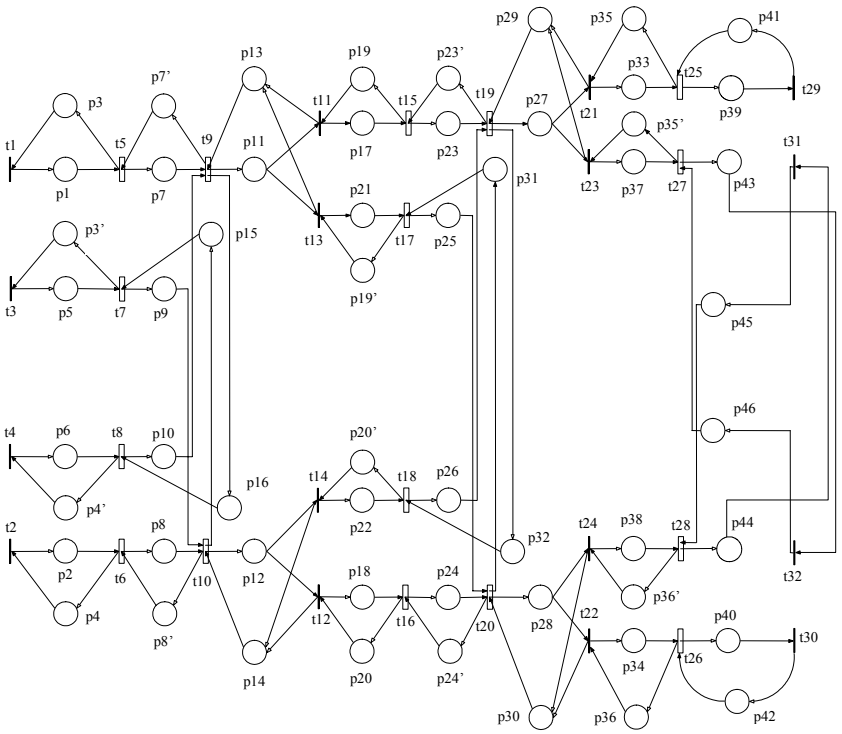

Figure 7. GSPN model of system S_3

Table 1. Place interpretation in the GSPN of figures 5 and 6

Name	Description
p_1 (p_5)	A lot of product A is transported to M_1 (M_2)
p_2 (p_6)	A lot of product B is transported to M_2 (M_1)
p_3 (p'_3)	Pool of available transporters to transfer a lot of A to M_1 (M_2)
p_4 (p'_4)	Pool of available transporters to transfer a lot of B to M_1 (M_2)
p_7 (p_9)	Lots of product A in M_1 (M_2) ready for processing
p_8 (p_{10})	Lots of product B in M_2 (M_1) ready for processing
p_{11}	Lots of product C in M_1 ready for transportation
p_{12}	Lots of product D in M_2 ready for transportation
p_{13} (p_{16})	Kanbans available for product A from manufacturer M_1 (M_2)
p_{15} (p_{14})	Kanbans available for product B from manufacturer M_2 (M_1)
p_{17}	Transportation of a lot of product C to M_3
p_{18}	Transportation of a lot of product D to M_4
p_{19} (p'_{19})	Pool of available transporter to transfer a lot of C to M_3 (M_4)
p_{20} (p'_{20})	Pool of available transporter to transfer a lot of C to M_3 (M_4)
p_{21}	Transportation of a lot of product C to M_4
p_{22}	Transportation of a lot of product D to M_3
p_{23} (p_{25})	Lots of product C in M_3 (M_4) ready for assembling
p_{24} (p_{26})	Lots of product D in M_4 (M_3) ready for assembling
p_{27}	Lots of product E in M_3 ready for transportation
p_{28}	Lots of product F in M_4 ready for transportation
p_{29} (p_{32})	Kanbans available for product C from manufacturer M_3 (M_4)
p_{30} (p_{31})	Kanbans available for product D from manufacturer M_4 (M_3)
p_{33}	Transportation of a lot of product E to R_1
p_{34}	Transportation of a lot of product F to R_2
p_{35} (p'_{35})	Pool of available transporters to transfer a lot of E to R_1 (R_2)
p_{36}	Pool of available transporters to transfer a lot of F to R_1 (R_2)
p_{37}	Transportation of a lot of product E to R_2
p_{38}	Transportation of a lot of product F to R_1
p_{39}	Lots of product E in R_1 ready for sale
p_{40}	Lots of product F in R_2 ready for sale
p_{41}	Kanbans available for manufacturer M_3
p_{42}	Kanbans available for manufacturer M_4
p_{43}	Lots of product E in R_2 ready for sale
p_{44}	Lots of product F in R_1 ready for sale
p_{45}	Kanbans available for manufacturer M_4
p_{46}	Kanbans available for manufacturer M_3

Table 2. Transition interpretation in the GSPN of figures 5, 6 and 7

Name	Description	Firing time [h]
t_1 (t_3)	Start of transport of a lot of product A to M_1 (M_2)	0
t_2 (t_4)	Start of transport of a lot of product B to M_2 (M_1)	0
t_5	Arrival of a lot of product A in M_1	10.00
t_6	Arrival of a lot of product B in M_2	11.70
t_7	Arrival of a lot of product A in M_2	8.30
t_8	Arrival of a lot of product B in M_1	6.67
t_9	End of production of a lot of product C	3.00
t_{10}	End of production of a lot of product D	4.00
t_{11} (t_{13})	Start of transport of a lot of product C to M_3 (M_4)	0
t_{12} (t_{14})	Start of transport of a lot of product D to M_4 (M_3)	0
t_{15}	Arrival of a lot of product C in M_3	16.70
t_{16}	Arrival of a lot of product D in M_4	1.90
t_{17}	Arrival of a lot of product C in M_4	2.20
t_{18}	Arrival of a lot of product D in M_3	14.20
t_{19}	End of production of a lot of product E	2.00
t_{20}	End of production of a lot of product F	1.50
t_{21} (t_{23})	Start of transport of a lot of product E to R_1 (R_2)	0
t_{22} (t_{24})	Start of transport of a lot of product F to R_2 (R_1)	0
t_{25}	Arrival of a lot of product E in R_1	1.70
t_{26}	Arrival of a lot of product F in R_2	1.33
t_{27}	Arrival of a lot of product E in R_2	2.50
t_{28}	Arrival of a lot of product F in R_1	5.80
t_{29} (t_{32})	Request of a lot of product E from R_1 (R_2)	0.50
t_{30} (t_{31})	Request of a lot of product F from R_2 (R_1)	0.50

Table 3. Place interpretation in the GSPN of figure 7

Name	Description
p_1 (p_5)	A lot of product A is transported to M_1 (M_2)
p_2 (p_6)	A lot of product B is transported to M_2 (M_1)
p_3 (p'_3)	Pool of available transporters to transfer a lot of A to M_1 (M_2)
p_4 (p'_4)	Pool of available transporters to transfer a lot of B to M_1 (M_2)
p_7 (p_9)	Lots of product A in M_1 (M_2) ready for processing
p_8 (p_{10})	Lots of product B in M_2 (M_1) ready for processing
p'_7 (p_{15})	Capacity of inventory in M_1 (M_2) for product A
p'_8 (p_{16})	Capacity of inventory in M_2 (M_1) for product B
p_{11}	Lots of product C in M_1 ready for transportation
p_{12}	Lots of product D in M_2 ready for transportation
p_{13}	Capacity of inventory in M_1 for product C
p_{14}	Capacity of inventory in M_2 for product D
p_{17}	Transportation of a lot of product C to M_3
p_{18}	Transportation of a lot of product D to M_4
p_{19} (p'_{19})	Pool of available transporter to transfer a lot of C to M_3 (M_4)
p_{20} (p'_{20})	Pool of available transporter to transfer a lot of C to M_3 (M_4)
p_{21}	Transportation of a lot of product C to M_4
p_{22}	Transportation of a lot of product D to M_3
p_{23} (p_{25})	Lots of product C in M_3 (M_4) ready for assembling
p_{24} (p_{26})	Lots of product D in M_4 (M_3) ready for assembling
p_{27}	Lots of product E in M_3 ready for transportation
p_{28}	Lots of product F in M_4 ready for transportation
p_{29}	Capacity of inventory in M_3 for product E
p_{30}	Capacity of inventory in M_4 for product F
p_{31} (p'_{23})	Capacity of inventory in M_4 (M_3) for product C
p_{32} (p'_{24})	Capacity of inventory in M_3 (M_4) for product D
p_{33}	Transportation of a lot of product E to R_1
p_{34}	Transportation of a lot of product F to R_2
p_{35} (p'_{35})	Pool of available transporters to transfer a lot of E to R_1 (R_2)
p_{36}	Pool of available transporters to transfer a lot of F to R_1 (R_2)
p_{37}	Transportation of a lot of product E to R_2
p_{38}	Transportation of a lot of product F to R_1
p_{39}	Lots of product E in R_1 ready for sale
p_{40}	Lots of product F in R_2 ready for sale
p_{41} (p_{46})	Capacity of inventory in R_1 (R_2) for product E
p_{42} (p_{45})	Capacity of inventory in R_2 (R_1) for product F
p_{43}	Lots of product E in R_2 ready for sale
p_{44}	Lots of product F in R_1 ready for sale

5. THE CASE STUDY PERFORMANCE ANALYSIS

5.1 The Performance Measures Definition

The performances of the industrial case study presented in Example 1 and modeled by the described GSPN are determined by the steady state probabilities of the MC embedded in the corresponding GSPN. The selected performance measures are the total inventory cost C_I and the total delay cost C_D. The first performance index accounts for costs related to stocks, while the second collects costs due to delays in deliveries. Clearly, such indices are complementary to each other: in a MTS strategy the first index is prevalent, while a MTO strategy is characterized by the second measure being predominant. The total cost associated to the SC operation is [20]:

$$C = C_I + C_D \tag{7}$$

In addition, we call I_1 the unitary cost for inventories at the first stage of the SC, while the cost per hour of delayed delivery at this stage is D_1. We consider two cases: D_1=1.5I_1 and D_1=40I_1 [20]. Moreover, product E is valued more than product F by 50%. In addition, inventory of final products E and F is assumed to be 20% more expensive than the inventory of products C and D that cost 20% more than materials A and B. Furthermore, without loss of generality we assume I_1=1.

The total inventory costs associated with the GSPN in systems S_1, S_2 and S_3 are calculated by determining the average number of tokens in all the places of the considered GSPN and the throughput rate of the system stochastic transitions as follows:

$$\begin{aligned} C_I = I_1 \sum_{i=7,8,9,10} ET(p_i) + \\ +1.2 \cdot I_1 \sum_{i=11,12,23,24,25,26} ET(p_i) + \\ +1.44 \cdot I_1 \sum_{i=27,28} ET(p_i) \end{aligned} \tag{8}$$

where the above expression accounts for costs of work in process during assembly and manufacturing operations (i.e., related to places p_7, p_8, p_9, p_{10}, p_{23}, p_{24}, p_{25} and p_{26}) and stocks in warehouses (i.e., related to places p_{11}, p_{12}, p_{27} and p_{28}). Similarly, the total delay costs associated to the GSPN are obtained as follows:

$$C_D = D_1 \cdot \big(WAIT(p_{38}) + WAIT(p_{34})\big) + \\ +1.5 \cdot D_1 \cdot \big(WAIT(p_{33}) + WAIT(p_{37})\big) \quad (9)$$

where the previous expression refers to the different costs of the waiting times of finished goods E and F (i.e., related to places p_{33} and p_{37} for product E and to p_{38} and p_{34} for product F). The steady state probability distributions necessary to calculate (7), (8) and (9) are obtained by using the SPNP™ software package [4].

Table 4. Capacities and Kanbans of the GSPN of figures 5, 6 and 7

Case	System	K_{13}= K_{14}= K_{15}= K_{16}	K_{29}= K_{30}= K_{31}= K_{32}	K_{41}= K_{42}= K_{45}= K_{46}	C_3=C_4	C_{19}= C_{20}	C_{35}= C_{36}
1	S_1, S_2	1	1	1	1	1	1
2	S_1, S_2	2	1	1	1	1	1
3	S_1, S_2	1	2	1	1	1	1
4	S_1, S_2	1	1	2	1	1	1
5	S_1	1	1	1	2	2	2
Case	System	C_{23}= C_{24}= C_{29}= C_{30}= C_{31}= C_{32}=	C_7= C_8= C_{13}= C_{14}= C_{15}= C_{16}=	C_{41}= C_{42}= C_{45}= C_{46}	C_3=C_4	C_{19}= C_{20}	C_{35}= C_{36}
6	S_3	1	1	1	1	1	1
7	S_3	2	1	1	1	1	1
8	S_3	1	2	1	1	1	1
9	S_3	1	1	2	1	1	1

Table 5. Performance measures for the GSPN of figures 5, 6 and 7

Case	System	Inventory costs	Delay costs	Total costs (D_1=1.5I_1)	Total costs (D_1=40I_1)
1	S_1	3.166I_1	13.452D_1	23.344I_1	541.246I_1
2	S_1	4.895I_1	13.640D_1	25.355I_1	550.495I_1
3	S_1	4.647I_1	13.685D_1	25.175I_1	552.047I_1
4	S_1	3.166I_1	12.849D_1	22.440I_1	517.126I_1
1	S_2	4.636I_1	13.464D_1	24.832I_1	543.196I_1
2	S_2	5.613I_1	13.466D_1	25.812I_1	544.253I_1
3	S_2	5.575I_1	13.469D_1	25.779I_1	544.335I_1
4	S_2	3.090I_1	13.468D_1	23.292I_1	541.810I_1
5	S_1	6.282I_1	13.450 D_1	26.457I_1	544.282I_1
6	S_3	4.712I_1	13.459D_1	24.901I_1	543.072I_1
7	S_3	7.809I_1	13.465D_1	28.007I_1	546.409I_1
8	S_3	6.868I_1	13.468D_1	27.070I_1	545.588I_1
9	S_3	3.907I_1	13.451D_1	24.084I_1	541.947I_1

5.2 The Performance Analysis

In this section the performance analysis of the described case study is carried out by two comparisons. First, we compare systems S_1 and S_2, managed by the MTO policy, considering a fixed number of transporter capacities (i.e., with $M_0(p_i)$=1 for each $p_i \in P_C$) and varying in each system the number of available Kanbans. More precisely, the defined costs are obtained for systems S_1 and S_2 in the cases 1, 2, 3 and 4 shown in Table 4. Moreover, in case 5 system S_1 has the number of available Kanbans equal to case 1 but a double number of transporters. Table 5 reports the performance measures obtained in each case and Figure 8 compares system S_1 and S_2 for similar values of delay and inventory costs (i.e., when it holds D_1=1.5I_1). More precisely, Figure 8 shows that if the transportation capacity is minimum and the number of Kanbans assigned to the first and second SC stages (i.e., SU_1, SU_2, M_1 and M_2 in Figure 1) increases, then total costs increase too. Indeed, in such a case the stock costs of the two stages rise. On the contrary, if the number of Kanbans assigned to manufacturers M_3 and M_4 increases, then the total costs suffer a reduction (basically due to reduced delay costs). Moreover, doubling the pool of transporters for each stage in system S_1, the costs increase for the higher inventory costs (compare the results of cases 1 and 5 for S_1 in Table 4 and in Figure 8).

Second, to compare the MTO and MTS strategy we consider systems S_2 and S_3. More precisely, we compare the performance measures evaluated for system S_2 in cases 1, 2, 3 and 4 with those obtained for system S_3 respectively in cases 6, 7, 8 and 9 (see Table 4). In each case systems S_2 and S_3 are characterized by the same transporter capacities. However, system S_2 has a finite number of Kanbans in all its stages to realize the MTO policy, while system S_3 exhibits a finite capacity of each manufacturer, so that the MTS policy does not lead the system to infinite inventory. The corresponding results for system S_3 are reported in Table 5.

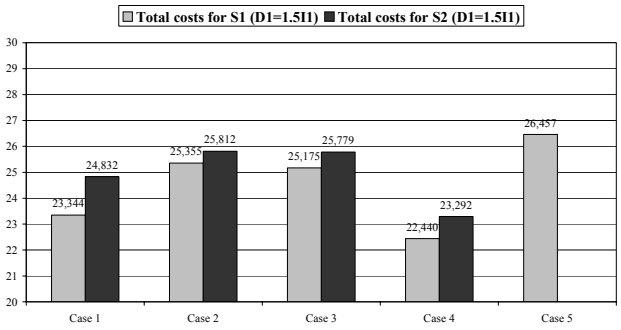

Figure 8. Total costs for systems S1 and S2 (D_1=1.5I_1)

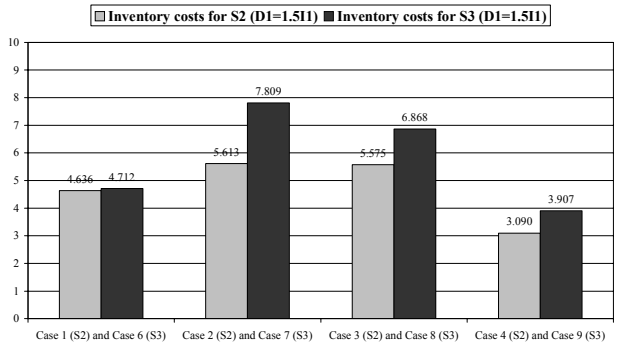

Figure 9. Inventory costs for systems S2 and S3 (D_1=1.5I_1)

Comparing the MTO and MTS results with D_1=1.5I_1, it can be inferred that the MTS policy leads to slightly lower delay costs than MTO. However, the MTS strategy is characterized by an increase in the inventory costs, that are limited in the Kanban system. Figure 9 depicts the different inventory costs obtained under the two management policies, while a graphical comparison of delay costs is neglected since the values of such

indices are very similar. Hence, the MTO policy is able to reduce stocks (and their costs) while restraining delays, so that the overall costs are lower than with the MTS strategy (see Figure 10).

In addition, Figures 11 and 12 respectively compare the total costs of system S_1 with S_2 and system S_2 with S_3 when delays are assigned much higher costs than stocks (i.e., $D_1=40I_1$). Clearly, in such a case an increase in transporters and in inventories does not always result in an increase in total costs, since the high delay costs may be balanced by the increased transport and inventory capacities (see Figure 11). Moreover, comparing the MTO and MTS results shows that similar costs are obtained, due to the high penalty assigned to delays in MTO, that counterbalances the larger stocks of MTS (see Figure 12).

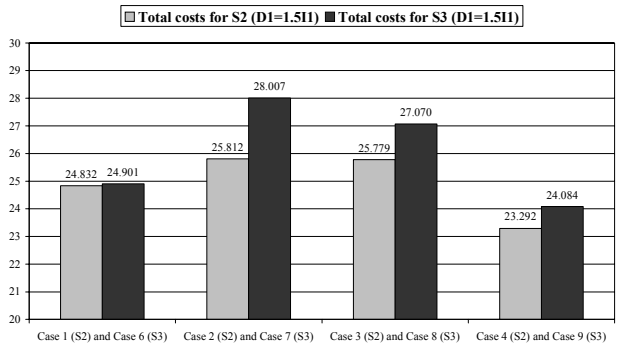

Figure 10. Total costs for systems S2 and S3 ($D_1=1.5I_1$)

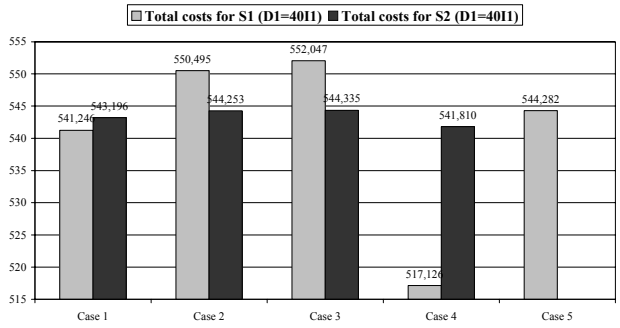

Figure 11. Total costs for systems S1 and S2 ($D_1=40I_1$)

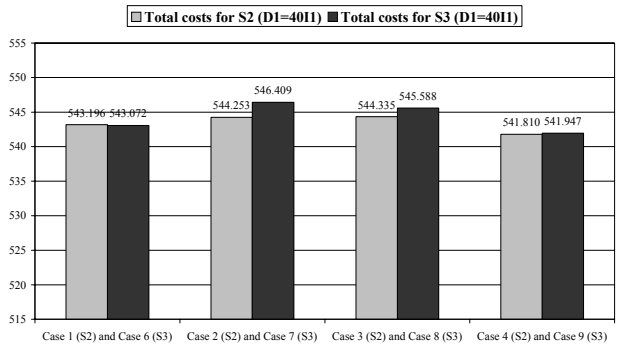

Figure 12. Total costs for systems S2 and S3 ($D_1=40I_1$)

6. CONCLUSIONS

This paper presents a technique to model a generic Supply Chain (SC) using Petri Nets (PN). The model may be successfully employed by practitioners in order to carry out the performance analysis of a generic SC and to choose the management technique of the system at the operational decision level. With this objective in mind, the choice of a PN based formalism is obvious, because of the well known PN effectiveness and straightforwardness in modeling concurrency and conflicts in systems driven by events. In particular, Generalized Stochastic Petri Nets (GSPN) are selected, since they are able to take into account the stochastic values of process and transportation times, while the performance measures of the modeled system can be obtained analytically by the many available software packages.

The proposed technique is illustrated via a case study, that is in turn controlled using a Make-To-Order (MTO) strategy employing the just in time philosophy based on Kanbans and the Make-To-Stock (MTS) technique. The steady state probabilities of the Markov chain embedded in the GSPN are evaluated to obtain the performance measures under the different management strategies. The results show the ability of the MTO approach to reduce inventory costs with respect to the MTS method.

The benefits of the presented modeling procedure are its accuracy as well as its simplicity and versatility. Moreover, the performance measures can be obtained analytically by using suited software packages, or by simulation, when larger systems are considered. However, a limitation of the introduced modeling technique is that discrete tokens can model lots or batches of products and discrete transmission of orders and information. Consequently, discrete amounts of materials and products are handled by SC entities such as transporters and manufacturers. To overcome this shortcoming, future research might generalize the model using more complex formalisms, such as for instance continuous or hybrid PN. Nevertheless, we remark that the presented methodology may be employed thanks to its straightforwardness for performing a preliminary analysis of a given SC, while letting more analytical investigation techniques (e.g. simulation) study the system in greater detail.

REFERENCES

[1] M. Ajmone Marsan, G. Balbo, G. Conte, S. Donatelli, G. Franceschini, Modeling with Generalized Stochastic Petri Nets. J. Wiley & sons, Great Britain, 1996.

[2] H. Chen, L. Amodeo, F. Chu, K. Labadi, "Modeling and Performance Evaluation of Supply Chains using Batch Deterministic and Stochastic Petri Nets", IEEE Transactions on Automation Science and Engineering, Vol. 2, no. 2, 2005, pp. 132-144.

[3] S. Chopra, P. Meindl, "Supply chain management: Strategy, planning, operation", Upper Sandle River, NJ: Prentice Hall, 2001.

[4] G. Ciardo, J.K. Muppala, K.S. Trivedi, "SPNP: Stochastic Petri Net Package", available at http://www.ee.duke.edu/?chirel/research.html.

[5] M. Davis, D. O' Sullivan, "System Design Framework for the Extended Enterprise", Production Planning and Control, vol. 10, no. 1, pp. 3-18, 1999.

[6] A. Desrochers, R.Y. Al-Jaar, Applications of Petri Nets in Manufacturing Systems. IEEE Press, New York, NY, USA, 1995.

[7] A. Desrochers, T. Deal, M.P. Fanti, "Complex Token Petri Nets", 2003 IEEE International Conference on Systems, Man and Cybernetics, October 2003, Washington, D.C., USA, pp. 1153-1160.

[8] M. Dotoli, M.P. Fanti, C. Meloni, M.C. Zhou, "A Multi-Level Approach for Network Design of Integrated Supply Chains", International Journal of Production Research, vol. 43, no. 20, pp. 4267-4287, 2005.

[9] I. Elmahi, O. Grunder, A. Elmoudni, "A Petri Net Approach for the Evaluation and Command of a Supply Chain Using the Max Plus Algebra", 2002 IEEE International Conference on Systems, Man and Cybernetics, October 2002, Hammamet, Tunisia.

[10] R. Ganeshan, T.P. Harrison, "An Introduction to Supply Chain Management", available at http://lcm.csa.iisc.ernet.in/scm/supply_chain_intro.html.

[11] R. Ganeshan, E. Jack, M.J. Magazine, P. Stephens, "A Taxonomic Review of Supply Chain Management", in Quantitative Models for Supply Chain Management, S. Tayur, R. Ganeshan, and M.J. Magazine (Eds). Kluwer Academic Publishers, Boston, MA, USA, pp. 840-879, 1999.

[12] R.S. Gaonkar, N. Viswanadham, "Collaboration and Information Sharing in Global Contract Manufacturing Networks", IEEE Transactions on Mechatronics, vol. 6, no. 4, pp. 366-376, 2001.

[13] H. Min, G. Zhou, "Supply Chain Modelling: Past, Present and Future", Computers & Industrial Engineering, vol. 43, pp. 231-249, 2002.

[14] J. Olhager, "Supply Chain Management: a Just-in-Time Perspective", Production Planning and Control, vol. 13, no. 8, pp. 681-687, 2002.

[15] K. Rota, C. Thierry, G. Bel, "Supply Chain Management: a Supplier Perspective", Production Planning and Control, vol. 13, no. 4, pp. 370-380, 2002.

[16] W. M. P. Van der Aalst, "Timed Colored Petri Nets and Their Application to Logistics", Ph.D. dissertation, Technical University of Eindhoven, Eindhoven, The Netherlands, 1992.

[17] C. Vidal, M. Goetschalckx, "Strategic Production-Distribution Models: a Critical Review with Emphasis on Global Supply Chain Models", European Journal of Operational Research, vol. 98, pp. 1-18, 1997.

[18] N. Viswanadham, R.S. Gaonkar, "Partner Selection and Synchronized Planning in Dynamic Manufacturing Networks", IEEE Transactions on Robotics and Automation, vol. 19, no. 1, pp. 117-130, 2003.

[19] N. Viswanadham, Y. Narahari, Performance Modeling of Automated Manufacturing Systems. Prentice-Hall, Englewood Cliffs, NJ, USA, 1992.

[20] N. Viswanadham, S. Raghavan, "Performance Analysis and Design of Supply Chains: a Petri Net Approach", Journal of the Operational Research Society, vol. 51, pp. 1158-1169, 2000.

[21] M. Von Mevius, R. Pibernik, "Process Management in Supply Chains - a New Petri-Net Based Approach", 37th Annual Hawaii International Conference on System Sciences, January 2004, pp. 71-80.

[22] T. Xu, A.A. Desrochers, R. J. Graves, "Performance Modeling of Dynamic Network-Based Decision Systems for Distributed Manufacturing", International Journal of Computer Integrated Manufacturing, vol. 18, no. 2-3, pp. 179-198, 2005.

[23] T. Wu, P. O'Grady, "A Network-Based Approach to Integrated Supply Chain Design", Production Planning and Control, vol. 16, no. 5, 2005, pp.444-453.

Biographies

Mariagrazia Dotoli received the Laurea degree in Electronic Engineering with honors in 1995 and the Ph.D. in Electrical Engineering in 1999, both from Politecnico di Bari (Italy). She has been a visiting scholar at the Paris 6 University and at the Technical University of Denmark. In 1999 she joined Politecnico di Bari (Italy) as Assistant Professor in systems and control engineering. Her research interests include modeling and control of discrete event systems, flexible production systems and distributed manufacturing systems, as well as Petri nets and computational intelligence techniques. Dr. Dotoli has been co-chairman of the Training and Education Committee of ERUDIT, the network of excellence for fuzzy logic and uncertainty modeling in information technology. She has also been key node representative of EUNITE, the EUropean Network of excellence on Intelligent TEchnologies. She is member of IEEE since 1996. Since 2003 she is expert evaluator of the European Commission. Dr. Dotoli belongs to the editorial advisory board of the Mediterranean Journal of Measurement and Control and of the International Journal of Automation and Control.

Maria Pia Fanti received the Laurea degree in Electronic Engineering from the University of Pisa (Italy), in 1983. She was a visiting researcher at the Rensselaer Polytechnic Institute of Troy (New York, USA) in 1999. Since 1983 she has been with the Department of Electrical and Electronic Engineering of the Polytechnic of Bari (Italy), where she was Assistant Professor from 1990 till 1998 and where she is now an Associate Professor in Automation. Her research interests include discrete event systems, Petri nets, control and modeling of automated manufacturing systems and computer integrated systems, supply chain modeling and management. Since 2002 she is Senior Member of IEEE. Prof. Fanti is Associate Editor of IEEE Transactions on Systems, Man, and Cybernetics: Part A and of IEEE Transactions on Automation Science and Engineering.

CONTROL OF SOLUTION COPOLYMERIZATION REACTORS

C. Rimlinger, N. Sheibat-Othman *, H. Hammouri
LAGEP-Université Lyon1 - CNRS/ESCPE, 69622 Villeurbanne CEDEX, France

ABSTRACT

The requirements of productivity, safety and quality impose the development of advanced control strategies for polymerization processes. Polymers produced by solution polymerization must have well-defined characteristics and physicochemical properties such as the polymer composition and molecular weight distribution. This work proposes a new observer-based control structure in order to control the composition and the molecular weight of the polymer. A high gain observer that allows estimating the concentration of radicals and the residual number of moles of monomers is developed. A nonlinear input-output linearizing geometric approach is then applied to control the composition and the polymer molecular weight by manipulating the inlet flow rate of monomers and chain transfer agent. The control strategy is validated by simulation during the solution copolymerization of methyl methacrylate and vinyl acetate.

Keywords

Nonlinear Control, Input-Output Linearisation, High Gain Nonlinear Observer, Solution Copolymerization, Semi Batch Reactor.

1. INTRODUCTION

The industrial requirements of productivity, safety and quality impose the development of advanced control strategies for the control of polymerization processes. The produced polymer must have well defined characteristics and physicochemical properties with respect to the specifications. The Polymer Molecular Weight Distribution (MWD) is a fundamental polymer property that influences the final polymer properties. Maintaining the instantaneous molecular weight constant during the polymerization process allows narrowing the final cumulative MWD, which influences the thermal properties, the impact resistance and the solution viscosity of many polymer systems. The polymer composition is also an important property that affects the glass transition temperature of the polymer.

*Corresponding author: *E-mail:* nida.othman@lagep.cpe.fr

 ISSN: 1743-9310

Some works have been done in order to control solution and emulsion copolymerization reactors in an open-loop manner. Dynamic optimization approaches were used [1] to calculate the optimal monomer addition and temperature profiles to obtain uniform polymer molecular weight and composition in batch and semi-batch solution copolymerization reactors.

Regarding closed-loop operations, most of them consisted of applying nonlinear techniques of estimation or control to the linearized system. However, a number of papers addressed nonlinear techniques to monitor and control these processes [2-4]. Congalidis et al. (1989) [5] studied the combination of feed-forward and feedback control to regulate the polymer production rate, copolymer composition and molecular weight. Model predictive control remains the algorithm the most commonly applied in closed-loop schemes; but usually on the linearized system [6, 7]. Nowadays, some applications of the nonlinear theory of model predictive control can be found in polymerization processes. Input-output linearization also seems to be a good way to take into account the nonlinearity of the model [8, 9].

Besides the nonlinearity of the system, the lack of on-line process sensors to measure the polymer properties makes the control of solution copolymerization reactors more difficult. Calorimetry is one of the most customarily used techniques to monitor the process [10, 11]. Nowadays, near infrared spectroscopy is also used to monitor the different concentrations in the reactor and seems to give good results in solution polymerizations since the system is homogeneous [12]. As a complement to these online sensors, observers were used to obtain information about the non-measured variables from the available online measurements. The typical observers employed consist of the Extended Kalman Filter, Kalman-like estimator and high gain observers [13, 14].

In a previous work [15] high gain observers and nonlinear input-output linearizing control were used to estimate the concentration of radicals and to control the polymer molecular weight in solution homopolymerization processes. In the present paper, copolymerization processes are considered. In this case, a simultaneous control of the instantaneous or cumulative polymer molecular weight and the polymer composition is an issue. The monomer overall conversion is assumed to be measured online.

In the first part of this paper, the process model is presented. It consists of the material balances of the initiator and monomers and the moment equations describing the polymer MWD. Then, as the proposed feedback algorithm requires the knowledge of the state of the system, a high gain observer is developed to estimate the concentration of radicals in the reactor. Finally, a nonlinear input-output linearizing geometric approach is adopted to control simultaneously the composition and the polymer molecular weight by manipulating the inlet

flow rate of the monomers. The control strategy is validated by simulation during the solution copolymerization of methyl methacrylate (MMA) and vinyl acetate (VA).

2. NONLINEAR FREE RADICAL COPOLYMERIZATION MODEL

The kinetic model of radical copolymerization comprises of the following steps: initiation, chain propagation, chain transfer to the chain transfer agent, and termination by combination or by disproportionation of radicals.

Under quasi steady-state hypothesis on radicals and long chain hypothesis [16, 17], the balances of initiator, monomers, chain transfer agent and the reactor volume take the following form:

$$\begin{cases} \dfrac{dN_I}{dt} = -k_d N_I \\ \dfrac{dN_1}{dt} = Q_1 - \underbrace{[M_1^\bullet]\left\{k_{p11}\dfrac{N_1}{V} + k_{p12}\dfrac{N_2}{V}\right\}}_{R_{P1}} \\ \dfrac{dN_2}{dt} = Q_2 - \underbrace{[M_2^\bullet]\left\{k_{p21}\dfrac{N_1}{V} + k_{p22}\dfrac{N_2}{V}\right\}}_{R_{P2}} \\ \dfrac{dN_T}{dt} = Q_T - k_{f1T}[M_1^\bullet]\dfrac{N_T}{V} - k_{f2T}[M_2^\bullet]\dfrac{N_T}{V} \\ \dfrac{dV}{dt} = \sum_{i=1,2}\dfrac{Q_i M_{wi}}{\rho_i} \end{cases} \quad (1)$$

The following notations are used in system (1):

$$[M_1^\bullet] = \varphi_1[M^\bullet] \quad \text{and} \quad [M_2^\bullet] = \varphi_2[M^\bullet] \quad (2)$$

where φ_1 and φ_2 are the mole fractions of radicals with the ultimate unit of type 1 or 2,

$$\varphi_1 = \frac{k_{p21}N_1}{k_{p21}N_1 + k_{p12}N_2} \quad (3)$$

And,

$$\varphi_2 = 1 - \varphi_1 = \frac{k_{p12}N_2}{k_{p21}N_1 + k_{p12}N_2} \quad (4)$$

The total concentration of live polymers $[M^\bullet]$ is derived by applying the quasi-steady-state hypothesis to live radical species which yields,

$$[M^\bullet] = \sqrt{\frac{2fk_d N_I / V}{k_{t11}\varphi_1^2 + 2k_{t12}\varphi_1\varphi_2 + k_{t22}\varphi_2^2}} \quad (5)$$

where f is the initiator efficiency factor.

The polymer MWD is represented by the method of moments. The moments for live and dead copolymer chain distributions are,

$$\begin{aligned} &\lambda_{ij} = \sum_m \sum_n \left(mM_{w1} + nM_{w2}\right)^j [M^\bullet_{m,n,i}] \\ &\textit{with } i=1,\ 2;\ j=1,\ 2,\ 3 \\ &\mu_k = \sum_m \sum_n \left(mM_{w1} + nM_{w2}\right)^k [P_{m,n}] \\ &\textit{with } k=0,\ 1,\ 2 \end{aligned} \quad (6)$$

where λ_{ij} is the j^{th} moment of live copolymer chain of type i and μ_k is the k^{th} moment of dead copolymer chain.

$$\begin{cases} \lambda_{10} = [M_1^\bullet] = \varphi_1[M^\bullet] \\ \lambda_{20} = [M_2^\bullet] = \varphi_1[M^\bullet] \\ \lambda_{11} = \dfrac{M_{w1}\left(k_{p11}\lambda_{10} + k_{p21}\lambda_{20}\right)N_1 + k_{p21}\lambda_{21}N_1}{k_{p12}N_2 + \left\{k_{t11}\lambda_{10} + k_{t12}\lambda_{20}\right\}V + k_{f1T}N_T} \\ \lambda_{21} = \dfrac{M_{w2}\left(k_{p12}\lambda_{10} + k_{p22}\lambda_{20}\right)N_2 + k_{p12}\lambda_{11}N_2}{k_{p21}N_1 + \left\{k_{t21}\lambda_{10} + k_{t22}\lambda_{20}\right\}V + k_{f2T}N_T} \\ \lambda_{12} = \dfrac{M_{w1}^2\left(k_{p11}\lambda_{10} + k_{p21}\lambda_{20}\right)N_1 + 2M_{w1}\left(k_{p11}\lambda_{11} + k_{p21}\lambda_{21}\right)N_1 + k_{p21}\lambda_{22}N_1}{k_{p12}N_2 + \left\{k_{t11}\lambda_{10} + k_{t12}\lambda_{20}\right\}V + k_{f1T}N_T} \\ \lambda_{22} = \dfrac{M_{w2}^2\left(k_{p12}\lambda_{10} + k_{p22}\lambda_{20}\right)N_2 + 2M_{w2}\left(k_{p12}\lambda_{11} + k_{p22}\lambda_{21}\right)N_2 + k_{p12}\lambda_{12}N_2}{k_{p21}N_1 + \left\{k_{t21}\lambda_{10} + k_{t22}\lambda_{20}\right\}V + k_{f2T}N_T} \end{cases} \quad (7)$$

$$\frac{d\mu_0}{dt} = k'_{t11}\lambda_{10}^2 + k'_{t22}\lambda_{20}^2 + \left(k'_{t21}+k'_{t12}\right)\lambda_{10}\lambda_{20} + k_{f1T}\lambda_{10}\frac{N_T}{V} + k_{f2T}\lambda_{20}\frac{N_T}{V}$$

$$\frac{d\mu_1}{dt} = \left(k_{td11}+k_{tc11}\right)\lambda_{10}\lambda_{11} + \left(k_{td22}+k_{tc22}\right)\lambda_{20}\lambda_{21} + \left(k_{td21}+k_{tc21}\right)\left(\lambda_{21}\lambda_{10}+\lambda_{11}\lambda_{20}\right) + k_{f1T}\frac{N_T}{V}\lambda_{11} + k_{f2T}\frac{N_T}{V}\lambda_{21} \tag{8}$$

$$\frac{d\mu_2}{dt} = \left(k_{td11}+k_{tc11}\right)\lambda_{12}\lambda_{10} + \left(k_{td22}+k_{tc22}\right)\lambda_{20}\lambda_{22} + \left(k_{td21}+k_{tc21}\right)\left(\lambda_{22}\lambda_{10}+\lambda_{12}\lambda_{20}\right) + k_{f1T}\frac{N_T}{V}\lambda_{12} + k_{f2T}\frac{N_T}{V}\lambda_{22} + 2k_{tc21}\lambda_{11}\lambda_{21} + k_{tc11}\lambda_{11}^2 + k_{tc22}\lambda_{21}^2$$

Applying the pseudo-steady state approximation to live polymers [18] leads to the equations given by (7) for live polymer chains. In these equations, transfer to monomer, polymer and solvent are neglected since transfer to the chain transfer agent is much more important. The moment equations for dead polymers are given by (8).

where,

$$k'_{tij} = \frac{1}{2}k_{tcij} + k_{tdij} \qquad i,j = 1,2 \tag{9}$$

The cumulated number and weight average molecular weights are calculated from the moments of the weight chain length distribution for the dead polymer,

$$\overline{M}_n = \frac{\mu_1+\lambda_{11}+\lambda_{21}}{\mu_0+\lambda_{10}+\lambda_{20}}, \quad \overline{M}_w = \frac{\mu_2+\lambda_{12}+\lambda_{22}}{\mu_1+\lambda_{11}+\lambda_{21}} \tag{10}$$

The instantaneous molecular weight is given by:

$$M_n = \frac{d\mu_1}{d\mu_0} \text{ and } M_w = \frac{d\mu_2}{d\mu_1} \tag{11}$$

The instantaneous polymer composition is defined as the fraction of the monomer units in the total polymer chain. This is equal to the reaction ratio of this monomer to the total reaction rate,

$$F_1 = \frac{R_{P1}}{R_{P1}+R_{P2}} \tag{12}$$

The system methyl methacrylate (MMA) and vinyl acetate (VA) is studied in this work. The kinetics of this system are presented in Table 1. In this system, Methyl Methacrylate is much more reactive than Vinyl Acetate. Benzene was used as a solvent, azobisisobutyronitrile (AIBN) as initiator, and acetaldehyde as chain transfer agent.

Table 1: Kinetic parameters

Parameter	Value	Parameter	Value
k_d	1.1317e-5 (s^{-1})	k_{td22}	0 (cm^3/mol/s)
f	1	k_{t11}	$k_{tc11}+k_{td11}$
k_{p11}	5.1480e5 (cm^3/mol/s)	k_{t12}	$k_{tc12}+k_{td12}$
k_{p12}	1.9793e4 (cm^3/mol/s)	k_{t21}	k_{t12}
k_{p21}	3.166e8 (cm^3/mol/s)	k_{t22}	$k_{tc22}+k_{td22}$
k_{p22}	1.0126e6 (cm^3/mol/s)	k_{f1T}	334.6935 (cm^3/mol/s)
k_{tc11}	2.549e10 (cm^3/mol/s)	k_{f2T}	6.6826e4 (cm^3/mol/s)
k_{tc22}	3.799e11(cm^3/mol/s)	M_{w1}	100 (g/mol)
k_{tc12}	$(k_{tc11}\times k_{tc22})^{0.5}$	M_{w2}	86.09 (g/mol)
k_{td11}	0 (cm^3/mol/s)	ρ_1	0.94 (g/cm^3)
k_{td12}	0 (cm^3/mol/s)	ρ_2	0.9317 (g/cm^3)

3. HIGH GAIN OBSERVER

In general, most of the modern feedback control strategies require the knowledge of the state of the system. Assuming the monomer conversion is measured either by calorimetry or by near infrared spectroscopy, the concentration of radicals becomes observable. As a result, a high gain observer [19, 20] is employed to estimate the concentration of radicals. The design procedure is described in what follows.

The observer is composed of two cascade observers. The first one allows the estimation of the number of moles of monomers N1 and N2 assuming the concentration of radicals is known. The second observer estimates the concentration of radicals using the estimated values of N_1 and N_2.

Based on the monomer overall conversion, and using the total number of moles of monomer introduced into the reactor, the total mass of residual monomer can be calculated. The overall conversion X is defined by,

$$X = \frac{M_{w1}\left(N_1^{tot}-N_1\right)+M_{w2}\left(N_2^{tot}-N_2\right)}{M_{w1}N_1^{tot}+M_{w2}N_2^{tot}} \tag{13}$$

The residual mass of monomer is therefore,

$$\begin{aligned} y &= (1-X)\left(M_{w1}N_1^{tot} + M_{w2}N_2^{tot}\right) \\ &= M_{w1}N_1 + M_{w2}N_2 \end{aligned} \tag{14}$$

3.1 Estimation of the number of moles of monomers

The general form of the model used to estimate N_1 and N_2 is given by:

$$\begin{cases} \dfrac{dN_1}{dt} = Q_1 - \varphi_1[M^\bullet]\left\{k_{p11}\dfrac{N_1}{V} + k_{p12}\dfrac{N_2}{V}\right\} \\ \dfrac{dN_2}{dt} = Q_2 - \varphi_2[M^\bullet]\left\{k_{p21}\dfrac{N_1}{V} + k_{p22}\dfrac{N_2}{V}\right\} \\ y = M_{w1}N_1 + M_{w2}N_2 \end{cases} \tag{15}$$

The following transformation is considered in order to put the system under a canonical form of observability. This transformation is based on the Lie derivative of the output y,

$$\begin{cases} z_1 = \phi_1(N) = y = M_{w1}N_1 + M_{w2}N_2 \\ z_2 = \phi_2(N) = -R_{P1}M_{w1} - R_{P2}M_{w2} \end{cases} \tag{16}$$

This yields the following new system,

$$\begin{cases} \dot{z} = \underbrace{\begin{bmatrix} 0 & 1 \\ 0 & 0 \end{bmatrix}}_{A} z + \begin{bmatrix} 0 \\ \phi(z) \end{bmatrix} + \begin{bmatrix} Q_1 \\ Q_2 \end{bmatrix} \\ y = \underbrace{\begin{bmatrix} 1 & 0 \end{bmatrix}}_{C} z \end{cases} \tag{17}$$

with,

$$\phi(z) = -\dot{R}_{P1}M_{w1} - \dot{R}_{P2}M_{w2} \tag{18}$$

System (17) is under a canonical form of observability. A high gain observer can therefore be constructed in order to estimate the state z. The inverse of the transformation z gives then an observer of the original states N_1 and N_2 as follows,

$$\begin{bmatrix} \dot{\hat{N}}1 \\ \dot{\hat{N}}2 \end{bmatrix} = \begin{bmatrix} Q_1 \\ Q_2 \end{bmatrix} + \begin{bmatrix} -\hat{R}_{P1} \\ -\hat{R}_{P2} \end{bmatrix} - \left(\frac{\partial z}{\partial \hat{N}_i}\right)^{-1} S_\theta^{-1} C^T (\hat{y} - y) \tag{19}$$

Where S_θ is the unique symmetric positive definite matrix satisfying the algebraic Lyapunov equation,

$$\theta S_\theta + A^T S_\theta + S_\theta A - C^T C = 0$$

3.2 Estimation of total concentration of live polymers

The concentration of radicals is denoted by $\omega = [M^\bullet]$. The same process output (y) is used to estimate ω. In order to construct the observer, we consider the following augmented system, where the unknown dynamic of is represented by ε,

$$\begin{cases} \dot{y} = M_{w1}\dot{N}_1 + M_{w2}\dot{N}_2 = -\alpha\omega \\ \dot{\omega} = \varepsilon \end{cases} \tag{20}$$

System (20) can be written in matrix form as,

$$\begin{cases} \dot{z} = B(u, z_1, s) + f(z_1, s)F(z_1, s)z + \bar{\varepsilon}(t) \\ y = h(z) = \begin{bmatrix} 1 & 0 \end{bmatrix} z \end{cases} \tag{21}$$

Where,

$$F(z_1, s) = \begin{bmatrix} 0 & \alpha \\ 0 & 0 \end{bmatrix}, \quad \bar{\varepsilon}(t) = \begin{bmatrix} 0 \\ \varepsilon(t) \end{bmatrix} \text{ and}$$

$$B(u, z_1, s) = \begin{bmatrix} M_{w1}Q_1 + M_{w2}Q_2 \\ 0 \end{bmatrix}$$

The observer of this system takes the following form [19]:

$$\begin{aligned} \dot{\hat{z}} = {} & B(u, \hat{z}, s) + f(\hat{z}, s)F(\hat{z}, s)\hat{z} \\ & - f(\hat{z}, s)\begin{bmatrix} 2\theta \\ \theta^2 F_1^{-1}(z_1, s) \end{bmatrix}(\hat{y} - y) \end{aligned} \tag{22}$$

Finally, the observer of the original coordinates is given by,

$$\begin{cases} \dot{\hat{y}} = M_{w1}Q_1 + M_{w2}Q_2 - \alpha\hat{\omega} - 2\theta(\hat{y} - y) \\ \dot{\hat{\omega}} = \dfrac{\theta^2}{\alpha}(\hat{y} - y) \end{cases} \tag{23}$$

It is important to notice that observers (19) and (23) estimate N_1, N_2 and ω simultaneously.

4. NONLINEAR GEOMETRIC CONTROL

Since the process states are now available, a feedback controller can be developed. We will consider controlling the polymer instantaneous composition combined first with the cumulative and second with the instantaneous number average molecular weight.

4.1 Control of the cumulative molecular weight and the polymer composition

In order to control the polymer composition, the ratio F_1/F_2 has to be maintained at a predefined value,

(24)

$$\frac{F_1}{F_2}=\frac{R_{P1}}{R_{P2}}=\frac{\overbrace{\left(\frac{k_{p21}N_1}{k_{p21}N_1+k_{p12}N_2}\right)}^{\varphi_1}\left\{k_{p11}\frac{N_1}{V}+k_{p12}\frac{N_2}{V}\right\}}{\underbrace{\left(1-\frac{k_{p21}N_1}{k_{p21}N_1+k_{p12}N_2}\right)}_{\varphi_2=1-\varphi_1}\left\{k_{p21}\frac{N_1}{V}+k_{p22}\frac{N_2}{V}\right\}}$$

However, (24) shows that it is sufficient to control the ratio of monomers N_1/N_2 in order to control the polymer composition. The desired ratio $(N_1/N_2)^d$ is calculated from the desired composition ratio (F_1/F_2) from the same equation. It is customary to use the flow rate of the most reactive monomer to control the polymer composition ($Q_{1,in}$). Therefore, the flow rate of the less reactive monomer ($Q_{2,in}$) will be used to control the number average molecular weight. First of all, let us analyze the controllability of the system.

$$\begin{cases}\underbrace{\begin{bmatrix}\dot N_1\\ \dot N_2\end{bmatrix}}_{\dot x}=\underbrace{\begin{bmatrix}1\\0\end{bmatrix}}_{g_1(x)}\underbrace{Q_1}_{u_1}+\underbrace{\begin{bmatrix}1\\0\end{bmatrix}}_{g_2(x)}\underbrace{Q_2}_{u_2}+\underbrace{\begin{bmatrix}-R_{P1}\\-R_{P2}\end{bmatrix}}_{f(x)}\\ y=\underbrace{\begin{bmatrix}N_1\\N_2\end{bmatrix}}_{h(x)}\end{cases} \tag{25}$$

The characteristic matrix of this system is non-singular [21, 22],

$$C(x)=\begin{bmatrix}L_{g_1}h_1 & L_{g_2}h_1\\ L_{g_1}h_2 & L_{g_2}h_2\end{bmatrix}=\begin{bmatrix}1 & 0\\ 0 & 1\end{bmatrix}$$

System (25) is a nonlinear multi-input multi-output (MIMO) system. We can apply a nonlinear input-output linearizing controller with the feedback,

$$u=\frac{v-L_f h(x)-\beta_1 h(x)}{L_{g_1}L_f^0 h(x)}=v+R_{P1}-\beta_1 N_1 \tag{26}$$

We define the external input v as a Proportional Integral (PI) loop,

$$v-\beta_1 N_1=\kappa_p\underbrace{(y^d-y)}_{\varepsilon}+\frac{1}{\tau_p}\int(y^d-y)dt \tag{27}$$

The complete control system becomes,

(28)

$$Q_1=R_{P1}+\underbrace{\kappa_{p1}\left(N_2\left(\frac{N_1}{N_2}\right)^d-N_1\right)}_{P}+\underbrace{\frac{1}{\tau_{p1}}\int\left(N_1^d-N_1\right)dt}_{I}$$

and,

(29)

$$Q_2=R_{P2}+\underbrace{\kappa_{p2}(N_2^d-N_1)}_{P}+\underbrace{\frac{1}{\tau_{p2}}\int(N_2^d-N_1)dt}_{I}$$

where N_2^d is calculated from (11).

4.2 Control of the instantaneous molecular weight and the polymer composition

In order to control the instantaneous molecular weight and the polymer composition, the same control laws presented above are used (28, 29) with the exception that the desired value is calculated by iteration from relation (10).

In the both cases, R_{P1} and R_{P2} permit to compensate the nonlinear dynamic of the model. The proportional action (P) is necessary in order to account for the set point and the integral action (I) allows to eliminate the errors due to modeling uncertainties. The controller is regulated by the parameters k_{p1}, k_{p2} and τ_{p1}, τ_{p2}.

The observers and the controllers are coupled to design a feedback controller for Cases a and b:

Case a, the objective is to control the polymer composition and the instantaneous molecular weight.

Case b, the objective is to control the polymer composition and the cumulative molecular weight.

The controller algorithm is shown on the following scheme.

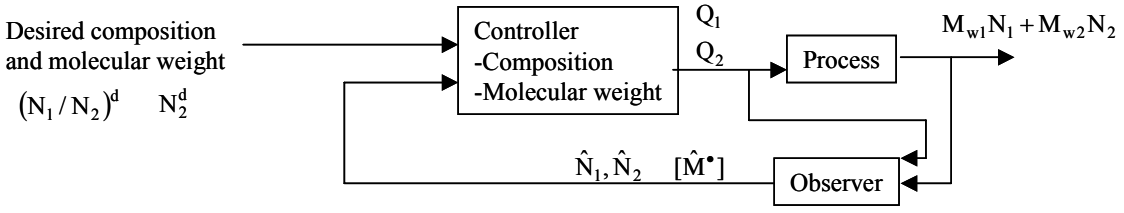

Control of the molecular weight and the polymer composition

5. RESULTS AND DISCUSION

The observers and controllers developed above were validated by simulation during the copolymerization of methyl methacrylate (MMA) and vinyl acetate (VA). In the first series of simulation (Case a), the objective was to maintain the polymer composition and the instantaneous molecular weight at a predefined trajectory.

Figures 1 and 2 show the estimated values of $[M^{\bullet}]$, N_1 and N_2 compared to the real values. In order to test the robustness of the observer, the measurement of the monomer conversion was corrupted by an additive Gaussian noise with amplitude equivalent to 5%. The figures show that the cascade observers work well with and without measurement noise. A rapid convergence to the real values could be observed.

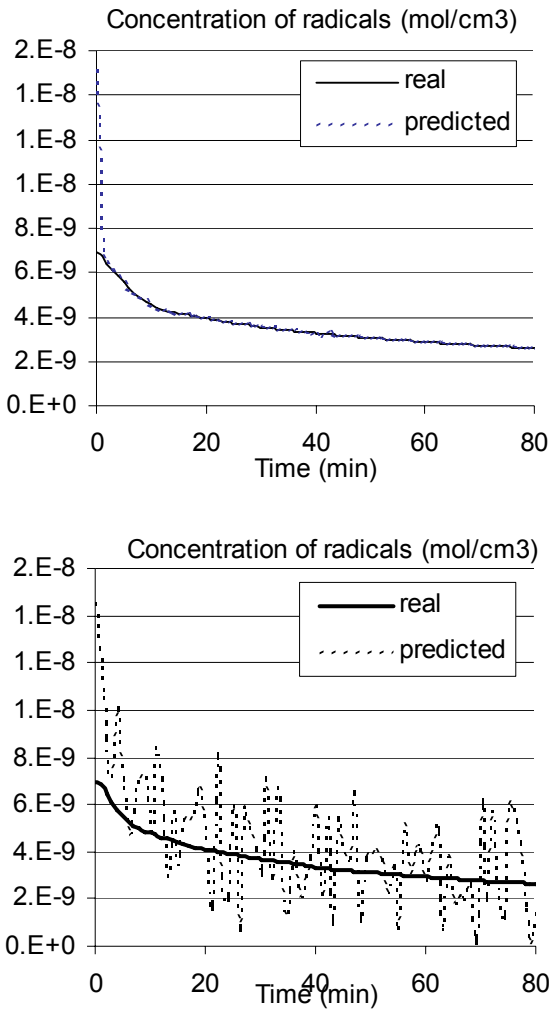

Figure 1. Estimation of the concentration of radicals. Case a: Control of the instantaneous molecular weight and the polymer composition (at top, without noise and at bottom, with measurement noise)

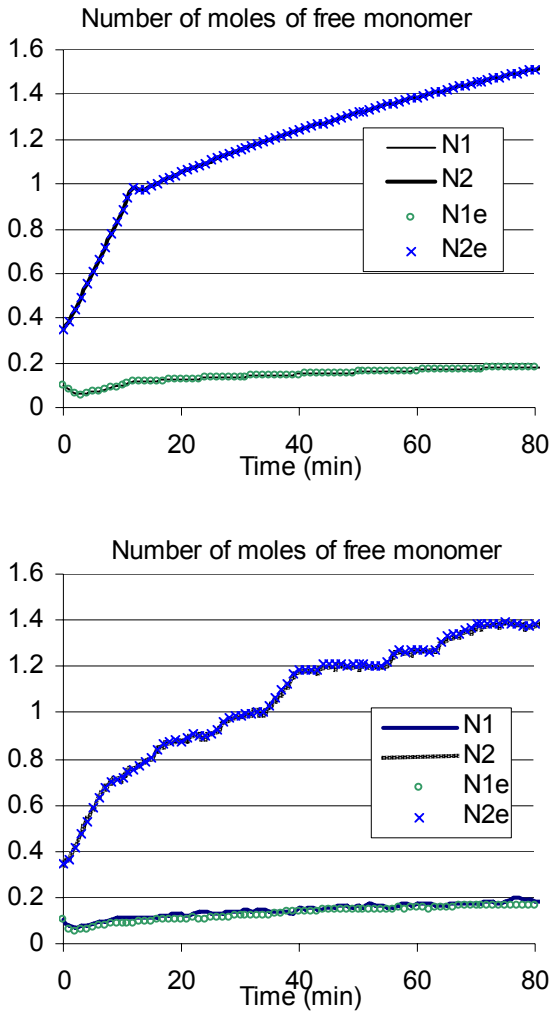

Figure 2. Estimation of the number of moles of monomers 1 and 2. Case a: Control of the instantaneous molecular weight and the polymer composition (at top, without noise and at bottom, with measurement noise)

Figures 3 to 5 show the performance of the controller. Figure 3 shows the evolution of the instantaneous molecular weight in presence and in the absence of measurement noise. It can be seen that it converges rapidly to the set-point. In parallel, the polymer composition converges very quickly to the set-point (Figure 4). Figure 5 shows the flow rates of monomers employed to obtain this comportment of the process states. The flow rates were assumed to be limited at $1e^{-3}$ (mol/s). The rapidity of convergence is a function of this saturation value. It is important to mention that the adjustment of the PI parameters in a multivariable system is very important in order to get good results.

In the second series of simulations (Case b), the objective was to maintain the polymer composition and the cumulative molecular weight at a predefined trajectory. This means that, the controller tries to maintain the average value of the molecular weight of the produced since the beginning of the reaction at a desired value. It can be imagined that this generates a forgetting factor on the molecular weight of

polymer that depends on the amount of polymer produced. Actually, an amount of polymer is produced at the beginning of the reaction with an error in molecular weight until the controller converges to the desired trajectory. This error is integrated in the cumulative molecular weight as can be seen on Figure 6. It is important to mention that the instantaneous molecular weight does not take into account the molecular weight of the produced polymer but only what is produced at each time (Figure 3). Figure 7 shows the evolution of the polymer composition in this simulation. The controller convergence is mainly affected by the saturation of the monomer flow rates as shown on Figure 8.

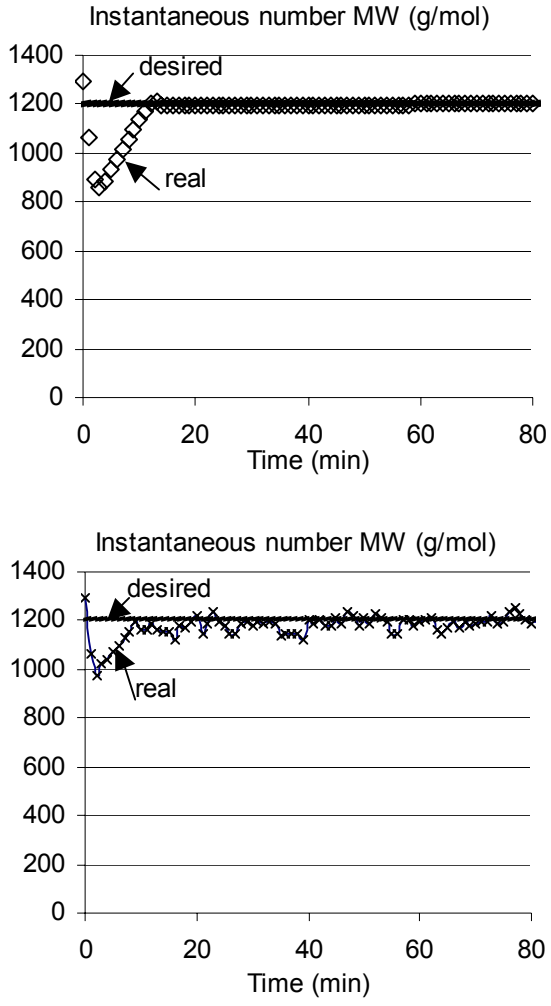

Figure 3. Evolution of instantaneous molecular weight. Case a: Control of the instantaneous molecular weight and the polymer composition (at top, without noise and at bottom, in presence of measurement noise)

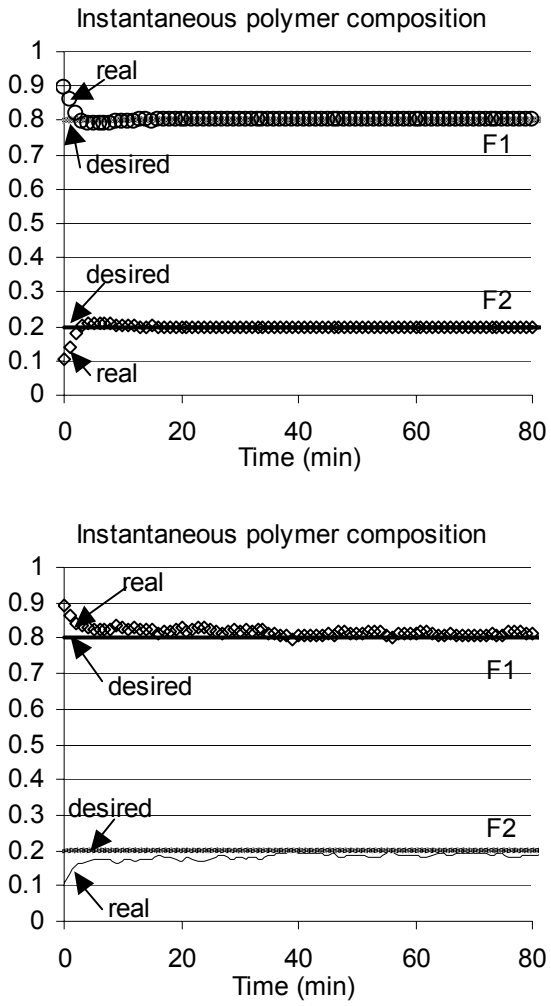

Figure 4. Evolution of the polymer composition. Case a: Control of the instantaneous molecular weight and the polymer composition (at top, without noise and at bottom, in presence of measurement noise)

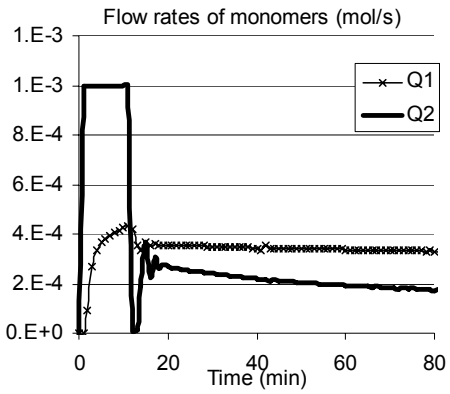

Figure 5. Flow rates of monomers 1 and 2. Case a: Control of the instantaneous molecular weight and the polymer composition.

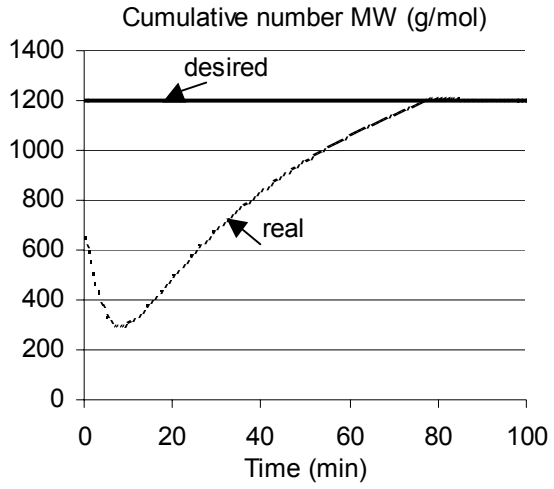

Figure 6. Evolution of the cumulative molecular weight. Case b: Control of the cumulative molecular weight and the polymer composition.

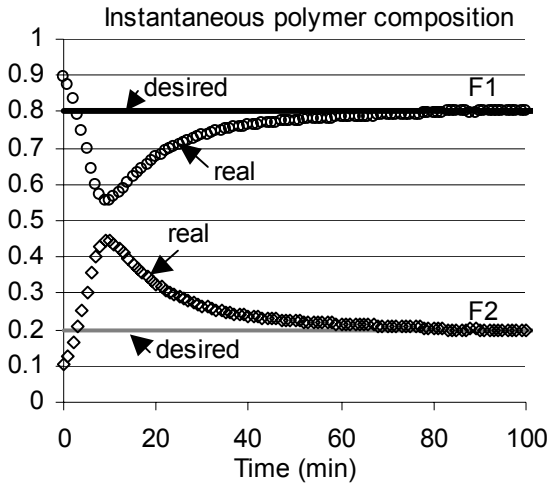

Figure 7. Evolution of the polymer composition. Case b: Control of the cumulative molecular weight and the polymer composition.

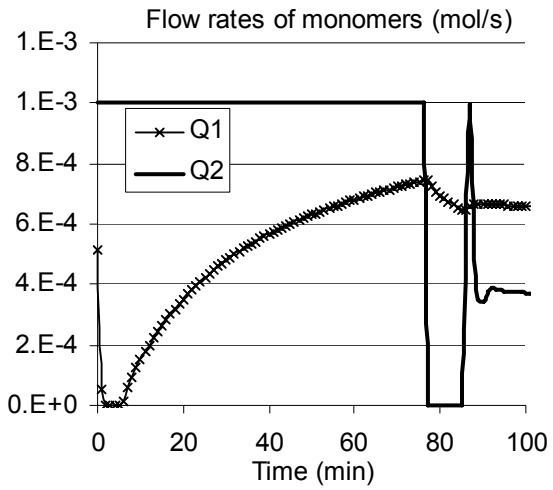

Figure 8. Flow rates of monomers 1 and 2. Case b: Control of the cumulative molecular weight and the polymer composition.

The decision of controlling the instantaneous or cumulative molecular weight of the polymer depends on the application and on the process time. For long processes, it is worthy to use the instantaneous molecular weight in order to have good information about the process. At a time t where a big amount of polymer has been produced, the cumulative molecular weight will not account well for what is being produced. The polymer quality would be better if the controller of the instantaneous molecular weight is applied in this case. In applications, where the average molecular weight is measured online or at discrete intervals, it is more interesting to use this information for process control.

As a result, it seems more interesting to control the cumulative average molecular weight at the beginning of the reaction and when the reaction volume increases considerably it becomes more interesting to use the controller of the instantaneous molecular weight.

6. CONCLUSIONS

In this work, a system of controlling semi batch solution copolymerization processes was developed. A high gain observer was developed to estimate the residual amounts of monomers and the concentration of radicals based on the measurement of the monomer conversion and on a detailed process model. The observer performance was validated by simulation. A nonlinear state feedback controller was then developed to control the instantaneous polymer composition and both the instantaneous and cumulative molecular weight of polymer. The controller takes into account the nonlinearity of the process by input-output linearization. A comparison between the controllers shows that the choice of the controller depends on the application. In order to obtain a homogeneous polymer, the instantaneous properties should be controlled. However, if the reaction time is small then it would be more interesting to concentrate on the cumulative properties.

NOTATIONS

k_d: Decomposition rate of initiator (s^{-1})
k_{pij}: Propagation rate of a radical with the ultimate unit of type i with monomer j (cm^3/mol/s)
k_{tcij}: Coefficient of the termination by combination of radicals of type i and j (cm^3/mol/s)
k_{tdij}: Coefficient of the termination by disproportion of radicals of type i and j (cm^3/mol/s)
k_{fiT}: Chain transfer rate coefficient of radicals of type i (cm^3/mol/s)
f: Initiator efficiency
F_i: Fraction of monomer i in the polymer chains
$\overline{M}_n, \overline{M}_w$: Cumulative number and weight average molecular weight
M_n, M_w: Instantaneous number and weight average molecular weight
N_I: Number of moles of initiator (mol)
N_i^{tot}: Total number of moles of monomer i introduced to the reactor (mol)
M_i: Molecular weight of monomer i (g/mol)
N_T: Number of moles of chain transfer agent (mol)
Q_i: Inlet flow rates of monomer i (mol/s)
Q_T: Inlet flow rates of chain transfer agent (mol/s)
R_{pi}: Rate of reaction of monomer i (mol/s)
V: Volume of the reacting mixture (cm^3)
X: Monomer conversion
$\omega = [M^\bullet]$: Concentration of radicals (mol/cm^3)
ρ_x: Density of monomer i (g/cm^3)
λ_{ij}: The j^{th} moment of live copolymer chain of type i.
μ_k: The k^{th} moment of dead copolymer chain.

REFERENCES

[1] D. Butala, K. Y. Choirand and M. K. H. Fans, "Multiobjective dynamic optimization of a semibatch freeradical copolymerization process with interactive CAD tools", Comput. Chem. Engng. Vol. 12, No. II, 1988, pp. 1115-1127.

[2] D.J. Kozub and J.F. MacGregor, "Feedback control of polymer quality in semi-batch copolymerization reactors", Chem. Eng. Sci. Vol. 47, No. 4, 1992, pp. 929-942.

[3] R.A.M. Vieira, M. Embirucu, C. Sayer, J.C. Pinto and E.L. Lima, "Control strategies for complex chemical processes. Applications in polymerization process", Comput. Chem. Engng., Vol. 27, 2003, pp. 1307-1327.

[4] M.H. Lee, C. Han, K.S. Chang, "Hierarchical time-optimal control of a continuous copolymerization reactor during start-up or grade change operation using genetic algotrithms", Comput. Chem. Engng., Vol. 21, 1997, pp. S1037-S1047.

[5] J.P. Congalidis, J.R. Richrads and W.H. Ray, "Feedforward and feedback control of a solution copolymerization reactor", AIChE J., Vol. 35, No. 6, 1989, pp. 891-907.

[6] L. Ozkan, M.V. Kothare and C. Georgakis, "Control of a solution copolymerization reactor using multi-model predictive control", Chem. Eng. Sci., Vol. 58, 2003, pp. 1207-1221.

[7] R. Bindlish and J.B. Rawlings, "Target linearization and model predictive control of polymerization processes", AIChE J, Vol. 49, No. 11, 2003, pp. 2885-2899.

[8] K.R. Harris and A. Palazaglu, "Studies on the analysis of nonlinear processes via functional explanations-III: Controller design", Chem. Eng. Sci., Vol. 53, No. 23, 1998, pp. 4005-4022.

[9] S. Padilla and J. Alvarez, "Control of continuous copolymerization reactors", AIChE J. Vol. 43, No. 2, 1997, pp. 448-462.

[10] M. Vicente, J.R. Leiza, J.M. Asua, "Maximizing production and polymer quality (MWD and composition) in emulsion polymerization reactors with limited capacity of heat removal", Chem. Eng. Sci., Vol. 58, 2003, pp. 215-22.

[11] G. Févotte, I. Barudio and J. Guillot, "An adaptive inferential measurement strategy for on-line monitoring of conversion in conversion in polymerization processes", Thermochimica acta, Vol. 289, 1996, pp. 223-242.

[12] N. Sheibat-Othman, D. Peycelon, J.B Egraz, J.M. Suau, G. Févotte, "Control of the polymer molecular weight using near infrared spectroscopy", AIChE J., Vol. 50, No. 3, 2004, pp. 654-664.

[13] H. Hammouri, T.F. McKenna S. Othman, "Applications of nonlinear observers and control: Improving productivity and control of free radical solution copolymerization", Ind. Eng. Chem. Res., Vol. 38, 1999, pp. 4815-4824.

[14] M.J. Park, H.K. Rhee, "Property evaluation and control in a semi-batch MMA/MA solution copolymerization reactor", Chem. Eng. Sci., Vol. 58, 2003, pp. 603-611.

[15] C. Rimlinger, N. Sheibat Othman, G. Févotte and H. Hammouri, "Estimation and control of the molecular weight distribution in free radical polymerization", ESCAPE 14, European Symposium on Computer Aided Process Engineering, Lisbon – Portugal, May 16-19 2004.

[16] B.L. Louie, D.S. Soong, "Optimization of batch polymerization processes- narrowing the MWD. I. Model simulation", J. of Appl. Polymer Sci., Vol. 30, 1985, pp. 3707-3749.

[17] R. Jaisinghani, W.H. Ray, "On the dynamic behavior of a class of homogeneous continuous stirred tank polymerization reactors", Chem. Eng. Sci., Vol. 32, 1977, pp. 811-825.

[18] J.S CHANG, P-H. LIAO, "Molecular weight control of a batch polymerization reactor: experimental study", Ind. Eng. Chem. Res., Vol. 38, 1999, pp. 144-153.

[19] M. Farza, H. Hammouri, S. Othman and K. Busawon, "Nonlinear observers for parameter estimation in bioprocesses", Chem. Eng. Sci., Vol. 52, No. 23, 1997, pp. 4251-4267.

[20] J.P. Gauthier, H. Hammouri, S.Othman, "A simple observer for nonlinear systems- application to bioreactors", IEEE Trans. Automat. Control, Vol. 37, 1992, 875-880.

[21] A. Isidori, "Control Systems, An Introduction" 2nde Edition. Berlin: Springer Verlag, 1989.

[22] C. Kravaris, J.C. Kantor, "Geometric methods for nonlinear process control II. Controller synthesis", Ind. Eng.Chem. Res., Vol. 29, 1990, pp. 2310-2323.

Biographies

Christel Rimlinger received her M.S. degree in industrial automation from Lyon University/France in 2001. She is currently Ph.D. student at the LAGEP at Lyon University. Her research interests include nonlinear control and observer design in the field of polymerisation processes.

Nida Sheibat-Othman is a CNRS researcher in the LAGEP at Lyon University. She obtained a Ph.D. in process engineering in 2000 at Lyon University. She was a post-doctoral fellow at the company Coatex in 2001. She is a secretary of the European Working Party of Polymer Reaction Engineering. Her research interests include monitoring and control of polymerization processes.

Hassan Hammouri is Professor of Control Theory at Lyon University/France. He obtained a Ph.D. of mathematics in 1983 at Joseph Fourier University and a Doctorate of Science in Automatic control in 1991 at Grenoble Polytechnic Institute. His research interests include nonlinear observation and control theory, optimization and fault detection and isolation with application to electrical and chemical processes.

A PIPELINE TRACKING CONTROL OF AN UNDERACTUATED REMOTELY OPERATED VEHICLE

C. S. Chin *, M. W. Shing Lau, E. Low, G. G. Lee Seet
Robotic Research Centre, Mechanical and Aerospace Eng. Department, Nanyang Tech.University, Singapore

ABSTRACT

In this paper, we propose a new pipeline tracking control of an underactuated remotely operated vehicle (ROV) based on a thruster allocation and a nonlinear PD heading control for inner and outer loops respectively. The thruster allocation control without constraint uses the vehicle's velocity feedback to detect the change in thrust required for the thrusters used in ROV's maneuvering. Generalized ROV models for decoupled horizontal and vertical plane motions are derived based on small roll and pitch angles that are self-stabilizing during operations. When compared with the Proportional-Derivative (PD) controller for all motions, the proposed cascaded controller is proven to render the tracking error dynamic globally k-exponentially stable with a lower control effort needed. Computer simulations are performed on these controllers and shown to be robust against parametric uncertainty.

Keywords

Pipeline Tracking Control, Remotely Operated Vehicle (ROV), Cascaded Controller, Nonlinear Control.

1. INTRODUCTION

Remote-operated vehicle (ROV) speed and position control systems have been highly interesting research areas, with respect to safety and performance issues. However, major part of research work in this field has been focused towards the design of the outer loop control system [2-6], that is positioning control systems while the design of the thruster allocation [1], and control loops have received less attention [7-10].

This paper focuses on the design of a cascade control system with thruster allocation, in inner or 'slave' loop, and positioning control, in outer or 'master' loop for different plane maneuvering. The motivations for this work are: (i) to reduce the voltage input to thruster in the presence of opposing thruster's axial velocity and thus reduces the control effort needed for ROV's maneuvering and (ii) to decouple the ROV motion into vertical and horizontal plane and used only a heading control.

Since the vehicle is underactuated and does not have pure lateral thruster for the uncontrollable degree of freedom, maneuvering of the ROV in these directions require all thrusters. Often techniques such as unconstrained thrust allocation using Moore-Penrose pseudoinverse and Singular Value Decomposition (SVD) are used to optimize the thrust require for the motions. This is inefficient since it requires real-time optimization due to the dynamic input requirement and may not be appropriate for ROV's positioning. The proposed thrust allocation is used in the inner loop. For conventional ROVs the basic motion is the movement in a horizontal plane with some variation due to diving. Often, they operate in a crab-wise manner in four DOF with small roll and pitch angles that can be neglected during normal operations. Therefore, it is purposeful to regard the vehicle's spatial motion as a superposition of two-displacement motion in the vertical plane and the motion in the horizontal plane. By considering only few DOF at a time, motions become decoupled. For example, the vehicle is first steered at constant forward speed towards a straight line that passes through the desired target point with desired vehicle's orientation. At the end of this phase, the vehicle will be following a vertical line with constant heading but an altitude change.

Besides thruster allocation for different plane motion in the inner loop is utilized while a nonlinear PD control law for the yaw motion in the outer loop of the cascade system is used to render the tracking error dynamics globally asymptotically stable. The thruster allocation is applied to all positions except yaw angle that requires all thrusters to be activated.

This paper is organized as follows: In Section 2, the general equation of motion for ROV is described. In Section 3, the description of the thruster's system consisting of thruster dynamics and allocations are given respectively. In Section 4, the nonlinear equations for horizontal and vertical dynamic are derived. Followed by the cascaded system design for the ROV. In Section 5, discussion on the computer simulations on the proposed design and comparison with PD control are shown followed by the conclusion.

2. DESCRIPTION OF GENERAL NONLINEAR ROV MODEL

The general motion of ROV with added mass and hydrodynamic damping terms in six degree of freedom (DOF), according to Fossen [1], is described by the following equations. The added mass coefficient are contained from principle of strip theory [1]. It involves dividing the submerged part of the vehicle into a number of strips. Here,

*Corresponding author: *E-mail:* chin0014@ntu.edu.sg

 ISSN: 1743-9310

two-dimensional hydrodynamic coefficients for the added mass can be computed for each strip and summarized over the length of the body to yield three-dimensional coefficients. By examining each parts of the ROV such as the left and right float, main chassis and thrusters as a slender body, as shown in Figure 1, the total added mass coefficients for each direction is computed.

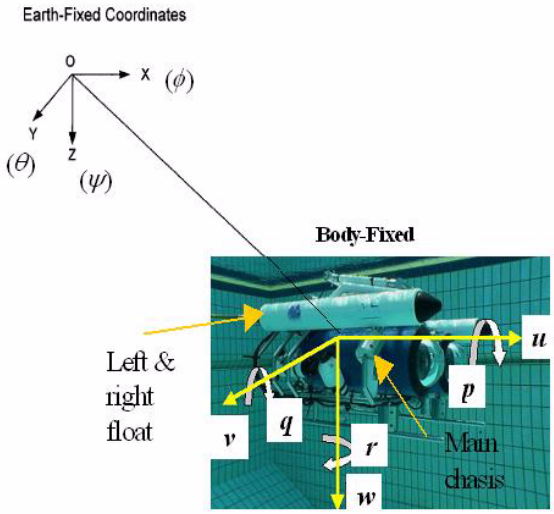

Figure 1. Coordinate system for underwater robot

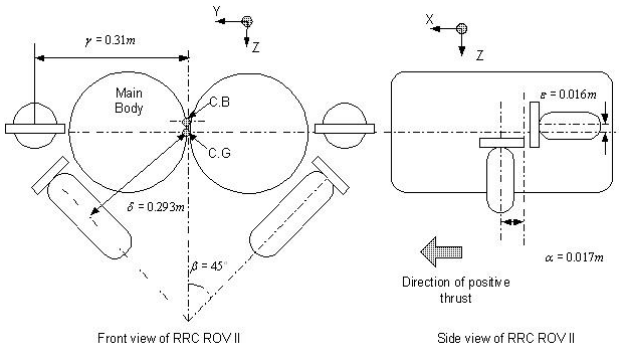

Figure 2. Front and side view of RRC ROV II

For ROV's slow speed application, off-diagonal terms in added mass matrix is smaller than their diagonal counterparts and hence a diagonal structure is adopted. Therefore, the general motion of a ROV can be described by using a body-fixed frame relative to an earth fixed frame in the compact form of:

$$M\dot{\mathrm{v}} + C(\mathrm{v})\mathrm{v} + D(\mathrm{v})\mathrm{v} + g(\eta) = \tau \qquad (1)$$

where $M = M_{RB} + M_A \in \Re^{6\times 6}$ is the sum of mass inertia and added mass matrix; $C = C_{RB} + C_A \in \Re^{6\times 6}$ is the sum of Coriolis and centripetal and added forces and moments matrix; $D \in \Re^{6\times 6}$ is the diagonal hydrodynamic forces and moments matrix; $g \in \Re^6$ is the vector of gravitational and buoyancy restoring forces and moments vector; $\tau \in \Re^6$ is the force and moment inputs vector; $\mathrm{V} = [\mathrm{V}_1,\mathrm{V}_2]^T \in \Re^6$ and are the linear and angular velocities vector consisting $\mathrm{V}_1 = [\mathrm{u,v,w}]^T$ and $\mathrm{V}_2 = [\mathrm{p,q,r}]^T$ respectively; $\eta = [\eta_1,\eta_2]^T \in \Re^3 \times S^3$ are the positions and orientation angles vector consisting $\eta_1 = [x,y,z]^T$ and $\eta_2 = [\phi,\theta,\psi]^T$ respectively. The kinematics equations or Euler transformation between the body and earth frames can be written as:

$$\dot{\eta} = J(\eta_2)\mathrm{v} \qquad (2)$$

where $J(\eta_2) \in \Re^{6\times 6}$ is the Euler transformation matrix. The notations used in ROV are shown in Table 1.

Remark 1: Since the position of the center of gravity x_g, y_g, z_g are designed to coincide with ROV origin, thus (1) can be further simplified. The ROV is neutrally buoyant and that center of buoyancy x_b and y_b coincide with the origin except z_b (located above the origin) as shown in Figure 2.

3. DESCRIPTION OF THE THRUSTER SYSTEM

In thruster allocation, the aim is to optimize some objective like minimum use of control input (optimization based control allocation in order to obtain an efficient used of voltage input to the thruster. But in some case, it is not necessary that optimized thrust is useful in the event of positioning control. Thus a thruster allocation control based on vehicle's velocity feedback is proposed. To render the thruster allocation control effective, a thruster dynamic with the effect of opposing axial velocity generated by rotating propeller is derived.

3.1 Thruster Configuration and Allocation

The layout of thrusters in the ROV platform is shown in Figure 2. There are four thrusters responsible for the six DOF motions. Since the roll and the pitch motion are not controllable but are self-stabilizable, the thrust allocation for these direction are not considered. As shown in (3), same set of thrusters has to be used for some DOF.

$$f = \begin{cases} T_1 + T_2 \text{ if } x > 0 \text{ (surge motion)} \\ T_3 - T_4 \text{ if } \mathrm{y} > 0 \text{ (sway motion)} \\ T_3 + T_4 \text{ if } z > 0 \text{ (heave motion)} \\ T_1 - T_2 + T_3 - T_4 \text{ if } \psi > 0 \text{ (yaw motion)} \end{cases} \qquad (3)$$

where T_1 to T_4 are the respective i-th thruster. For horizontal plane motion, T_1 and T_2 are generating a propulsion force acting in the longitudinal axis. T_3 and T_4 ensure the motion in sway is maintained while T_1 to T_4 provides the yaw motion. For vertical plane motion, T_1 and T_2 are generating a propulsion force acting in the longitudinal axis while T_3 and T_4 ensure the motion in heave is maintained. Note that the roll and pitch motion, there are no direct thrusters used due its self-stabilizing behavior.

In practical applications the vector of propulsion forces and moment acting on the vehicle in the horizontal and vertical plane can be described as a function of the thrust vector f by the followings expression:

$$\tau = TP\, f \qquad (4)$$

where

$$\tau = \begin{bmatrix} \tau_u & \tau_v & \tau_w & \tau_r \end{bmatrix}^T$$

τ_u - force in the longitudinal axis

τ_v - force in the transversal axis

τ_w, τ_r - force and moment in the vertical axis

T – thruster configuration matrix

$$T = \begin{bmatrix} t_1 \\ t_2 \\ t_3 \\ t_4 \end{bmatrix} = \begin{bmatrix} 1 & 1 & 0 & 0 \\ 0 & 0 & \sin\beta & -\sin\beta \\ 0 & 0 & \cos\beta & \cos\beta \\ \gamma & -\gamma & \alpha\sin\beta & -\alpha\sin\beta \end{bmatrix} \quad (5)$$

where $\alpha = 0.017m$, $\beta = 45°$, $\gamma = 0.31m$, $\delta = 0.293m$, $\varepsilon = 0.016m$ as shown in Figure 2.

$f = [f_1, f_2, f_3, f_4]^T$ is the thrust vector subjected to $f_{min} \le f \le f_{max}$, and P is a diagonal matrix of the readiness of the thruster:

$$p_{ii} = \begin{cases} 0 & \text{if the i-th thruster is off} \\ 1 & \text{if the i-th thruster is active.} \end{cases} \quad (6)$$

In the thruster allocation as indicated in (4), it produces the level of thrust without any feedback from the vehicle motion. The open-loop nature of this thrust allocation is undesired in the event of vehicle's is making a maneuvering. Hence, the following thruster allocation is proposed.

The $u_e(t_i), v_e(t_i), w_e(t_i), r_e(t_i)$ are the velocity error signal at time t_i where $i = 1 \ldots n$. T is the configuration matrix, and P is the diagonal matrix of the readiness of the thruster as in (6). All matrices are appropriately dimensioned.

$$\tau = \begin{cases} \text{sign}(u_e(t_i))TPfu_e(t_i) = \begin{cases} P = \text{diag}(1,1,0,0), u_e(t_i) > 0 \\ P = \text{diag}(-1,-1,0,0), u_e(t_i) < 0 \end{cases} \\ \text{sign}(v_e(t_i))TPfv_e(t_i) = \begin{cases} P = \text{diag}(1,-1,0,0), v_e(t_i) > 0 \\ P = \text{diag}(-1,1,0,0), v_e(t_i) < 0 \end{cases} \\ \text{sign}(w_e(t_i))TPfw_e(t_i) = \begin{cases} P = \text{diag}(0,0,1,1), w_e(t_i) > 0 \\ P = \text{diag}(0,0,-1,-1), w_e(t_i) < 0 \end{cases} \\ \text{sign}(r_e(t_i))TPfr_e(t_i) = \begin{cases} P = \text{diag}(1,-1,1,-1), r_e(t_i) > 0 \\ P = \text{diag}(-1,1,-1,1), r_e(t_i) < 0 \end{cases} \end{cases} \quad (7)$$

3.2 Thruster Dynamic

Without a good thruster model, thruster allocation may not function probably. In this section, an unsteady state thruster model is derived using the Bernoulli's Equation applied to the streamlines upstream and downstream of the propeller and assuming that the flow is incompressible, inviscid and irrotational. The thrust output from the propeller can be defined as:

$$f = \rho A_p l \dot{u}_a + 2\rho A_p u_a^2 \quad (8)$$

where u_a is the axial fluid velocity at the propeller (fluid advance speed) in m/s, A_p is the axial projected area of the propeller in m^2, l is the length of the area projected in m and ρ is the density of the seawater (3.5% salinity) at 20°C in kg/m^3. It is not difficult to see that $A_p l$ is actually the control volume in m^3. Note that f refers to the thrust produced by each thruster namely: f_1, f_2, f_3 and f_4 as shown in (4).

The relationship between axial velocity and rotational speed can be obtained from the energy balance equation. Since there is a difference in the thrust due to disturbances in the water inflow to the thruster blades, thruster-to-ROV surfaces interactions, underwater current and ROV velocities, a factor K_R is included in the energy from input to output:

$$u_a = \frac{Q\Omega}{K_R f} \quad (9)$$

where Q is the shaft's torque in N/m, Ω is the rotational speed in rad/s and f is the thrust generated from propeller rotation in Newton. The relationship between the torque and thrust is obtained from the water tank experiment [11] that is: $f = 40Q$ (forward) and $f = -54Q$ (reverse). The $K_R = 1.923$ is an average value obtained from the ratio of $Q\Omega / f u_a$ at ROV's surge velocity of $u = 0.01$ to 2 m/s under open loop condition. While the u_a, is defined as function of the vehicle's surge velocity u:

$$u_a = (1-W)u \tag{10}$$

where W refers to the wake fraction number [1] between 0.1 to 0.4. By examining (9) it is not difficult to see that $u_a \infty \Omega$. By applying $f = 40Q$ (forward), $f = -54Q$ (reverse) and substituting (9) into (8) gives:

$$f = K_{Tdo}\dot{\Omega} + K_{Td}\Omega^2 \tag{11}$$

where the constant for both forward and reverse are:

Forward: $K_{Qdo} = \dfrac{\rho A_p l D_p}{40 K_R}$, $K_{Qd} = \dfrac{\rho A_p D_p}{800 K_R{}^2}$

Reverse: $K_{Qdo} = -\dfrac{\rho A_p l D_p}{54 K_R}$, $K_{Qd} = -\dfrac{\rho A_p D_p}{1458 K_R{}^2}$

Similarly the torque become:

$$Q = K_{Qdo}\dot{\Omega} + K_{Qd}\Omega^2 \tag{12}$$

where the constant for both forward and reverse are:

Forward: $K_{Qdo} = \dfrac{\rho A_p l D_p}{40 K_R}$, $K_{Qd} = \dfrac{\rho A_p D_p}{800 K_R{}^2}$

Reverse: $K_{Qdo} = -\dfrac{\rho A_p l D_p}{54 K_R}$, $K_{Qd} = -\dfrac{\rho A_p D_p}{1458 K_R{}^2}$

From the experimental results, the thruster model without considering the time dependent term, $\dot{\Omega} = 0$ portion of the thrust and torque in (11) and (12) can be obtained as:

$$f = K_{Td}\Omega^2 \tag{13}$$

$$Q = K_{Qd}\Omega^2 \tag{14}$$

where the constant for both forward and reverse are: K_{Td} = 0.0022(forward), K_{Td} = -0.0013(reverse), K_{Qd} = (forward), K_{Qd} = 5.5 x 10^{-5} (reverse). By substituting K_R=1.923, l = 0.01m, D_p=0.09 and ρ =1024 kg/m3 into equation (11), the forward and reverse thrust in steady and non-steady condition coincides (due to the K_{Tdo} in the equation is small).

Forward: $f = 0.000847\dot{\Omega} + 0.022\Omega^2$ (15)

Reverse: $f = -0.000627\dot{\Omega} - 0.00121\Omega^2$ (16)

Similarly, this applies to the forward and reverse torque, Q in (12). For the DC motor shaft dynamics, the electromechanical model assuming small electrical time constant as compared to the mechanical time constant.

In general, the unified hydro-electromechanical dynamic model for both the dc motor shaft speed and propeller dynamic can be written as:

$$J_m\dot{\Omega} + \frac{K_m K_e}{R_m}\Omega = \frac{K_m}{R_m}V_m - K_{Qd}\Omega^2 \tag{17}$$

where V_m is the armature voltage, L_m is the armature inductance in Henry, R_m is the armature resistance in Ohms, K_m is the motor torque constant Nm/A, K_e is the motor back emf in Vs/rad, J_m is the rotor moment of inertia in Nm.s^2/rad and K_{Qd} is obtained from (12) at steady state. Equation (15) and (16) imply that the unsteady state model in (11) to (12) can be approximated by the steady state model in (13) to (14) respectively. The model steady state response match those observed in the experiments [11] as shown in Figure3. However, the approximated transient response does not match very well with the observed oscillatory response. It is observed that most oscillations diminish within 0.5s. This is relatively shorter than ROV dynamics response time.

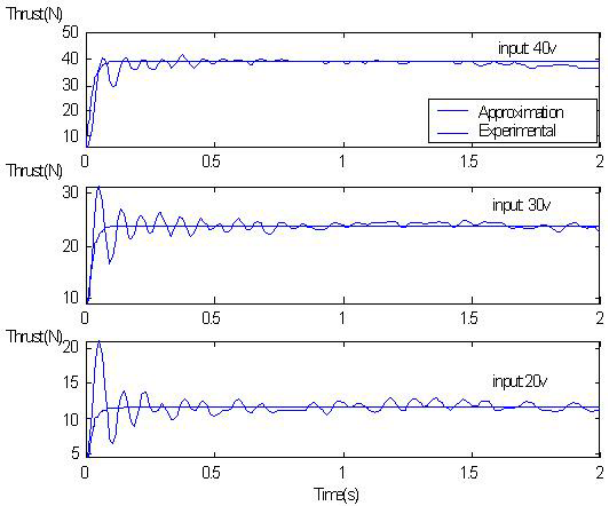

Figure 3. Time responses of the measured thrust and the thruster model

4. NONLINEAR PLANE DYNAMIC

Basically in all maneuvers, it is restricted to a horizontal and vertical plane. The horizontal plane motions consist of making a turn to the left or right at a constant altitude. States involve are simply the surge, sway and yaw motions while in the vertical plane motion moves at fixed heading or orientation with change in altitude. States involve are the surge, heave and pitch motions.

4.1 Horizontal Plane Dynamic

From the open-loop simulation with T_1 and T_2 activated, the ROV does not leave the horizontal plane. Instead the ROV's yaw and exhibit the self-regulating in roll and pitch. Hence the roll, pitch and yaw velocities are bounded as the ROV is following along the *x*-axis or $y = 0$ at a constant z that defines the horizontal dynamic. The horizontal plane dynamic with added mass terms $X_{\dot{u}}$, $Y_{\dot{v}}$ and $N_{\dot{\gamma}}$ are written as:

$$(m - X_{\dot{u}})\dot{u} + X_u u + (Y_{\dot{v}} - m)vr = \tau_u \quad (18a)$$

$$(m - Y_{\dot{v}})\dot{v} + Y_v v + (m - X_{\dot{u}})ur = \tau_v \quad (18b)$$

$$(I_z - N_{\dot{r}})\dot{r} + N_r r + (X_{\dot{u}} - Y_{\dot{v}})uv = \tau_r + u_r \quad (18c)$$

where location of the center of gravity coincide with the origin of the earth-fixed frame, that is $x_g = y_g = z_g = 0$ and the hydrodynamic damping is assumed to be linear. In (18), the dynamics in the u and v are coupled with r respectively. Using the Euler transformation matrix, the positions and orientation x, y and ψ become:

$$\dot{x} = u\cos\psi - v\sin\psi \quad (19a)$$

$$\dot{y} = u\sin\psi + v\cos\psi \quad (19b)$$

$$\dot{\psi} = r \quad (19c)$$

The z_1 to z_3 are:

$$z_1 = x\cos\psi + y\sin\psi \quad (20a)$$

$$z_2 = -x\sin\psi + y\cos\psi \quad (20b)$$

$$z_3 = \psi \quad (20c)$$

The reference variables $z_{1,r}$, $z_{2,r}$ and $z_{3,r}$ are defined correspondingly. Next, we define the tracking error as $u_e = u - u_r$, $v_e = v - v_r$. We obtain the tracking error dynamics as:

$$\dot{u}_e = -\frac{X_u}{(m - X_{\dot{u}})}u_e - \frac{(Y_{\dot{v}} - m)}{(m - X_{\dot{u}})}(v_e r_e + v_e r_r + v_r r_e) + \frac{\tau_u}{(m - X_{\dot{u}})} \quad (21a)$$

$$\dot{v}_e = -\frac{Y_v}{(m - Y_{\dot{v}})}v_e - \frac{(m - X_{\dot{u}})}{(m - Y_{\dot{v}})}(u_e r_e + u_e r_r + u_r r_e) + \frac{\tau_v}{(m - Y_{\dot{v}})} \quad (21b)$$

$$\dot{r}_e = -\frac{N_r}{(I_z - N_{\dot{r}})}N_e - \frac{(X_{\dot{u}} - Y_{\dot{v}})}{(I_z - N_{\dot{r}})}(u_e v_e + u_e v_r + u_r v_e) + \frac{\tau_r + u_r - u_{r,r}}{(I_z - N_{\dot{r}})} \quad (21c)$$

$$\dot{z}_{1,e} = u_e + z_{2,e}r_e + z_{2,e}r_r(t) + z_{2,r}r_e \quad (21d)$$

$$\dot{z}_{2,e} = v_e - z_{1,e}r_e - z_{1,e}r_r(t) - z_{1,r}r_e \quad (21e)$$

$$\dot{z}_{3,e} = r_e \quad (21f)$$

We study the problem of stabilizing the tracking error dynamics (21) by using the thruster allocation and nonlinear PD controller on the yaw dynamic. Next the problem is to find appropriate state feedback laws u_r. Similarly the vertical dynamic can be modeled as shown.

4.2 Vertical Plane Dynamic

For the T_3 and T_4 are activated during altitude change in the vertical plane, the ROV does not leave the vertical. Instead the ROV's yaw with the self-regulating in roll and pitch. Hence the roll, pitch and yaw velocities are bounded as the ROV is following along the *z*-axis or $x = 0$ at a constant y that defines the vertical plane dynamic. The vertical plane dynamic for both the translational and rotational direction with added mass term $X_{\dot{u}}$, $Y_{\dot{w}}$ and $M_{\dot{q}}$ can be written as:

$$(m - X_{\dot{u}})\dot{u} + X_u u + (m - Z_{\dot{w}})wq = \tau_u \quad (22a)$$

$$(m - Z_{\dot{w}})\dot{w} + Z_w w + (X_{\dot{u}} - m)uq = \tau_w \quad (22b)$$

$$(I_y - M_{\dot{q}})\dot{q} + M_q q + (Z_{\dot{w}} - X_{\dot{u}})uw = u_q \quad (22c)$$

where location of the center of gravity coincide with the origin of the earth-fixed frame, that is $x_g = y_g = z_g = 0$ and the hydrodynamic damping is linear. From the Euler transformation matrix, the positions and orientation x, z and θ becomes:

$$\dot{x} = u\cos\theta + w\sin\theta \quad (22d)$$

$$\dot{z} = -u\sin\theta + w\cos\theta \quad (22e)$$

$$\dot{\theta} = q \quad (22f)$$

coordinates x-x_r, w-w_r, q-q_r, since these position errors depend on the choice of the inertia frame. This problem is solved by defining the change of coordinates as proposed in [12] that considered the dynamics in a frame with an earth-fixed origin having the x, z-axis always orientated along the ROV surge and heave axis.

$$z_1 = x\cos\theta - z\sin\theta \tag{23a}$$

$$z_2 = x\sin\theta + z\sin\theta \tag{23b}$$

$$z_3 = \theta \tag{23c}$$

The reference variables $z_{1,r}$, $z_{2,r}$ and $z_{3,r}$ are defined correspondingly. Next, we define the tracking error

$$u_e = u - u_r \tag{24a}$$

$$w_e = w - w_r \tag{24b}$$

$$q_e = q - q_r \tag{24c}$$

$$z_{1,e} = z_1 - z_{1,r} \tag{24d}$$

$$z_{2,e} = z_2 - z_{2,r} \tag{24e}$$

$$z_{3,e} = z_3 - z_{3,r} \tag{24f}$$

In this way, we obtain the tracking error dynamics

$$\dot{u}_e = -\frac{X_u}{(m-X_{\dot{u}})}u_e - \frac{(m-Z_{\dot{w}})}{(m-X_{\dot{u}})}(w_e q_e + w_e q_r + w_r q_e) + \frac{\tau_u - \tau_{u,r}}{(m-X_{\dot{u}})} \tag{25a}$$

$$\dot{w}_e = -\frac{Z_w}{(m-Z_{\dot{w}})}w_e - \frac{(X_{\dot{u}}-m)}{(m-Z_{\dot{w}})}(u_e q_e + u_e q_r + u_r q_e) + \frac{\tau_w - \tau_{w,r}}{(m-Z_{\dot{w}})} \tag{25b}$$

$$\dot{q}_e = -\frac{M_q}{(I_y - M_{\dot{q}})}q_e - \frac{(Z_{\dot{w}} - X_{\dot{u}})}{(I_y - M_{\dot{q}})}(u_e w_e + u_e w_r + u_r w_e) + \frac{\tau_q}{(I_y - M_{\dot{q}})} \tag{25c}$$

$$\dot{z}_{1,e} = u_e + z_{2,e}q_e + z_{2,e}q_r(t) + z_{2,r}q_e \tag{25d}$$

$$\dot{z}_{2,e} = w_e - z_{1,e}q_e - z_{1,e}q_r(t) - z_{1,r}q_e \tag{25e}$$

$$\dot{z}_{3,e} = q_e \tag{25f}$$

We study the problem of stabilizing the tracking error dynamics (21) and (25) by using the thruster allocation and nonlinear PD controller on the yaw dynamic as shown in (21c) and left pitch motion uncontrolled.

5. CASCADED CONTROLLER DESIGN

Due to the nature of the ROV operation, the velocity and position must be controlled during the pipeline tracking respectively. This inevitably leads to a cascade control structure consisting of an inner loop for thruster allocation control and outer loop for position control in particular the yaw angle. Hence controller design aims at arriving at a closed-loop error dynamic of the form $\dot{x} = f(t, x)$ can be written as:

$$\dot{x}_1 = f_1(t, x_1) + h(t, x_1, x_2)x_2 \tag{26a}$$

$$\dot{x}_2 = f_2(t, x_2) \tag{26b}$$

where $x_1 \in \Re^n$, $x_2 \in \Re^m$ is continuously differentiable in (t, x_1) and $f_1(t, x_2)$, $h(t, x_1, x_2)$ are continuously differentiable in their arguments, and locally Lipschitz in x_2 and (x_1, x_2) respectively. Notice that if $x_2 = 0$, (26a) reduces to $\dot{x}_1 = f_1(t, x_1)$. Therefore, we can view (26a) as the system:

$$\Sigma_1 : \ \dot{x}_1 = f_1(t, x_1) \tag{27}$$

that is perturbed by the output of the system

$$\Sigma_2 : \ \dot{x}_2 = f_2(t, x_2) \tag{28}$$

For example if Σ_1 and Σ_2 are asymptotically stable, the x_2 tends to zero. In that case, the dynamics (26a) reduces to (27). Hence the (26) become asymptotically stable. But this is not true in general as the cascade system has a finite escape time or implies that the solution can be infinite at the finite time. However, in [12], it was mentioned that if the system (27) and (28) are globally uniformly asymptotically stable and the solutions of the cascaded system is globally uniformly bounded, then the system is globally uniformly asymptotically stable. Hence to ensure that the cascaded system is globally uniformly bounded, the following Corollaries are used. A slightly weaker notation than global exponential stability is the Corollary 1 [13].

Corollary 1 [13]: Assume that both (27) and (28) are globally K-exponentially stable and that continuous functions k_1: $\Re_+ \to \Re$ and k_2: $\Re_+ \to \Re$ exist such that

$$\left\|h(t, x_1, x_2)\right\| \le k_1(\left\|x_2\right\|) + k_2(\left\|x_2\right\|)\left\|x_1\right\| \tag{29}$$

Then the cascaded system (26) is globally K-exponentially stable. Next, we required the time-varying liner system (that eventually the closed-loop system will become) to be uniformly controllable. This requirement is needed before designing the controller. The details can be find in the linear system theory. The result we need in this paper is a corollary of [13].

Corollary 2 [14]: Consider the time-varying linear system

$$\dot{x} = A(\mu(t))x + Bu \tag{30}$$

$$y = C_x x \tag{31}$$

where $A(\mu(t))$ is continuous, $A(0) = 0, \mu: \Re \to \Re$ continuous. Assume that for all $\mu \neq 0$, the pair $(A(\mu), B)$ is controllable. If the following three conditions are met:

(i) $\mu(t)$ is bounded $\Rightarrow \mu(t) \leq K, \forall t \geq 0, K > 0$,

(ii) Lipschitz in $t \Rightarrow |\mu(t) - \mu(t')| \leq L|t - t'|, L > 0$, and

(iii) constants $\delta_c > 0$ and $\varepsilon > 0$ exist such that

$$\forall t \geq 0, \exists s : t - \delta_c \leq s \leq t : \left| \mu(s) \right| \geq \varepsilon \tag{32}$$

then the system (30) is uniformly completely controllable. It is also known as the "persistence of excitation condition". The Corollary 2 [14], consider a time-varying linear system is uniformly completely controllable or known as the "persistence of excitation condition" that is required before controller design. As mentioned in Section 4, the controller design aims at arriving at a closed-loop error dynamics in (37). To begin, we try to obtain the closed-loop in (37). With that, we can use one input for stabilization of the subsystem of the control system (26b). By defining the preliminary feedback:

(33)

$$u_r = u_{r,r} - (N_{\dot{r}} - X_{\dot{u}})(uv - u_r v_r) + N_r r_e + (I_z - N_{\dot{r}})\bar{v}$$

where $\bar{v}$ is a new input, the subsystem (21c) and (21f) reduces to the linear system:

$$\dot{r}_e = \bar{v} \qquad \dot{z}_{3,e} = r_e \tag{34}$$

which can easily be stabilized by choosing a suitable control law for $\bar{v}$, for example:

$$\bar{v} = -c_1 r_e - c_2 z_{3,e}, \qquad c_1, c_2 > 0 \tag{35}$$

As a result, the subsystem (21c) and (21f) are rendered globally exponentially stable. Now z_1 is left and should be chosen such that the overall closed-loop system is rendered asymptotically stable. We aim for the closed-loop system of the form (37). Besides, for asymptotic stability of the system $\dot{z}_2 = f_2(t, z_2)$, it is necessary that the part:

$$\dot{z}_1 = f_1(t, z_1) \tag{36}$$

in

$$\dot{z}_1 = f_1(t, z_1) + h(t, z_1, z_2) z_2 \tag{37}$$

$$\dot{z}_2 = f_2(t, z_2) \tag{38}$$

to be asymptotically stable. This is something that should be guaranteed by the thruster allocation control. From corollary 1, we further know that it is sufficient since both $\dot{z}_2 = f_2(t, z_2)$ and $\dot{z}_1 = f_1(t, z_1)$ (that guaranteed by the controller design) are asymptotically stable and the part $h(t, z_1, z_2) z_2$ can be ignored.

Remark 2: Considering the horizontal plane model, the closed-loop system is designed as follow. Since the pitching motion in vertical pane model is self-stabilizing, hence the control for this motion is not required. Emphasis is on the designing of heading control with the thruster allocation control on x, y, z incorporated in the cascaded system.

To begin, we designed a control law for z_2 such as way that the subsystem in closed-loop form was stabilized. Before we proceed with the controller design we assume that the stabilization of this subsystem worked out to be, $r_e \equiv 0$ and $z_{3,e} \equiv 0$. All that remains to be done is to show that the thruster allocation control using (7) for τ_u and τ_v stabilizes the system (21). It follows from Corollary 2 that the system (21) is uniformly completely controllable if the reference pitch velocity $r_r(t)$ is persistently exciting. If the $r_r(t)$ is persistently exciting, we can use any of the control laws available in literature for stabilizing the linear time-varying systems. In addition to these results, we propose the following control law.

Proposition 1: Consider the system (21) in closed loop with control law:

$$\tau_u = -\text{sign}(u_e) T_{1\times4} P_{4\times1} f_1 u_e \tag{39}$$

$$\tau_v = -\text{sign}(v_e) T_{1\times4} P_{4\times1} f_2 v_e \tag{40}$$

where T_{1x4} is the 1 x 4 thruster configuration matrix of (5), $P_{4\times1}$ is the 4 x 1 thruster readiness matrix of (6), f_1 and f_2 in (4). If $r_r(t)$ is persistently exciting than the closed-loop system with (39) and (40) are globally exponentially stable.

Proof: Consider the positive definite Lyapunov function candidate in [15]:

$$V = \frac{1}{2} x_e^T M x_e + z_e^T P z_e \tag{41}$$

Differentiating the Lyapunov function yields:

$$\begin{aligned} \dot{V} &= x_e^T M \dot{x}_e + z_e^T P \dot{z}_e \\ &= x_e^T M \left(f_1(z_1) + h_1(t, z_1, z_2) \right) + z_e^T P f_2(z_2) \\ &= x_e^T M f_1(z_1) + x_e^T M h_1(t, z_1, z_2) + z_e^T P f_2(z_2) \end{aligned} \tag{42}$$

Since the value $f_1(z_1), f_2(z_2) < 0$, $g_2(t, z_1, z_2) < 0$ and hence $\dot{V} < 0$. It is well known [16] that the origin of the closed-loop system is globally exponentially stable if the pair is uniformly completely observable (UCO). If is persistently exciting, it follows from Corollary 2 that the pair is UCO, which completes the proof.

Combining the controllers (33), (39) and (40), we are able to formulate the cascaded systems based solution to the tracking control law.

Proposition 2: Consider the ship tracking error dynamics (21) for cruising in closed loop with the control law (39), (40) and:

$$u_r = u_{r,r} - (X_{\dot{u}} - N_{\dot{r}})(u_e v_e + u_r v_e + u_r v_e) - k_d r_e - k_p z_{3,e} \tag{43}$$

where k_p and k_d are the controller constant.

If u_r, v_r, $z_{1,r}$ and $z_{2,r}$ are bounded and $r_r(t)$ is persistently exciting, then the closed-loop system (44) and (45) are globally K-exponentially stable.

Proof: Due to the design, the closed-loop system has a cascaded structure as shown in the (44) and (45). From the Proposition 1 we know that the system $\dot{z}_1 = f_1(t, z_1)$ is globally exponentially stable and from standard linear control that the system $\dot{z}_2 = f_2(t, z_2)$ is globally exponentially stable. Furthermore, due to the fact that u_r, r_r, $z_{1,r}$ and $z_{2,r}$ are bounded, $h_1(t, z_1, z_2)$ satisfies k-exponential stability. Applying Corollary 1 provides the desired result.

Notice that the only property of the system $\dot{z}_1 = f_1(t, z_1)$ that we need in this proof, is the fact that it is globally exponentially stable. Under the assumption that $r_r(t)$ is persistently exciting (which yields uniform complete controllability according to Corollary 2), more control laws are in literature that also guarantee global exponential stability of the system. In the case, we replace u_r with other control law, the proof is still holds. Therefore several other choices of u_r can be made:

$$\begin{bmatrix} \dot{u}_e \\ \dot{w}_e \\ \dot{z}_{1,e} \\ \dot{z}_{2,e} \end{bmatrix} = \underbrace{\begin{bmatrix} -\frac{X_u}{m - X_{\dot{u}}} - \frac{1}{m - X_{\dot{u}}} sign(u_e) T_{1\times 4} P_{4\times 1} f_1 & -\frac{Y_{\dot{v}} - m}{m - X_{\dot{u}}} r_r(t) & 0 & 0 \\ -\frac{m - X_{\dot{u}}}{m - Y_{\dot{v}}} r_r(t) & -\frac{Y_v}{m - Y_{\dot{v}}} - \frac{1}{m - Y_{\dot{v}}} sign(v_e) T_{1\times 4} P_{4\times 1} f_2 & 0 & 0 \\ 1 & 0 & 0 & r_r(t) \\ 0 & 1 & -r_r(t) & 0 \end{bmatrix}}_{f_1(t, z_1)} \begin{bmatrix} u_e \\ v_e \\ z_{1,e} \\ z_{2,e} \end{bmatrix} + \underbrace{\begin{bmatrix} \frac{Y_{\dot{v}} - m}{m - X_{\dot{u}}}(v_e + v_r) & 0 \\ -\frac{m - X_{\dot{u}}}{Y_{\dot{v}} - m}(u_e + u_r) & 0 \\ z_{2,e} + z_{2,r} & 0 \\ -(z_{1,e} + z_{1,r}) & 0 \end{bmatrix}}_{h_1(t, z_1, z_2)} \begin{bmatrix} r_e \\ z_{3,e} \end{bmatrix} \tag{44}$$

$$\begin{bmatrix} \dot{r}_e \\ \dot{z}_{3,e} \end{bmatrix} = \underbrace{\begin{bmatrix} -\frac{N_r + k_d}{I_z - N_{\dot{r}}} & -\frac{k_p}{I_z - N_{\dot{r}}} \\ 1 & 0 \end{bmatrix} \begin{bmatrix} r_e \\ z_{3,e} \end{bmatrix}}_{f_2(t, z_2)} \tag{45}$$

Similarly Proportional 1 and 2 can be applied to the tracking error dynamic of the vertical plane in (25).

6. COMPUTER SIMULATION

To verify our design, we performed some simulations using a block diagram simulation package in MATLAB™, SIMULINK™. In the simulation, we used the ROV parameters in [17]. The reference trajectory to be tracked is namely, the pipeline profile as shown in Figure 4. The ROV starts at the launch position with a prior knowledge of the locations. Once the ROV completed the planned path, it moves back to the initial position or stay for further instruction. At each breakpoint, the position is highlighted in the box with zero velocity. This condition is known as station keeping.

The schematic block diagram as the result of the above control system design is shown in Figure 5. Using SIMULINK™ as shown in Figure 6, the outer loop controller (as shown in Figure 7) consists of the new PD heading control with the thruster allocation in the inner loop (as shown in Figure 8). For the thruster allocation control used in the inner loop, it mainly represents the proposed thruster allocation in (39) and (40). It determines the thrusters to be activated using the velocity as its input signal. Thruster dynamic block consists mainly the thruster fluid dynamic and electro-mechanical models with the axial velocity term, u_a. Since the roll and pitch positions are self-stabilizable, they are not feedback to the controllers that as shown in the feedback filter block diagram. The gains for the control law are $K_p = K_d = 1$.

During the simulation, the ROV moves vertically down by z = 50m from its launch position followed by: (i) z = -50m, ψ = 1.57rad, (ii) z = -50m, x = 1.5m (iii) z = -45m, (iv) z = -45m, x = 3m, (v) z = -50m, ψ = -1.57rad, (vi) z = -50m, x =5m. In each phase, a constant altitude is maintained. The duration of the simulation is 2000 seconds and was done in a Pentium IV,

2.4 GHz computer. The resulting performance of this controller is shown in Figure 9. The "New-Alloc" refers to the proposed cascaded controller for the heading and the thruster allocation control while the PD-Alloc refers to the PD control for all motions with the same thruster allocation control.

To check the validity of the Corollary 1, term in the right-hand side and left-hand side are plotted and shown to be valid throughout the simulation. Besides validating the Corollary 1, the Corollary 2 (known as state controllability or the "persistence of excitation condition") of the system is verified. The pair $(A(\mu(t)), B)$ is controllable since the three condition as follows are met: (i) μ is bounded, (ii) μ is Lipschitz in t, and (iii) constants $\delta_c > 0$ and $\varepsilon > 0$ exist such that

$$\forall t \geq 0, \exists s : t - \delta_c \leq s \leq t : \left| \mu(s) \right| \geq \varepsilon$$

As compared with the PD for all DOF with the same thruster allocation control, the overshoot in sway motion is smaller that the proposed controller. But to achieve the desired position, the settling time for the proposed controller is longer. Both roll and pitch angles are self-stabilizing at all time. As shown in Figure 10, the voltage input to the thrusters is smaller and less peaking in the proposed controller. As observed, only some thrusters are activated for certain time due to the requirement of the ROV's maneuvering.

Hence the presented cascaded controller can be applied on the ROV RRC II. To determine the robustness of the controller, for example a ten percents variation in the mass inertia and hydrodynamic damping terms are introduced in the model. As shown in Figure 11, the proposed controller has some degree of robustness against the parametric uncertainty.

7. CONCLUSIONS

In this paper, the general equation for ROV was described and applied on the RRC ROV II. The thruster dynamics and allocation were formulated for the inner loop control. The thruster allocation control uses the vehicle's velocity feedback for thrust allocation instead of using an open-loop real-time thrust optimization while the outer loop uses the nonlinear PD controller on the yaw dynamic.

As compared to conventional Proportional-Derivative (PD) controller used for all motions, the proposed cascaded controller provides a simple structure for outer loop control and better thrust allocation for the ROV's plane maneuvering. Besides the overall cascaded control was proven to render the tracking error dynamic globally k-exponentially stable.

Computer simulations are performed on these controllers and shown to be robust against parametric uncertainty due to model inaccuracy.

Table 1. Notations used in ROV

DOF	Motion Descriptions	Positions and Orientations	Linear and Angular Velocities
1	Motions in the x-direction (surge)	x	u
2	Motions in the y-direction (sway)	y	v
3	Motions in the z-direction (heave)	z	w
4	Rotations about the x-axis (roll)	ϕ	p
5	Rotations about the y-axis (pitch)	θ	q
6	Rotations about the z-axis (yaw)	ψ	r

Acknowledgement

The authors would like to thanks all the project team members from NTU Robotics Research Centre especially Mr. Lim Eng Cheng, Ms. Agnes S.K. Tan, Ms. Ng Kwai Yee and Mr. You Kim San.

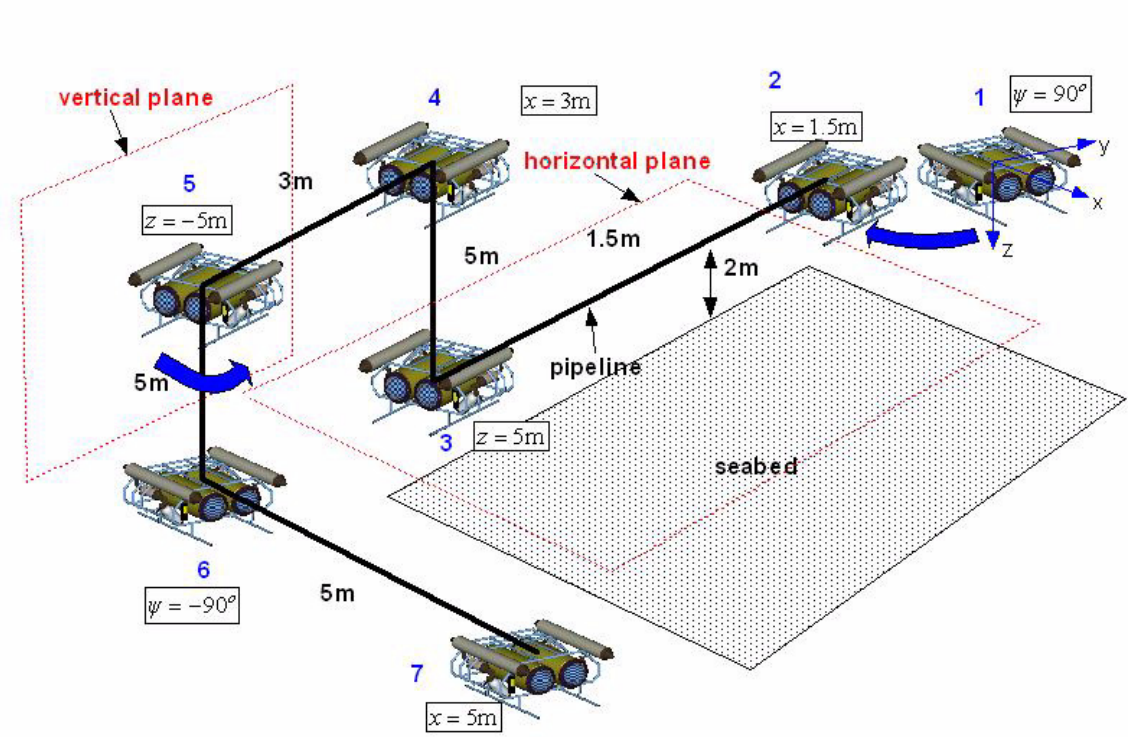

Figure 4. Pipeline profile for RRC ROV II

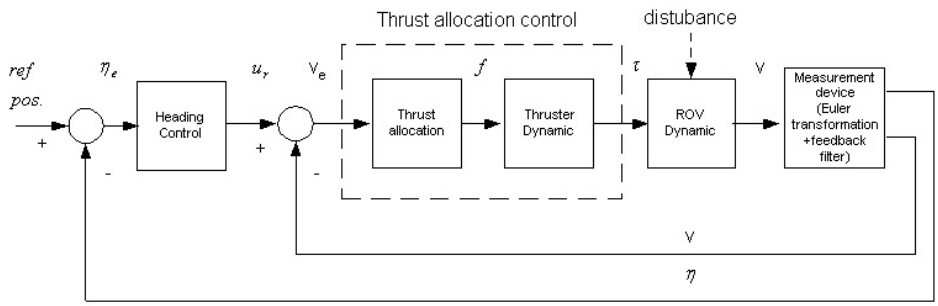

Figure 5. RRC ROV II schematic block diagram

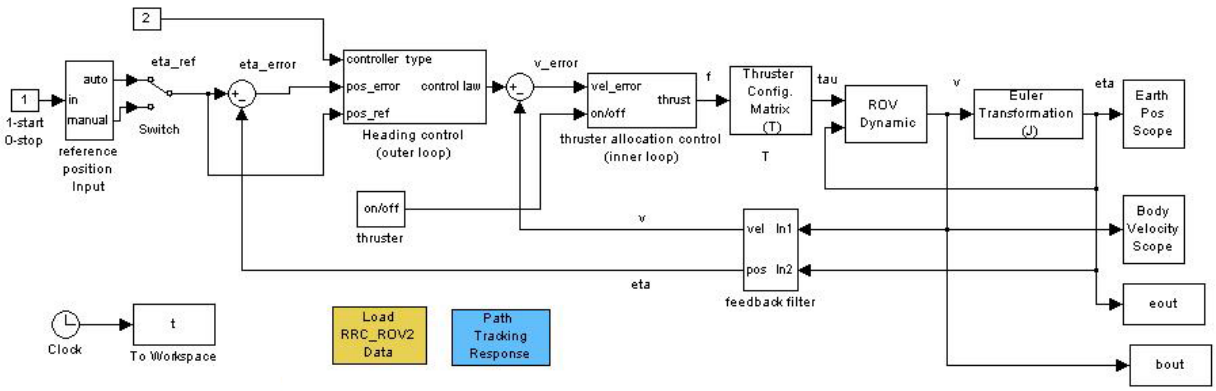

Figure 6. RRC ROV II simulation block diagram by SIMULINK™

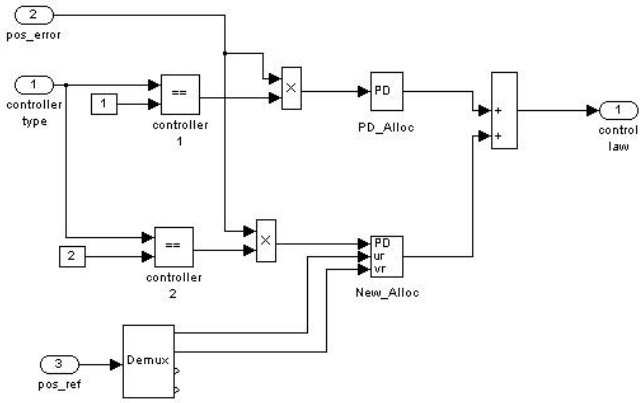

Figure 7. Heading control (for outer loop) block diagram by SIMULINK™

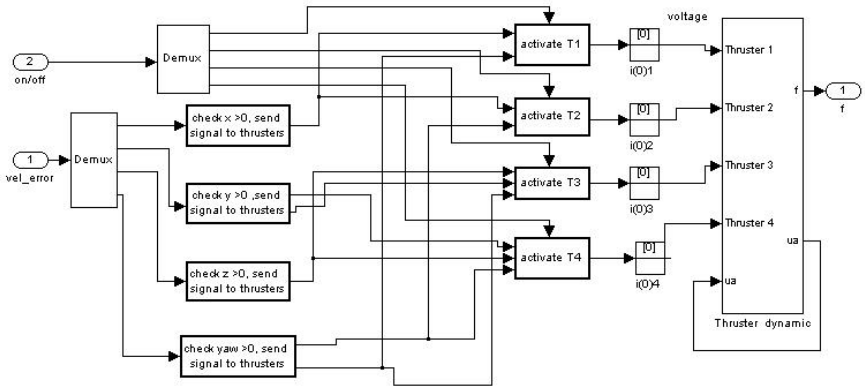

Figure 8. Thruster allocation control (for inner loop) block diagram by SIMULINK™

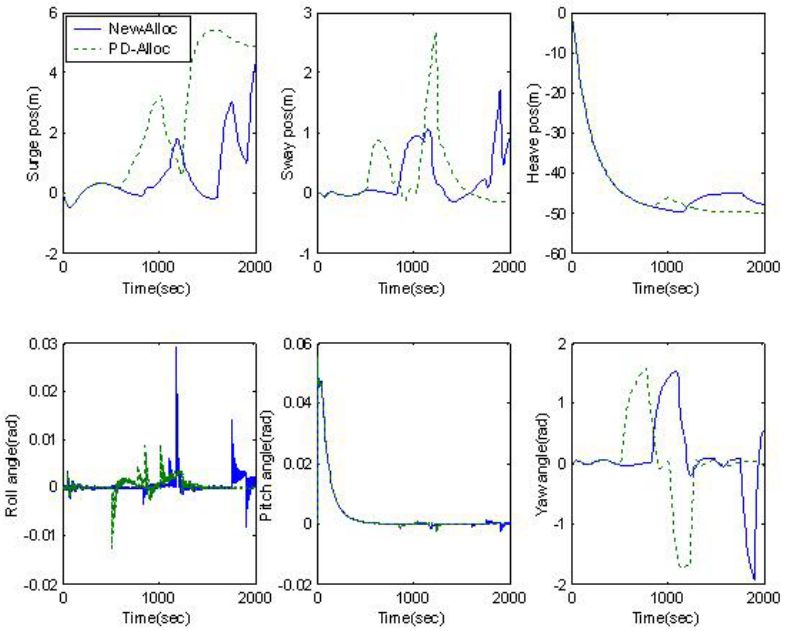

Figure 9. Position response of the controllers

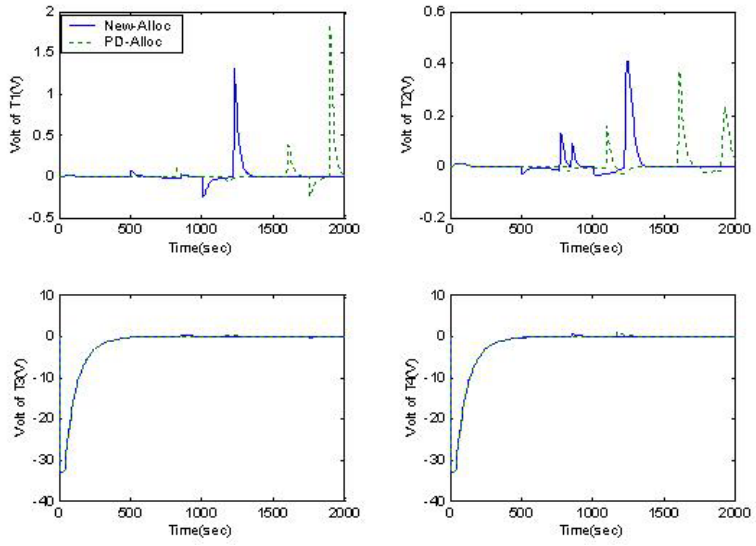

Figure 10. Voltage input to T_1 to T_4

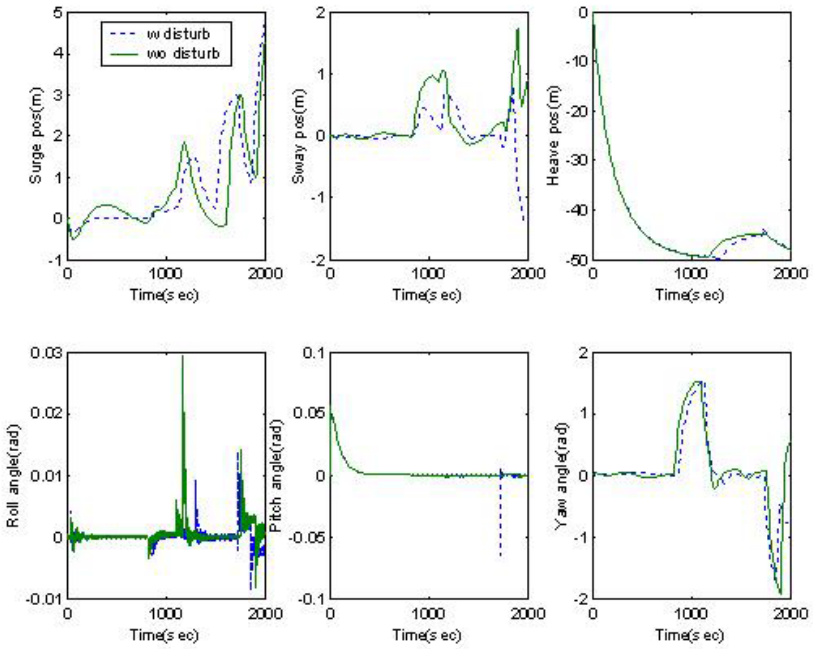

Figure 11. Position response of system under parametric uncertainty

REFERENCES

[1] T. I. Fossen, "Guidance and Control of Ocean Vehicles, Chichester", Wiley, 1994.

[2] W. C. Canudas, D. Olguin & M. Perrer, "Robust nonlinear control of an underwater vehicle", Proc. IEEE Int. Conf. Robotics and Automation, Leuven, Belgium, 1998, pp. 452–457.

[3] P. J. Craven, R. Sutton & R. S. Burns, "Control Strategies for Unmanned Underwater Vehicles", J. Navig., Vol. 51, No. 2, 1998, pp. 79–105.

[4] T. I. Fossen, "Marine Control Systems", Trondheim, Marine Cybernetics AS, 2002.

[5] J. Garus & Z. Kitowski, "Sliding control of motion of underwater vehicle", Marine Technology III (T. Graczyk, T. Jastrzebski and C.A. Brebia, Eds.), Southampton: WIT Press, 1999, pp. 603–611.

[6] M. R. Katebi & M. J. Grimble, "Integrated control, guidance and diagnosis for reconfigurable underwater vehicle control", Int. J. Syst. Sci., Vol. 30, No. 9, 1999, pp. 1021–1032.

[7] S. Berge & T. I. Fossen, "Robust control allocation of overactuated ships: Experiments with a model ship", Proc. 4-th IFAC Conf. Manoeuvring and Control of Marine Craft, Brijuni, Croatia, 1997, pp. 161–171.

[8] J. Garus, "A method of power distribution in power transmission system of remotely operated vehicle", J. Th. Appl. Mech., Poland, Vol. 42, No. 2, 2004, pp. 239–251.

[9] O. J. Sordelen, "Optimum thrust allocation for marine vessels", Contr. Eng. Pract., Vol. 5, No. 9, 1997, pp. 1223–1231.

[10] L. L.Whitcomb & D. Yoerger, "Preliminary experiments in model-based thruster control for underwater vehicle position control", IEEE J. Ocean. Eng., Vol. 24, No. 4, 1999, pp. 481–494.

[11] P.L. Cheng, M.W.S. Lau, E. Low & G.G. L. Seet, "Modeling of a thruster for an underwater robotic vehicle", Proceedings of the 11th International Symposium on Unmanned Untethered Submersible Technology (UUST'99), Autonomous Undersea Systems Institute, New Hampshire, August 1999, pp. 455-466.

[12] E. Panteley & A. Loría, "Growth rate conditions for uniform asymptotic stability of cascaded time-varying systems," Automatica, vol. 37, Mar 2001, pp. 453–460.

[13] O. Sørdalen & O. Egeland, "Exponential stabilization of nonholonomic chained systems," IEEE Trans. Automat. Contr., Vol. 40, Jan 1995, pp.35–49.

[14] G. Kern, "Uniform controllability of a class of linear time-varying systems," IEEE Trans. Automat. Contr., vol. 27, Feb 2002, pp. 208–210.

[15] T. I. Fossen & J. P. Strand, "Passive nonlinear observer design for ships using Lyapunov methods: Experimental results with a supply vessel," Automatica, Vol. 35, No. 1, 1999, pp. 3–16.

[16] H. Khalil, "Nonlinear Systems", 2nd ed. Upper Saddle River, NJ: Prentice- Hall, 1996.

[17] T.H. Koh, M.W.S. Lau, E. Low, G.G. L. Seet & P. L. Cheng, "Preliminary studies of the modeling and control of a twin-barrel underactuated underwater robotic vehicle", ICARCV, 2002, pp. 1043-1047.

Biographies

Cheng Siong Chin is the PhD candidate in School of Mechanical and Aerospace Engineering at Nanyang Technological University, Singapore. He received the M.Sc. in Advanced Control and System Engineering from The University of Manchester (formerly known as University of Manchester Institute of Science and Technology) in 2001 and was a Research Assistant in Control and Power group at Imperial College London. His interests are in control application on linear and nonlinear dynamic systems. He is a member of IEE and a Chartered Engineer (C.Eng) registered in UK.

Micheal Wai Shing Lau is the Director of Mechatronic and Control and Associate Professor in School of Mechanical and Aerospace Engineering at Nanyang Technological University, Singapore. He graduated with Ph.D from Aston University, in United Kingdom. His interests are in active vibration control, modelling and control of underwater robotic vehicles and mechatronics system design. He is an associate member of IEEE.

Eicher Low is the Associate Professor in School of Mechanical and Aerospace Engineering at Nanyang Technological University, Singapore. Graduated with Ph.D from University of Minnesota, in USA. His interests are in Mathematical modeling of dynamical and physiological systems, control-oriented system identification, robust control system synthesis with applications in helicopter flight control, unmanned aerial vehicle (UAV) and underwater robotic vehicles. He is a senior member of AIAA, a member of IEEE and ASME.

Gerald Gim Lee Seet is the Director of Robotic Research Centre and also the Associate Professor in School of Mechanical and Aerospace Engineering at Nanyang Technological University, Singapore. Graduated with Ph.D from Aston University, in United Kingdom. His interests are in mechatronics, robotics and hydraulics. He is a member of IEE, a fellow of IMechE and a Chartered Engineer (C.Eng) registered in UK.

APPROXIMATE OBSERVER ERROR LINEARIZATION FOR A CLASS OF SEMI-EXPLICIT DIFFERENTIAL-ALGEBRAIC EQUATIONS

K. Röbenack
Institut für Regelungs- und Steuerungstheorie, Fakultät Elektrotechnik und Informationstechnik, Technische Universität Dresden, Germany

ABSTRACT

Many complex systems can be described by network models or modelling languages. From a mathematical point of view, these systems are modelled by differential-algebraic equations. Quite often, several quantities occurring in the model cannot be measured directly and must therefore be reconstructed by observer schemes. We consider the problem of observer design for nonlinear differential-algebraic equations. Our approach is based on an approximate observer error linearization technique. The design method is applicable to a class of semi-explicit differential-algebraic equations. The observer design is illustrated on an example system.

Keywords

Observer design, Observer Canonical Form, Differential-Algebraic Equations.

1. INTRODUCTION

Using differential-geometric concepts, several observer design methods for (explicit) nonlinear state-space systems have been developed [1-4]. Most of these methods rely on certain normal forms (see [5, 6]). For example, the design method developed in [7] uses the observability canonical form. Similarly, the Byrnes-Isidori normal form is used in [8].

One particularly interesting approach suggested in [9, 10] uses the observer canonical form, where linear dynamics are driven by a nonlinear output injection. Unfortunately, the existence conditions for this normal form are very restrictive. Therefore, several approaches to circumvent this difficulty have been developed. These methods are often based on an approximate observer canonical form [11-13].

Quite often, real-world systems are modelled by differential-algebraic equations (DAEs), see [14] and references cited there. Although there are many observer design methods for explicit nonlinear systems available, systematic design methods for implicit systems are rare [15-17]. For example, the work in [7] is extended in [18] to index one DAEs. Another approach is suggested in [19, 20], where implicit observers in Hessenberger form of index one and two are used for nonlinear state-space systems. This method is extended in [21] to observe semi-explicit DAEs.

We consider the problem of observer design for nonlinear semi-explicit DAEs. This paper is based on the observer error linearization approach known from nonlinear state-space systems [9, 10, 22]. To relax the existence conditions we take the approximations suggested in [11-13] into account.

In Section 2 we recall the existence conditions of the normal forms required for the observer design. The observer design procedure is explained in Section 3, where we also discuss conditions for convergence. Our approach is applied to an example system in Section 4. Finally, the conclusions are drawn in Section 5.

2. NORMAL FORMS

2.1 Observer Canonical Form

We consider a single-output (possibly multi-input) system in form of a semi-explicit DAE

$$\begin{aligned} \dot{x} &= f(x,w,u) \\ 0 &= g(x,w,u) \\ y &= h(x) \end{aligned} \tag{1}$$

with smooth maps $f : \Re^n \times \Re^m \times \Re^r \to \Re^n$ and $g : \Re^n \times \Re^m \times \Re^r \to \Re^m$. The map $h : \Re^n \to \Re$ is the output map. Given an smooth input signal u, we assume that (1) has an unique smooth solution for all initial values belonging to a manifold $\mathbf{M} \subset \Re^n \times \Re^m$, i.e., $\mathbf{M}$ is the manifold of consistent initial values [14, 23].

Without loss of generality we can rewrite the first subsystem of (1) as

$$\dot{x} = f_0(x) + f_1(x,w,u) \tag{2}$$

with $f_0 : \Re^n \to \Re^n$ and $f_1 : \Re^n \times \Re^m \times \Re^r \to \Re^n$. We want to find a diffeomorphic change of coordinates

$$z = T(x), \quad x = S(z) \tag{3}$$

that transforms subsystem (2) into *observer canonical form* [5, 6]

$$\dot{z} = Az + \alpha_0(y) + \alpha_1(y,w,u), \quad y = c^T z, \tag{4}$$

*Corresponding author: *E-mail:* klaus@roebenack.de

 ISSN: 1743-9310

where w is treated as an additional input. The pair (A, c^T) is in dual Brunovsky form

$$A=\begin{pmatrix}0 & 0 & \cdots & 0\\ 1 & 0 & & \vdots\\ & \ddots & \ddots & 0\\ 0 & & 1 & 0\end{pmatrix},\quad c^T=\begin{pmatrix}0 & \cdots & 0 & 1\end{pmatrix}, \tag{5}$$

the map $\alpha_0 : \Re \times \Re^n$ is a pure output injection, and $\alpha_1 : \Re \times \Re^m \times \Re^r \to \Re^n$ acts as an input-output injection. The existence of (4) is governed by the following theorem [9, 22]:

Theorem 1: *Let $x_0 \in \Re^n$. There exists a local diffeomorphism (3) in a neighbourhood of x_0 transforming (2) into (4) if*

A1. $$\dim\left(dh, L_{f_0}dh, \ldots, L_{f_0}^{n-1}dh\right) = n$$

A2. $$\left[ad_{f_0}^i, ad_{f_0}^j\right] = 0,\ 0 \le i, j \le n-1$$

A3. $$\left[f_1, ad_{f_0}^i v\right] = 0,\ 0 \le i \le n-2$$

holds for all x in a neighbourhood of x_0, where the vector field v is the unique solution of

$$L_v L_{f_0}^i h = \begin{cases}0 & \text{for} \quad i = 0, \ldots, n-2\\ 1 & \text{for} \quad i = n-1.\end{cases} \tag{6}$$

The notation of Lie derivatives and Lie brackets used in Theorem 1 is by now standard in nonlinear control theory (see [24, 25] and the appendix of this paper). Condition A1 is the well-known observability rank condition, where "dim" stands for dimension. Unfortunately, the integrability condition A2 is violated for many systems of practical relevance. Condition A3 concerns the occurrence of the inputs in normal form coordinates.

If A1 holds, the vector field v can be obtained from (6). Based on the Simultaneous Rectification Theorem [25, Theorem 2.36] we can compute the inverse transformation

$$x = S(z) = \Phi_{z_1}^{v} \circ \Phi_{z_2}^{ad_{-f_0}v} \circ \cdots \circ \Phi_{z_2}^{ad_{-f_0}^{n-1}v}\left(x_0\right) \tag{7}$$

with $z = (z_1, \ldots, z_n)^T$, where Φ_t^v denotes the flow of a vector field v at time t. Unfortunately, the calculation of the flows required in (7) is often difficult. However, the flows can be approximated by Lie series, the coefficients of which can be calculated using Taylor series arithmetic [26, 27]. Alternative approaches to compute the form (4) have been suggested in [28, 29].

2.2 Approximate Observer Canonical Form

Only a small class of nonlinear systems can be transformed into observer canonical form (4). To circumvent this difficulty several approximation techniques have been developed [11-13]. The main idea of these approaches is the decomposition of the system into (2) such, that the unforced part

$$\dot{x} = f(x), \quad y = h(x)$$

can be transformed into (4). If we apply the associated transformation (3) to the first subequation of (1) we obtain an *approximate observer canonical* form

$$\dot{z} = Az + \alpha_0(y) + \hat{\alpha}_1\left(y, Hz, w, u\right), \quad y = c^T z \tag{8}$$

with a matrix $H \in \Re^{n \times q}$

and a map $\hat{\alpha}_1 : \Re \times \Re^q \times \Re^m \times \Re^r \to \Re^n$. In the additional nonlinearity $\hat{\alpha}_1$, the component z_n of the state vector z is replaced by $y = c^T z$. In general, the map $\hat{\alpha}_1$ will also depend on $q < n$ other components z_n of z. These q components are selected by the matrix H. Based on Theorem 1 we can summarize the existence conditions for (8) as follows [13]:

Theorem 2: *Consider the first subsystem (2) of system (1) in a neighbourhood of $x_0 \in \Re^n$. Assume conditions A1 and A2 of Theorem 1 hold. Then there exists a local diffeomorphism (3) in a neighbourhood of x_0 transforming subsystem (2) into (8).*

The vector field f_0 is used to construct the change of coordinates (7). This transformation is then applied to the vector field f_1 in order to obtain $\hat{\alpha}_1$, i.e.,

$$\hat{\alpha}_1\left(y, Hz, w, u\right) = \left(S'(z)\right)^{-1} f_1\left(S(z), w, u\right)\Big|_{z_n = y}.$$

3. OBSERVER DESIGN

3.1 Structure of the Observer

Assume subsystem (2) fulfils the conditions of Theorem 2. For system (1) we suggest an observer of the following structure:

$$\begin{aligned}\dot{\hat{z}} &= A\hat{z} + \alpha_0(y) + \hat{\alpha}_1\left(y, H\hat{z}, \hat{w}, u\right) + k\left(y - c^T\hat{z}\right)\\ 0 &= g(\hat{x}, \hat{w}, u)\\ \hat{x} &= S\left(\hat{z}\right)\end{aligned} \tag{9}$$

with a constant gain vector $k \in \Re^n$. The observation error $\tilde{z} = z - \hat{z}$ of the first subsystems of plant (1) and the observer (9) is governed by the error dynamics

$$\dot{\tilde{z}} = \left(A - kc^T\right)\tilde{z} + \hat{\alpha}_1(y, Hz, w, u) - \hat{\alpha}_1(y, H\hat{z}, \hat{w}, u). \tag{10}$$

The output injection α_0 is cancelled out between (8) and (9). Moreover, the maps $\hat{\alpha}_1$ in (10) differ only in the second and third argument. To obtain a prescribed characteristic polynomial

$$\det\left(sI - \left(A - kc^T\right)\right) = p_0 + p_1 s + \cdots + p_{n-1}s^{n-1} + s^n$$

of the linear part of (10) we set $k = (p_0, \ldots, p_{n-1})^T$. If additionally the conditions of Theorem 1 are fulfilled, the second argument of the nonlinearities in (10) can be omitted and the map $\hat{\alpha}_1$ can be replaced by α_1, by which we simplify the error dynamics (10).

In practical applications, it is often convenient to implement the observer (9) in original coordinates. In this case, we obtain

$$\begin{aligned} \dot{x} &= f(\hat{x},\hat{w},u)+\ell(y,\hat{x},\hat{w},u) \\ 0 &= g(\hat{x},\hat{w},u) \end{aligned} \tag{11}$$

with the correction term

$$\begin{aligned} \ell(y,\hat{x},\hat{w},u) &= \left(T'(\hat{x})\right)^{-1}\left[\alpha_0(y)+\hat{\alpha}_1(y,H\hat{z},\hat{w},u)\right. \\ &- \left.\alpha_0(h(\hat{x}))-\hat{\alpha}_1(h(\hat{x}),H\hat{z},\hat{w},u)+k(y-h(\hat{x}))\right]. \end{aligned}$$

3.2 Notes on the Convergence

The index of the DAE system (1) plays a crucial role concerning its analytical and numerical properties [14]. In fact, there exist several different index concepts. The most prominent examples are the differentiation index, the perturbation index, and the tractability index (e.g., see [31, 32]). Up to now, we made no assumption regarding the index of (1). Indeed, the observer design procedure given in Section 3.1 can be carried out for any index.

To analyze the convergence of the observer (9) or (11) we will restrict ourselves to the index one case. Consider system (1) at a point $(x_0, w_0) \in \mathbf{M}$ with

$$\det\left(\frac{\partial g}{\partial w}(x_0,w_0)\right)\neq 0$$

By the Implicit Function Theorem there exists a smooth map Ξ defined in a neighbourhood of x_0 such that

$$g(x,\Xi(x,u),u)=0$$

We define a map γ by

$$\gamma(y,z,u)=\hat{\alpha}_1(y,Hz,\Xi(S(z),u),u)$$

whereby (10) becomes

$$\dot{\tilde{z}}=\left(A-kc^T\right)\tilde{z}+\gamma(y,z,u)-\gamma(y,\hat{z},u). \tag{12}$$

The observer trajectories converge to the trajectories of the original system (1) if the equilibrium $\tilde{z} = 0$ of (12) is asymptotically stable. Note that the map γ can be obtained from

$$\gamma(y,z,u)=\left(S'(z)\right)^{-1} f(S(z),\Xi(S(z),u),u)\Big|_{z_n=y}.$$

The nonlinearities occurring in (12) differ only in one argument. Moreover, these nonlinearities are symmetric w.r.t. z and $\hat{z}$. By construction, the map γ is smooth and therefore Lipschitz on any compact subset of its domain. Error dynamics of the form (12) are well-known from high gain observer design [33]. The choice of the gain vector k depends of the Lipschitz constant of the nonlinear map γ. Conditions for the convergence of the observer and procedures for the computation of k can be found in [34, 35]. We recall the following result [35]:

Theorem 3: *Consider the error dynamics (12). Assume that γ has a Lipschitz constant $\nu > 0$ in the domain of interest. The equilibrium $\tilde{z} = 0$ of (12) is (locally) asymptotically stable if $k \in \Re^n$ can be chosen such that*

$$\left\|\left(sI-\left(A-kc^T\right)\right)^{-1}\right\|_\infty < \frac{1}{\nu}$$

where $\|\bullet\|_\infty$ denotes the $\boldsymbol{H}_\infty$ norm of a transfer function [36].

4. EXAMPLE

We consider the model

$$\begin{aligned} \dot{I} &= \frac{1}{L}(U_1-U_2) \\ \dot{U}_2 &= \frac{1}{C}\left(I-\phi(U_2)\right) \\ 0 &= \frac{1}{R}\left(U_1-U_{op}\right)+I \\ y &= I \end{aligned} \tag{13}$$

of a tunnel diode oscillator [37] with the cubic nonlinearity

$$\phi(U)=a_1U+a_2U^2+a_3U^3$$

and the (normalized) parameter values $L = 1$, $C = 10^{-7}$, $R = 1$, $U_{op} = 0.25$, $a_1 = 1.80048$, $a_2 = -8.766$ and $a_3 = 10.8$. The circuit is sketched in Figure 1. The state $x = (I, U_2)^T$ of the first subsystem consists of the current I flowing through the inductivity and the voltage U_2 over the tunnel diode. For the decomposition (2) we choose $f_0 = f|_{U_1 = 0}$.

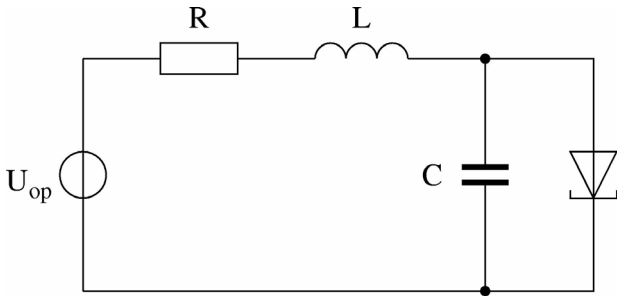

Figure 1. Circuit of the tunnel diode oscillator

With the measured current I we will estimate the voltages U_1 and U_2 using the observer (9). Based on (6) we obtain the vector fields

$$v(x)=\begin{pmatrix} 0 \\ -L \end{pmatrix}$$

and

$$ad_{-f_0}v(x)=\begin{pmatrix} 1 \\ \frac{L}{C}\phi'(x_2) \end{pmatrix}=\begin{pmatrix} 1 \\ \frac{L}{C}\left(a_1+2a_2x_2+3a_3x_2^2\right) \end{pmatrix}$$

The flow of both vector fields can be computed symbolically, but the flow of the vector field $ad_{-f_0}v(x)$ is quite complicated. However, the transformation (3) can be simplified by an appropriate choice of x_0. Indeed, for $x_0 = (0, U_{20})^T$ with

$$U_{20} = -\frac{a_2}{a_3} \pm \frac{1}{3a_3}\sqrt{a_2^2 - 3a_1a_3}$$

we obtain the linear transformation

$$x = S(z) = \begin{pmatrix} z_2 \\ U_{20} - Lz_1 \end{pmatrix}$$

The resulting observer (9) has the form

$$\begin{aligned} \dot{\hat{z}}_1 &= \frac{1}{LC}\left(\phi(U_{20} - L\hat{z}_1) - y\right) + p_0(y - \hat{z}_2) \\ \dot{\hat{z}}_2 &= \hat{z}_1 + \frac{1}{L}(U_1 - U_{20}) + p_1(y - \hat{z}_2) \\ 0 &= \frac{1}{R}(U_1 - U_{op}) + \hat{I} \\ \hat{I} &= \hat{z}_2 \\ \hat{U}_2 &= U_{20} - L\hat{z}_1 . \end{aligned} \tag{14}$$

The simulation was carried out with the tool SCILAB [38] using the differential-algebraic system solver DASSL [14]. We used the initial values $I(0) = 0.1$, $U_2(0) = 0.1$, $\hat{z}_1(0) = 0$, $\hat{z}_2(0) = 0$. The observer eigenvalues were placed at -50 and -100, i.e., $p_0 = 5000$ and $p_1 = 500$. Figure 2 shows the computed trajectories. We used solid lines for system (13) and dashed lines for the observer (14). The plant (13) has a limit cycle. It can be seen that the trajectories of the observer (14) synchronize with this limit cycle.

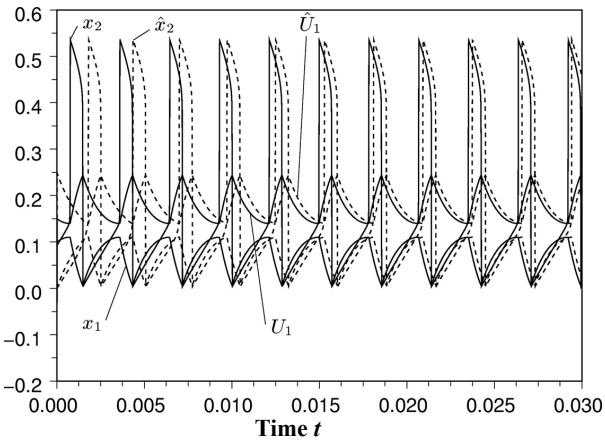

Figure 2. Trajectories of System (13) and observer (14)

5. CONCLUSIONS

A new method for observer design for nonlinear semi-explicit DAE systems has been proposed. The design procedure is based on an appropriate transformation. The new coordinates are chosen such that the error dynamics can be seen as a linear system with nonlinear perturbations. Moreover, some nonlinearities (namely the output injection of the underlying unforced system) do not occur at all in the error dynamics. In case of an index one system, the convergence of the observer can be achieved using high gain techniques known from nonlinear state-space systems.

APPENDIX

In the following we recall some definitions of differential geometry used in nonlinear control. Further details can be found in [24, 25].

Let $\Re^n$ denote the n-dimensional real vector space consisting of vectors (column vectors). Moreover, consider a vector field $v : \Re^n \to \Re^n$. The Lie derivative of a scalar field $h : \Re^n \to \Re$ along v is defined by

$$L_v h(x) = dh(x)v(x) = \frac{\partial h(x)}{\partial x} v(x)$$

where $dh = h'$ denotes the gradient of h. Iterated Lie derivatives along the same vector field are denoted by

$$L_v^m h(x) = L_v^{m-1} L_v h(x) \quad \text{with} \quad L_v^0 h(x) = h(x)$$

The dual space of $\Re^n$ denoted by $\Re^{n*}$ consists of covectors (row vectors). A map $\omega : \Re^n \to \Re^{n*}$ is called covector field. A covector field is called a differential form if it is the gradient of a scalar field. The Lie derivative of the covector field ω along the vector field v is given by

$$L_v \omega(x) = v^T(x)\left(\frac{\partial \omega^T(x)}{\partial x}\right) + \omega(x)\frac{\partial v(x)}{\partial x}$$

where the superscript T denotes transposition. As above, iterated Lie derivatives along the vector field v are denoted by

$$L_v^m \omega(x) = L_v^{m-1} L_v \omega(x) \quad \text{with} \quad L_v^0 \omega(x) = \omega(x)$$

Let $g : \Re^n \to \Re^n$ be a second vector field. The Lie derivative of g along v defined by

$$[v, g](x) = \frac{\partial g(x)}{\partial x} v(x) - \frac{\partial v(x)}{\partial x} g(x)$$

is also called Lie bracket. Iterated Lie brackets are denoted by

$$ad_v^m g(x) = \left[v, ad_v^{m-1} g(x)\right](x) \quad \text{with} \quad ad_v^0 g(x) = g(x)$$

REFERENCES

[1] B. Jakubczyk, W. Respondek, & K. Tchon, K., Eds., "Geometric Theory of Nonlinear Control Systems", Wroclaw: Wroclaw Technical University Press, Poland, 1985, ISSN: 0324-9794.

[2] B.L. Walcott, M. Corless, & S.H. Zak, "Comparative study of non-linear state-observation techniques", International Journal of Control, Vol. 45, No. 2, 1987, pp. 2109–2132.

[3] E.A. Misawa, & J.K. Hedrick, “Nonlinear observers — a state-of-the art survey,” Journal of Dynamic Systems, Measurement, and Control, Vol. 111, 1989, pp. 344–352.

[4] H. Nijmeijer, & T.I. Fossen, Eds., “New Directions in Nonlinear Observer Design”, Vol. 244 of Lecture Notes in Control and Information Science, London: Springer-Verlag, UK, 1999, ISBN: 1-85233-134-8.

[5] M. Zeitz, “Canonical forms for nonlinear systems”, Jakubczyk et al [1], 1985, pp. 255–278.

[6] M. Zeitz, “Canonical forms for nonlinear systems”, Proc. IFAC-Symposium Nonlinear Control System Design, Capri, Italy, 1989.

[7] J.P. Gauthier, H. Hammouri, & S. Othman, “A simple observer for nonlinear systems — application to bioreactors”, IEEE Transactions on Automatic Control, Vol. 37, No. 6, 1992, pp. 875–880.

[8] N.H. Jo, & J.H. Seo, “Input output linearization approach to state observer design for nonlinear system”, IEEE Transactions on Automatic Control, Vol. 45, No. 12, 2000, pp. 2388–2393.

[9] A.J. Krener, & A. Isidori, “Linearization by output injection and nonlinear observers”, Systems & Control Letters, Vol. 3, 1983, pp. 47–52.

[10] D. Bestle, & M. Zeitz, “Canonical form observer design for non-linear time-variable systems”, International Journal of Control, Vol. 38, No. 2, 1983, pp. 419–431.

[11] A. Banaszuk, & W. Sluis, “On nonlinear observers with approximately linear error dynamics”, Proc. American Control Conferences, Albuquerque, NM, USA, 1997, pp. 3460–3464.

[12] A.F. Lynch, & S.A. Bortoff, “Nonlinear observers with approximately linear error dynamics: The multivariable case”, IEEE Transactions on Automatic Control, Vol. 46, No. 7, 2001, pp. 927–932.

[13] J.A. Moreno, “Approximate observer error linearization by dissipativity”, Meurer et al. [30], 2006, pp. 35–51.

[14] K.E. Brenan, S.L. Campbell, & L.R. Petzold, “Numerical Solution of Initial-Value Problems in Differential-Algebraic Equations”, Philadelphia, PA: SIAM, USA, 1996, ISBN: 0-89871-353-6.

[15] M. Boutayeb, & M. Darouach, “Observer design for non linear descriptor systems”, Proc. 34th IEEE Conf. Decision and Control, New Orleans, LA, USA, 1995, pp. 2369–2374.

[16] G. Zimmer, & J. Meier, “On observing nonlinear descriptor systems”, Systems & Control Letters, Vol. 32, No. 1, 1997, pp. 43–48.

[17] N. Kidane, Y. Yamashita, & H. Nishitani, “Observer based I/O-linearizing control of high index DAE systems”, Proc. American Control Conference, Denver, CO, USA, 2003, pp. 3537– 3542.

[18] H. Hammouri, & N. Marchand, “High gain observer for a class of implicit systems”, Proc. 39th IEEE Conf. Decision and Control, Sydney, Australia, 2000, pp. 804-808.

[19] D. von Wissel, R. Nikoukhah, S.L. Campbell, & F. Delebecque, “Nonlinear observer design using implicit system descriptions”, Proc. Computational Engineering in Systems Applications, Lille, France, 1996, pp. 404–409.

[20] R. Nikoukhah, “A new methodology for observer design and implementation”, IEEE Transactions on Automatic Control, Vol. 43, No. 2, 1998, pp. 229–234.

[21] E. Frisk, & J. Aslund, “An observer for semi-explicit differential-algebraic equations”, Preprints of the 16th IFAC World Congress, Prague, Czech Republic, 2005.

[22] R. Marino, “Adaptive observers for single output nonlinear systems”, IEEE Transactions on Automatic Control, Vol. 35, No. 9, 1990, pp. 1054–1058.

[23] P.J. Rabier, & W.C. Rheinboldt, “A general existence and uniqueness theory for implicit differential-algebraic equations”, Differential and Integral Equations, Vol. 4, No. 3, 1991, pp. 563–582.

[24] A. Isidori, “Nonlinear Control Systems: An Introduction”, Berlin: Springer-Verlag, Germany, 1995, ISBN: 3-540-19916-0.

[25] H. Nijmeijer, & A.J. van der Schaft, „Nonlinear Dynamical Control systems“, Berlin: Springer-Verlag, Germany, 1990, ISBN: 3-540-97234-X.

[26] W. Gröbner, „Die Lie-Reihen und ihre Anwendung“, Berlin: Deutscher Verlag der Wissenschaften, Germany, 1967.

[27] K. Röbenack, „Regler- und Beobachterentwurf für nichtlineare Systeme mit Hilfe des Automatischen Differenzierens“, Aachen: Shaker Verlag, Germany, 2005, ISBN: 3-8322-4414-X.

[28] H. Keller, “Non-linear observer design by transformation into a generalized observer canonical form”, International Journal of Control, Vol. 46, No. 6, 1987, pp. 1915–1930.

[29] A.R. Phelps, “On constructing nonlinear observers”, SIAM Journal on Control and Optimization, Vol. 29, 1991, pp. 516–534.

[30] T. Meurer, K. Graichen, & E.D. Gilles, Eds., “Control and Observer Design for Nonlinear Finite and Infinite Dimensional Systems”, Vol. 322 of Lecture Notes in Control and Information Science, Berlin: Springer-Verlag, Germany, 2006, ISBN: 3-540-27938-5.

[31] E. Griepentrog, M. Hanke, & R. März, “Toward a better understanding of differential algebraic equations (Introduction survey)”, Seminarbericht Nr. 92-1, Seminar on Differential-Algebraic Equations, Berlin: Humboldt-Universität zu Berlin, Fachbereich Mathematik, Informationsstelle, Germany, 1992, pp. 2–13, ISSN: 0863-0968.

[32] E. Hairer, C. Lubich, & M. Roche, “The Numerical Solution of Differential-Algebraic Systems by Runge-Kutta Methods”, Vol. 1409 of Lecture Notes in Mathematics, Berlin: Springer-Verlag, Germany, 1989, ISBN: 3-540-51860-6.

[33] F.E. Thau, “Observing the state of nonlinear dynamical systems”, International Journal of Control, Vol. 17, No. 3, 1973, pp. 471–479.

[34] S. Raghavan, & J.K. Hedrick, “Observer design for a class of nonlinear systems”, International Journal of Control, Vol. 59, No. 2, 1994, pp. 515–528.

[35] R. Rajamani, “Observers for Lipschitz nonlinear systems”, IEEE Transactions on Automatic Control, Vol. 43, No. 3, 1998, pp. 397–401.

[36] J.C. Doyle, K. Glover, P.P. Khargonekar, & B.A. Francis, “State-space solutions to standard H2 and control problems”, IEEE Transactions on Automatic Control, Vol. 34, No. 8, 1989, pp. 831–847.

[37] W. Kampowsky, P. Rentrop, & W. Schmidt, “Classification and numerical simulation of electric circuits”, Surveys on Mathematics for Industry, Vol. 2, 1992, pp. 23–65.

[38] C. Gomez: “Engineering and Scientific Computing with Scilab”, Boston, MA: Birkhäuser, USA, 1999, ISBN: 0-8176-4009-6.

Biographies

Klaus Röbenack was born in Halle/Saale, Germany in 1967. He received his Dipl.-Ing. and Dr.-Ing. degrees in electrical engineering from the Technische Universität Dresden in 1993 and 1999, respectively. Additionally, he received the Dipl.-Math. degree with honours in 2002 and the university teaching qualification (Dr.-Ing. habil.) in 2005. Dr. Röbenack is associated with the Institut für Regelungs- und Steuerungstheorie at Technische Universität Dresden. His research interests include nonlinear control, observer design, descriptor systems and scientific computing.

MODEL PREDICTIVE CONTROL BASED ON RADIAL BASIS FUNCTION NETWORKS AND ITS APPLICATION

A. A. AbdulRahman *, M. H. Melhi, Y. M. Alwan
Department of Mechanical Engineering, Faculty of Engineering, Sana'a University, Sana'a, Yemen

ABSTRACT

This work primarily is concerned with developing a nonlinear predictive control methodology based on radial basis function (RBF) networks for nonlinear dynamical systems. The RBF model of the nonlinear process is developed using the orthogonal least squares (OLS) training algorithm. The nonlinear sequential quadratic programming (SQP) optimisation technique is employed to calculate the optimal actuation sequence for the nonlinear predictive control based on the RBF model of the system. The proposed control methodology is tested using a stirred tank heat exchanger nonlinear process. The proposed control strategy proved to be successful. The controller is capable of tracking various set-point changes and its performance is compared with the performance of the conventional PID controller.

Keywords

Radial Basis Function (RBF) Networks, Model Predictive Control, Sequential Quadratic Programming (SQP).

1. INTRODUCTION

Model predictive control (MPC) is known to be an effective control strategy for a wide variety of process industries. The advantages of MPC include the relative ease with which the input and output constraints, time delay, non-minimum phase and multivariable systems can be handled. The dynamic matrix control (DMC) [1] and the generalised predictive control (GPC) [2, 3] algorithms are the most commonly used control algorithms to date. They have been extended to incorporate many enhancements such as [4, 5]. Moreover, the DMC algorithm has been applied for integrating processes by Gupta [6]. The fundamental idea behind the MPC technique is to predict the output of the process over a long-range horizon and to use this information to determine the control sequence over a control horizon.

Despite the success enjoyed by MPC in industry there are some processes, which pose a challenge for the standard linear model-based algorithms mentioned above. Thus, there is an incentive to develop extensions of MPC to tackle nonlinear systems [7 – 9] and for more review [10, 11]. Most of the current nonlinear MPC strategies are based on physical process models, which are often inaccurate or not available at all. However, if empirical models are identified from plant input/output data, nonlinear MPC techniques can be applied to a wide range of nonlinear processes [12 - 15]. Beside these nonlinear models, recently neural networks have been used as an alternative framework for empirical model development and control [16 – 21] and for review of neural network application see [22]. The neural networks properties such as their adaptive and nonlinear nature, and their learning and approximation capabilities have contributed to make them a useful tool in dealing the problem of controlling nonlinear dynamic systems. Multilayer perceptrons (MLPs) and RBF networks are the tow most commonly used types of feedforward network. They have much in common and the fundamental difference is the way in which the hidden units combine values coming from preceding layers in the network. MLPs use inner products, while RBFs use Euclidean distance; the customary methods for training MLPs and RBFs are different, although, most methods for training MLPs can also be applied to RBF networks. The approaches for training MLPs networks involve the solution of a nonlinear problem with local minima. However, training RBF networks with Gaussion (Figure 1) function in the hidden layer using OLS training algorithm has the advantage of not being locked into local minima as do the training algorithms for MLPs networks [19, 21, 23].

Hunt and Sbarbaro [19] have trained the RBF network to learn both systems input/output relationship and the corresponding inverse relationship imposed these models into the internal model control (IMC) algorithm, on other hand, Pottmann and Seborg have trained RBF network to obtain a process model of a neutralization process and an approximate RBF controller network for the nonlinear predictive control algorithm [22].

In this paper we propose the possibility of modelling a nonlinear process using RBF network and integrating this model into the MPC algorithm to control nonlinear system, the SQP optimisation technique is used for obtaining the control sequence over the control horizon. The important and brief issue of RBF network is discussed in Section 2.

2. RADIAL BASIS FUNCTION NETWORKS

A radial basis function arises naturally in problems of hyper-surface interpolation and approximation and in problems of learning input/output mappings from given sets of data. RBF networks usually have only one hidden layer, for which the combination function is based on the Euclidean distance between the input vector and the weight vector. There are various well known RBFs [20, 21], for example;

The Gaussion distribution function,

*Corresponding author: *E-mail:* galil12 @yahoo.com

 ISSN: 1743-9310

$$y = \exp(-a^2 / v), \quad v > 0 \tag{1}$$

the thin plate spline function

$$y = a^2 \log(a) \tag{2}$$

the multiquadratic function

$$y = (a^2 + v)^{0.5}, \quad v > 0 \tag{3}$$

and the reciprocal multiquadratic function

$$y = (a^2 + v)^{-0.5}, \quad v > 0 \tag{4}$$

where $a = \|x - x_i\|$, has been introduced for brevity. Gaussian RBFs (Figure 1.) seem to be the most popular function used in the hidden unit of RBFs networks. RBFs that use Gaussian function have a width associated with each hidden unit or with the entire hidden layer. Instead of adding it in the combination function like a bias, the Euclidean distance is divided by the width.

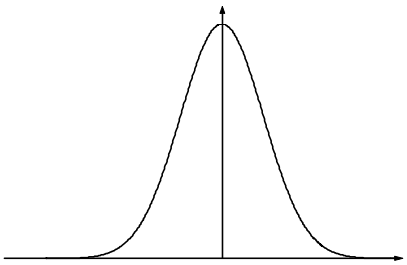

Figure 1. Gaussian Function

The output of the Gaussian activation function is

$$y = \exp(-a^2 / v) \tag{5}$$

where $a = \|w - \varphi\|$, the distance between the input φ presented at the input layer and the point w presented by the hidden unit, and v is a variance value that is required to shape the Gaussian function. As can be seen from Figure 1, the output from the Gaussian function is at its peak when the distance is zero, and falls to smaller values as the distance from the centre increases. As a result, the hidden unit gives an output of one when the input is centered, but it reduces as the input become more distant from the centre. In general, the RBF network can be described as constructing global approximations to functions using combinations of basis functions centered around weight vectors. In fact, it has been shown that RBF networks are universal function approximators [20, 21, 23].

3. RADIAL BASIS FUNCTION MODELS OF DYNAMICAL SYSTEMS

The RBF network (Figure 2) having Gaussian function in the hidden layer has the ability to approximate any nonlinear continuous function to an arbitrary degree of exactness [20, 21, 23]. Using past system n_u input and n_y output signals as an input to the RBF network, future outputs can be predicted,

$$\hat{y}(t) = f_{nn}[y(t-1),.....,y(t-n_y), u(t-t_d),.....,u(t-t_d-n_u)] \tag{6}$$

By feeding back the model outputs to the input nodes of the network, dynamical models are generated, although networks perform a static nonlinear mapping,

$$\hat{y}(t) = f_{nn}[\hat{y}(t-1),.....,\hat{y}(t-n_y), u(t-t_d),.....,u(t-t_d-n_u)] \tag{7}$$

where f_{nn} is some function realised by a RBF network, and t_d is the time delay, which is assumed to be at least one. For a given set of input/output data, an approximation of equation (6) will be generated. Choosing the RBF network approach with Gaussian functions in the hidden layer, the dynamical system is approximated by a linear combination of the Gaussian function,

$$\hat{y}(t) = \sum_{j=1}^{n_h} W_j K_j + W_0 \tag{8}$$

where W denotes the connection weight between the hidden unit and the network output, and K_j is the activation value of the hidden units.

The activation level of a hidden unit in a RBF network depends only on the distance between the input vector and the centre of the Gaussian function of that unit. The activation level K_j of the hidden unit j is defined as

$$K_j = f_G\left(\sum_{i=1}^{n}\left(\frac{w_{ij} - \varphi_i}{v_{ij}}\right)^2\right) \tag{9}$$

where the distance function

$$\rho_j = \sum_{i=1}^{n}(w_{ij} - \varphi_i)\Delta(w_{ij} - \varphi_i)$$

for hidden unit j represents the scaled distance between the centre of the function w_{ij} for that unit and the input vector φ_i:

$$\varphi(t) = [y(t-1),....,y(t-n_y),u(t-t_d),...,u(t-t_d-n_u)]^T$$

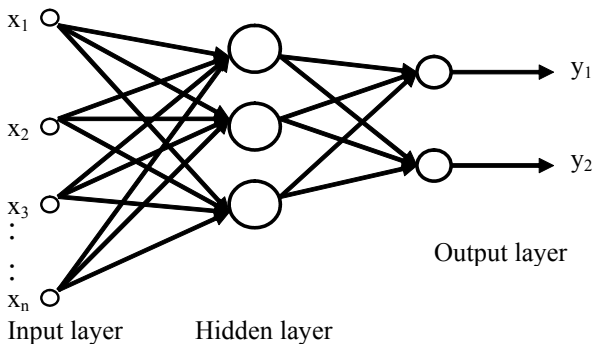

Figure 2. Two-layer neural network

The problem of determining the RBF network connections (weights) for the hidden and output layers is essentially an optimisation task and is called training.

RBF networks are often trained by 'hybrid' methods [20, 21, 23], in which the hidden weights (centres) are first obtained by unsupervised learning, after which the output weights are obtained by supervised learning. Unsupervised methods for choosing the centres include:

1.Distribute the centres in a regular grid over the input space.

2.Choose a random subset of the training cases to serve as centres.

3.Cluster the training cases based on the input variables and use the mean of each cluster as a centre.

The selection of significant RBF centres and the estimation of the weight output parameters could be performed simultaneously by combined orthogonal estimation and linear regression techniques. The combined orthogonal estimation and linear regression techniques are called the orthogonal least squares (OLS) training algorithm. The OLS algorithm is computationally efficient and tends to produce parsimonious RBF networks with excellent generalisation properties refer as in [23]. Hybrid training will usually require more hidden units than supervised training, since supervised training optimises the locations of the centres while hybrid training does not refer as in [21, 23]. Identification of the RBF network model using OLS training algorithm has been generated using neural network MATLAB™ Toolbox software package.

4. MODEL PREDICTIVE CONTROL BASED ON RBF NETWORKS

Model predictive control (MPC) scheme (Figure 3) is based on the receding horizon control approach, which can be summarised by the following steps:

1.Predict the system output over the range of future times.

2.Assume that the desired outputs are known.

3.Choose a set of future control, which minimises the future errors between the predicted future output and the future desired output.

4.Use the first element of future control moves as a current input, and repeat the whole process at the next instant.

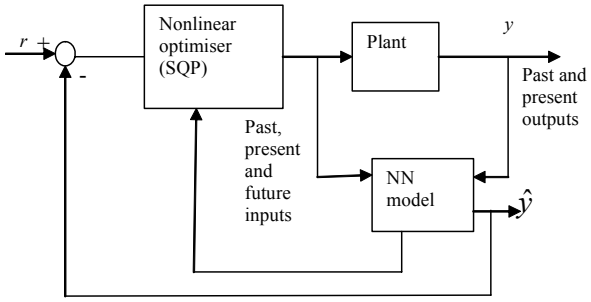

Figure 3. Neural network model predictive control structure

The first step in receding horizon control is to predict the system over the range of future times. This could be done by using a one-step ahead predictor equation (6). The k-step ahead prediction of the system output can be calculated by shifting the expression forward in time while substituting predictions for actual measurements where these do not exist equation (10).

(10)

$$\hat{y}(t+k) = f_{nn}[\hat{y}(t+k-1),.....,\hat{y}(t+k-\min[k,n_y]),\\ y(t-1),.....,y(t-\max[n_y-k,0]),\\ u(t+k-t_d),.....,u(t+k-t_d-n_u)]$$

It is assumed that the observation of the output is available up to time *t-1* only; for this reason, the output $\hat{y}(t)$ of the RBF network model enters the expression instead of the real output *y(t)*.

The objective function is the sum of square errors of the residuals between predicted outputs and the setpoint values over the prediction horizon, a term penalising the rate of change of the manipulated variable is often included as well. Mathematically, the neural network MPC problem can be stated in vector form as follows:

(11)

$$J(t,U(t)) = \Gamma^y[R(t+1)-\hat{Y}(t+1)]^T[R(t+1)-\hat{Y}(t+1)]\\ +\Gamma^u\Delta U^T(t)\Delta U(t)\\ =\Gamma^y E^T(t+1)E(t+1)+\Gamma^u\Delta U^T(t)\Delta U(t)$$

where

$$R(t+1)=[r(t+1),\ldots,r(t+p)]^T$$

$$E(t+1)=[e(t+1/t),\ldots,e(t+p/t)]^T$$

$$\hat{Y}(t+1)=[\hat{y}(t+1/t),....,\hat{y}(t+p/t)]^T$$

$$\Delta U(t)=[\Delta u(t),....,\Delta u(t+m-1)]^T$$

$$e(t+k/t)=r(t+k)-\hat{y}(t+k/t) \quad for \;\; k=1,....,p$$

subjected to,

$$y_{low} \le \hat{y} \le y_{high}$$
$$u_{low} \le u \le u_{high} \quad (12)$$

where m is the control horizon, p is the prediction horizon, Γ^u and Γ^y are the weighting coefficients matrices, $\hat{Y}(t+1)$ is the predicted output vector, $R(t+1)$ is the set point vector, and $\Delta U(t)$ is the rate of change of the manipulated variable $\Delta U(t) = U(t) - U(t-1)$.

It is beyond the scope of this paper to provide a survey of methods to solve the nonlinear programming model -based control problem, namely SQP is chosen for solving the previous problem, equation (11), subjected to constraints equation (12). Introducing constraints to the problem improves the computational aspects of nonlinear optimisation by eliminating significant regions of the area in which to search for a solution, and improving the ability to generate only feasible iterates, where inequality constraints are satisfied. In carrying out an SQP solution, the gradient information of the model prediction is needed and if the problem is constrained, then one needs to calculate the gradient of the Lagrangian function. For the analytical computation of the gradient $\partial J/\partial u$ of the objective function refer to [21]. In this work the gradient of the objective function $\partial J/\partial u$ necessary for the solution of the quadratic sub-problem were computed numerically and not analytically because, it has been mentioned by DE Souza et. al. [24] that the additional analytical effort of computing the gradient of the objective function and constraints does not produce significant difference in the results.

5. THE APPLICATION OF MODEL PREDICTIVE CONTROL BASED ON RBF NETWORKS ALGORITHM

The neural network (NN) MPC algorithm was tested with highly nonlinear process using a stirred tank heat exchanger process that was studied by Marlin [25]. The goal of this process is to control the dynamic response of the tank temperature subjected to a change in the coolant flow rate. The mathematical model for the system (liquid) in the stirred tank heat exchanger was obtained under these assumptions.

- The tank is well insulated, so that negligible heat is transferred to the surroundings.
- The accumulation of energy in the tank walls and cooling coil is negligible compared with the accumulation in the liquid.
- The tank is well mixed.
- Physical properties are constant.
- The system is initially at steady state (T_s = 85.49°C, F_c = 0.5 m^3/min).

The overall material and energy balances on the system are required to determine the flow rate and temperature from the tank. The final resulting model of the system in the stirred tank exchanger [25] is given by:

$$F\rho C_p(T_o - T) - \frac{aF_c^{b+1}}{F_c + \frac{aF_c^b}{2\rho_c C_{pc}}}(T - T_{cin}) = \rho C_p V \frac{d(T)}{dt} \quad (13)$$

Where;

$$F = 0.085\,m^3/\min;\ V = 2.1m^3;\ \rho = 10^3\,kg/m^3;\ C_p = 1cal/(g°C);$$
$$T_o = 150°C;\ T_{cin} = 25°C;\ C_{pc} = 1cal/(g°C);\ \rho_c = 10^3\,kg/m^3;$$

The first step to apply the NNMPC is to obtain a suitable representation of the system. The strong nonlinearity due to the variable F_c raised to the powers b and $b+1$ and to the product of variables F_c and T. Therefore, the foremost requirement for development of any neural network model is to obtain data that captures the relationship between the input and output of the process. In addition, these data should span across the entire scope of possible variation. The training data were generated by forcing the coolant flow rate ($u = F_c$) with a uniform random signal of minimum and maximum values of 0.01 and 1.0 respectively, see Figure 4 for samples data for the training the actual data for training is 2400 samples.

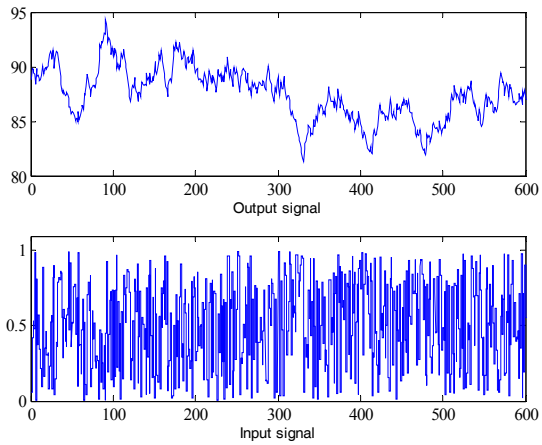

Figure 4. The training data

An important issue in neural network training is that of optimal training, which seeks to improve generalisation, reduce the number of training examples required and improve speed of learning. More importantly, as the number of parameters increases overfitting problems may arise, which degrades performance on generalisation. A solution to stop overfitting is to stop training just before the network starts to fit the sampling noise. In this work we followed the early stopping technique suggested by neural network MATLAB™ Toolbox software package where, the data are divided into three subsets, (i) one fourth of the data for the validation, (ii) another one fourth for testing, and (iii) the rest of the data for training. The content of the input vector and the number of hidden nodes define the network configuration. The network configuration should be large enough in order to give an acceptable performance but should not be too large because of stability properties and unnecessarily increasing calculation time. RBF networks with Gaussian functions require a reasonable large number of hidden units to approximate well. The model

structure is selected to be an auto-regressive with eXogenous (ARX) input with two past inputs and outputs to the input layer, resulting in 811 weights and biases in the hidden layer.

Once the RBF model is obtained, some validation tests should be considered. Model validation was performed by application on unseen data Figure 5. the output is generated and compared with the output of the nonlinear simulation with the same inputs. The results of this test shows good agreement between the output of the plant (target data) and NN (output data).

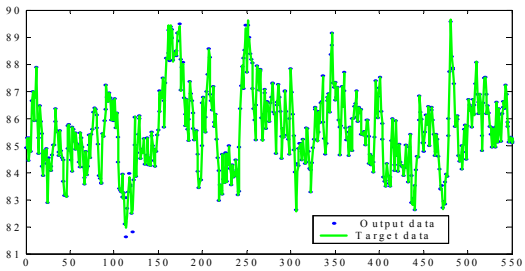

Figure 5. The validation data

Another option to measure validation of the RBF network model in more detail is to perform a regression analysis between the RBF network response and the corresponding targets as shown in Figure 6, it can be noticed that the coefficient of slope is very close to 1, the *y*-intercept is small and the correlation coefficient *R* between the outputs and targets is very close to 1.which indicate the perfect fit between the outputs and targets.

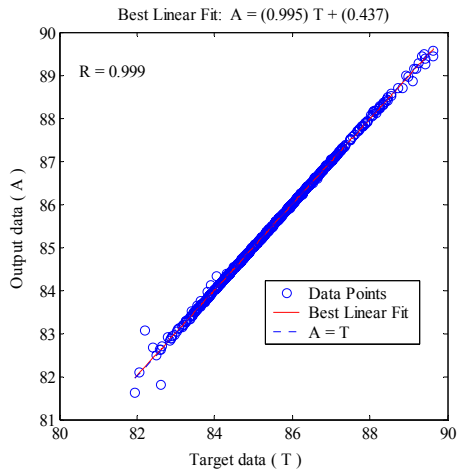

Figure 6. The regression analysis

A comparison between NNMPC algorithm and proportional-Integral (PI) controller is presented. The PI is somehow tuned based on linear model of the process. Therefore the nonlinear model of the process is linearised about the steady-state values (T_s = 85.49°C, F_c = 0.5 m^3/min) through a Taylor series in two variables. The approximate linear model of the system is expressed in deviation variables in t-domain [25] as follows:

$$\frac{dT'}{dt}+\frac{1}{\tau}T'=\frac{K_{Fc}}{\rho C_p V}F_c \qquad with \qquad \tau=\left(\frac{F}{V}-\frac{K_T}{\rho C_p V}\right)^{-1} \tag{14}$$

and the resulting linear model in s-domain can be obtained by getting the Laplace transform of the linear differential equation (14);

$$G(s)=\frac{K}{\tau s+1} \tag{15}$$

where

$$\Rightarrow K=\frac{K_{Fc}\tau}{\rho C_p V}=-33.9\frac{°C}{m^3/\min}$$

$$\tau=\left(\frac{F}{V}-\frac{K_T}{\rho C_p V}\right)^{-1}=11.9\,\min$$

The open loop step response for the nonlinear system, linear model and the RBF network model was obtained by applying a coolant flow rate (F_c) step response (0.5 ± 0.1 m3/min) as shown in Figure 7, it can be noticed that the linear model predicts the process time constant to a reasonable accuracy but fails to accurately predict the gain of the system, while the RBF network model predicts both time constant and gain with acceptable accuracy.

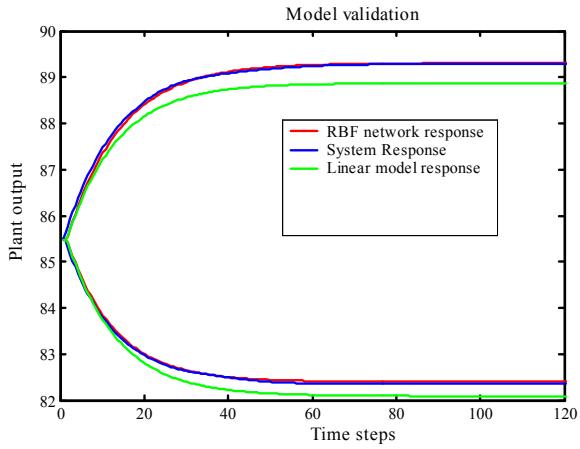

Figure 7. Open loop response for step changes of ± 0.1 m3/min from nominal value of 0.5 m^3/min for the nonlinear System response (dashed) RBF model response (solid), linear model response (dash-dotted)

For the closed-loop simulation, the control algorithm was set up with the RBF network model described earlier, and the new set points were introduced. The tuning parameters were chosen so that the integrated square error (ISE) between the simulated output and set point is minimised, as p = 25, m = 2, Γ^u = 0.95 and Γ^y = 1. The set point changes were implemented as step changes and no filtering was included in the feedback path. Moreover, the conventional PI controller was tuned based on

the design of PI and PID controllers with transient performance specification proposed by Basilio and Matos [26], the resulting tuning parameters are K_p = -0.2649 and T_i = 6.176.

Figures 8 and 9 respectively present the closed loop response of the system for PI and NNMPC algorithms. It can be noticed that both controllers bring the reactor to the new set point and perform the task in a short time. However, the nonlinear MPC takes less time than the PI. In all situations, the NNMPC controller outperforms the PI controller by considerably reducing the ISE between the system output and set point tracking. This is due to the perfect modelling using RBF networks and due the fact that the PI is tuned around the operating point so the response will be good as long as the system is working around the linearsied nominal model, thus not good response can be expected for the PI controller for setpoints far away from the operating point. The nonlinear MPC controller based on RBF network captures the nonlinear dynamics of the stirred tank heat exchanger and responds well to the set point changes.

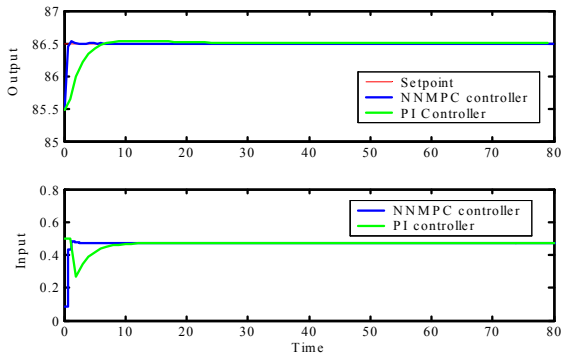

Figure 8. Closed-loop response to set point change of 86.5°C for NNMPC (solid), PI (dashdotted)

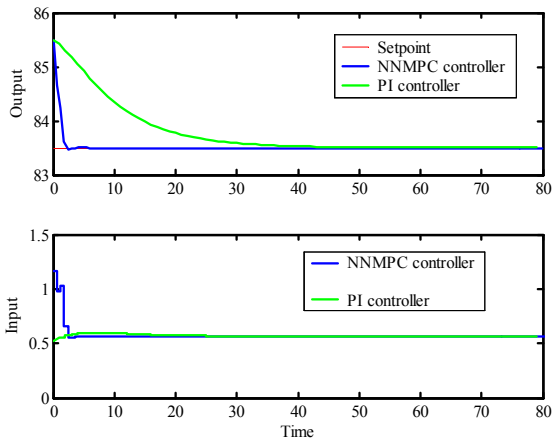

Figure 9. Closed-loop response to set point change of 82.5°C for NNMPC (solid), PI (dashdotted)

6. CONCLUSIONS

A nonlinear MPC algorithm based on RBF network has been presented. The model was identified using the RBF network with Gaussian function in the hidden layer. The RBF model was successfully incorporated into the MPC framework and significantly improved the accuracy of control of systems with significant nonlinearities. The nonlinear MPC algorithm applied to control a nonlinear process showed better performance than the conventional PI controller and ability to respond to the set point changes. The developed nonlinear MPC controller would therefore be of significant advantage to the process industry.

REFERENCES

[1] C. R. Cutler, & B. L. Ramaker, “Dynamic matrix control algorithm”, AIChE 86th National Meeting. Houston, TX, 1978.

[2] D. W. Clarke, C. Mohtadi, & P. S. Tuffs, “Generalised predictive control - Part I, the basic algorithm”, Automatica, Vol. 23, No.2, 1998, pp. 137-148.

[3] D. W. Clarke, C. Mohtadi, & P. S. Tuffs, “Generalised predictive control - Part II, extensions and interpretations”, Automatica, Vol. 23, No.2, 1987, pp. 149-160.

[4] H. Demericioglu, & D. W. Clarke, “Generalised predictive control with end-point state weighting”, IEE Proceedings-D, Vol. 140, No. 4, 1993, pp. 275-282.

[5] J. H. Lee, M. Morari, & C. E. Garcia, “State-Space interpretation of model predictive control”, Automatica, Vol. 30, No. 4, 1994, pp. 707-717.

[6] Y. P. Gupta, “Control of integrating processes using dynamic matrix control”, Institution of Chemical Engineers Trans IChemE, Vol. 76, pt A, May, 1998, pp.465-470.

[7] D. D. Brengel, & W. D, Seider, “Multistep nonlinear predictive controller”, Industrial Engineering Chemical Research, Vol. 28, No. 12, 1989, pp. 1812-1822.

[8] E. Ali, & E. Zafiriou, “Optimization-based tuning of nonlinear model predictive control with state estimation”, Journal of Process Control, Vol. 3, No. 2, 1993, pp. 97-107.

[9] P. A. Wisnewski, & F. J. Doyle III, “A reduced model approach to estimation and control of a kamyr digester”, Computers and Chemical Engineering, Vol. 20, No. 8, 1996, pp. S1053-S1058.

[10] R. Di Marco, D. Semino, & A. Brambilla, “From linear to nonlinear model predictive control: Comparison of different algorithms”, Industrial Engineering Chemical Research, Vol.36, No.5, 1997, pp. 1708-1716.

[11] M. A. Henson, “Nonlinear model predictive control: current status and future directions”, Computers and Chemical Engineering, Vol. 23, No. 2, 1998, pp. 187-202.

[12] M. Mackay, M. Thomson, & M. Soufian, “A bilinear non-parametric model based predictive controllers”, Proceedings IFAC 13th World Congress, June, California, 1996, pp. 459-364.

[13] E. Hernandez, & Y. Arkun, “Control of nonlinear systems using polynomial ARMA models”, AIChE Journal, Vol. 39, No. 3, 1993, pp. 446-460.

[14] B. R. Maner, F. J. Doyle III, “Polymerization reactor control using auto-regressive plus Volterra-based MPC”, AIChE Journal, Vol. 43, No. 7, 1997, pp. 1763-1784.

[15] G. R. Sriniwas, & Y. Arkun, "A global solution to the nonlinear model predictive control algorithms using polynomial ARX models", Computers and Chemical Engineering, Vol. 21, No. 4, 1997, pp. 431-439.

[16] H. T. Su, & T. J. McAvoy, "artificial neural networks for nonlinear process identification and control", in M. A. Henson & D. E. Seborg edition of nonlinear process control, Englewood Cliffs, NJ: prentice-Hall, UK, 1997, pp. 371-428.

[17] K. Temeng, P. D. Schnelle, & T. J. McAvoy, "Model predictive control of an industrial packed bed reactor using neural networks", Journal of Process Control, Vol. 5, No. 1, 1995, pp. 19-27.

[18] A. Aoyama, J. F. Doyle III, & V. Venkatasubramaniantt, "Control-affine neural network approach for non-minimum-phase nonlinear process control", Journal of Process Control, Vol. 6, No. 1,1996, pp. 17-26.

[19] K. J. Hunt, & D. Sbarbaro, "Neural networks for nonlinear internal model control", IEE Proceedings-D, Vol. 138, No. 5, 1991, pp. 431-438.

[20] M. Pottmann, & D. E. Seborg, "A nonlinear predictive control strategy based on radial basis function models", Computers and Chemical Engineering, Vol. 21, No. 9, 1997, pp. 965-980.

[21] D. P. Atherton, & G. I. Irwin, "Neural network applications in control", London: The Institution of Electrical Engineers, UK, 1995.

[22] M. A. Hussain,"Review of the applications of neural networks in chemical process control---Simulation and online implementation", Artificial Intelligence in Engineering, Vol. 13, No. 1, 1999, pp. 55-68.

[23] S. Haykin, "Neural networks: A comprehensive foundation, Second edition", New Jersey: Prentice-Hall, USA, 1999.

[24] M. B. De Souza, J. C. Pinto, & E. L. and Lima, "Control of a chaotic polymerization reactor: A neural network based model predictive approach", Polymer Engineering and Science, vol. 36, no. 4, 1996, February, pp. 448-457.

[25] T. E. Marlin, "Process control: designing processes and control systems for dynamic performance", London, McGraw-Hill, UK, 1995.

[26] J. C. Basilio, & S. R. Matos, "Design of PI and PID controllers with transient performance specification", IEE. Transaction on Education, Vol. 45, No. 4, 2002, pp. 364-371.

Biographies

Adel Abdulrahman obtained his MSc in Aviation field from the Mechanical Division and Flight Control Systems in 1994, this degree was a continuation from the BSc degree in the same field at Geoshuve Technical University, Geoshuve, Poland. He was appointed as an assistant lecturer in the Mechanical Engineering Department at Sana'a University in July 1995; Later on he obtained his MSc in computational and experimental stress analysis from UMIST, Manchester, UK. He obtained his PhD in the area of neural network model predictive control. He has also conducted specific studies and publication in the field of nonlinear model predictive control. Recently, he is working as assistant Professors in the Department of Mechanical Engineering at Sana'a University. He is working in advance control using conventional control and modern control, in addition he is interested in nonlinear system identification and the Mechatronic field.

Mohammed Melhi obtained his B.Sc in Computer Science and Engineering in 1987 from King Fahd University of Petroleum and Minerals (KFUPM), Dhahran, KSA. Later he obtained his M.Sc in Information and Computer Science in 1990 from the same university. Since 1991, he worked as a lecturer with the Faculties of KFUPM and Sana'a University until he obtained his Ph.D. from University of Bradford, UK in Cybernetics, Internet and Virtual Systems in 2001. From 2003 to 2004, he was the chairman of Computer Science Department, Sana'a University, Yemen.

Yasser M. Alwan obtained his B.Sc., degree in Electrical Engineering (2004). Assistant lectrurer in Faculty of engineering, Sana'a University. Supervisor of more than 20 mini-projects for one year in electrical engineering. Interested and working in control engineering researches since 2003.

Table of Contents

INSTRUCTIONS FOR AUTHORS (Title is Helvetica size 18)

Author 1[a,*], Author 2[b], Author 3[c] (Helvetica size 12)

[a]Affiliation a (Helvetica size 10)

[b]Affiliation b (Helvetica size 10)

[c]Affiliation c (Helvetica size 10)

ABSTRACT (Times New Roman size 12)

An abstract, not exceeding 200 words, is required for all papers (font is Times New Roman size 9).

Keywords (Times New Roman size 12)

The author should provide a list of key words, up to a maximum of six (font is Times New Roman size 9).

1. INTRODUCTION (Times New Roman size 12)

(Body text is Times New Roman size 9). The introduction of the paper should explain the nature of the problem, previous work, purpose, and the contribution of the paper. It is assigned the number "1" and following sections are assigned numbers as needed. format. The paper must be (Letter) page size with margins of 1.25" for the top of first page, 0.75" for left, right, and bottom, and 0.75" for top, bottom, left, and right of ALL subsequent pages. The paper must be double column format, single line spacing with an extra line added between paragraphs. Please limit the title to a maximum length of 10 words. The author's name(s) follows and is also centered on the page. A blank line is required between the title and the author's name(s). Last names should be spelled out in full and preceded by author's initials. The author's affiliation, complete mailing address, and e-mail address are provided below. Phone and fax numbers do not appear. Do not underline any of the headings, or add dashes, colons, etc. The headings, starting with "1. INTRODUCTION", appear in upper case letters and should be set in bold and aligned flush left. All headings from the Introduction to Conclusions are numbered sequentially using 1, 2, 3, etc. Subheadings are numbered 1.1, 1.2, etc. If a subsection must be further divided, the numbers 1.1.1, 1.1.2, etc. are used and the number and associated title are set in italics instead of bolded. A colon is inserted before an equation is presented, but there is no punctuation following the equation. All equations are numbered and referred to in the text solely by a number enclosed in a round bracket (i.e. (2) reads as "equation 2"). Ensure that any miscellaneous numbering system you use in your paper cannot be confused with a reference [3] or an equation (2) designation.

*Corresponding author: *E-mail:*

For more details, please visit

www.medjmc.com

1.1 Initial Submission

The manuscript must be a single file (including tables, figures, etc.) using either an Adobe-compatible portable document format (*.pdf) or an MS Word (*.doc) or Adobe FrameMaker (*.fm). Submit the manuscript without the authors' names, affiliation, and biographies. Along with it, submit a cover page that includes the manuscript title, authors' names and affiliation, and the corresponding author's name and contact information (full postal and e-mail addresses, phone and fax numbers), and biographies. The corresponding author will be given a reference number assigned to the paper and it is to be used in all future correspondence. Formatting your paper correctly saves a great deal of editing time, which in turn ensures publication of papers in a timely manner. Authors submit electronic versions of their manuscript to:

isubmission@medjmc.com

1.1.1 Figures

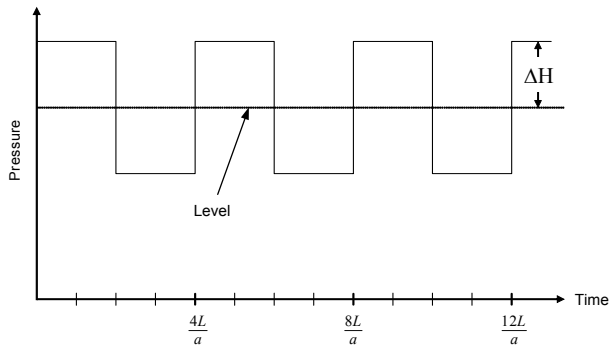

Figure 1. Sample graph

A reference list must be included. Only cited text references are included. Each reference is referred to in the text by a number enclosed in a square bracket (i.e., [3]). References must be numbered and ordered according to where they are first mentioned in the paper, not alphabetically.

REFERENCES

[1] Anderson, B. O. D. and D. J. Clements, "Algebraic Characterization", Vol. 17, 1981, pp. 703-712.

The Mediterranean Journal of Measurement and Control
www.medjmc.com

Published by SoftMotor Ltd. ISSN: 1743-9310

For complete information regarding
subscription and ordering,
please contact

SoftMotor Ltd
Provincial House, Solly Street, Sheffield S1 4BA
United Kingdom

Tel: (+44) 0114 201 4916
Fax: (+44) 0114 201 3524
E-mail: order@medjmc.com
Website: www.medjmc.com
Website: www.softmotor.co.uk

Volume 2 / Number 1 / 2006